Biomimetic Design Applied to the Redesign of a PEM Fuel Cell Flow Field

by

Jessica Marie Currie

A thesis submitted in conformity with the requirements
for the degree of Master of Applied Science

Mechanical and Industrial Engineering
University of Toronto

Biomimetic Design Applied to the Redesign of a PEM Fuel Cell Flow Field

Jessica Marie Currie

Master of Applied Science

Mechanical and Industrial Engineering
University of Toronto

2010

Abstract

In this thesis biomimetic design is applied to the redesign of a PEM fuel cell flow field. A number of designs inspired by biological phenomena were developed to address the problem of attaining a uniform current density distribution across a PEM fuel cell. These designs are evaluated using a numerical model. One design, inspired by Murray's law of branching in plants and animals, is further evaluated using and a physical model and comparing it to a commercial triple serpentine flow field. Improvements in pressure drop were seen for the Murray's law inspired flow field, however, it was found to be prone to flooding. If this flow field design were to be applied to high temperature membrane materials, materials that can operate above 100 °C where water is always in the vapor state, the mass transfer and reduced pressure drop advantages of the Murray flow field could be fully achieved.

Acknowledgments

I would first like to gratefully acknowledge the continued support of my supervisors, Professor Jim Wallace and Professor Li Shu, who didn't give up on me when I decided to take a job while still finishing my thesis.

I would also like to acknowledge the financial support of Natural Sciences and Engineering Research Council through a strategic projects grant, technical support of Hydrogenics, our industrial partner in the project, and Tony Mazza and Nathan Joos for their helpful discussions.

I would like to thank Professor Olivera Kesler and her student Craig Metcalfe for the use of the "hogs" for solving my simulations.

Huge thanks to Professor Aimy Bazylak and her students, James Hinebaugh, Zach Fishman and Jongmin Lee, for the use of the computer and fuel cell and for help whenever I needed it. A special thanks to Jongmin for running testing for me in these last weeks, I couldn't have done it without you.

Another big thanks to Joel Kuhn who has been amazing in so many ways. For being able to construct anything, for his skill in cad, and for always being able to help me forget about my stress.

And finally, thanks to my parents for teaching me that giving up is not an option and for always supporting me and believing in me whatever I do.

Table of Contents

List of Tables

List of Figures

List of Nomenclature

Variables

a_i	Activity of species i
c_i	Molar concentration of species i
Cap_m	Ionic capacity of the membrane
D_i	Diffusion coefficient of species i
E^o	Reference potential
F	Faraday's constant
Δg_f^o	Change in gibbs free energy of formation
$h_{e/c}$	Evaporation/condensation rate constant
h_m	Membrane/channel mass transfer coefficient
i	Current density
i_o	Reference current density
k_i	Conductivity of species i
M_i	Molecular weight of species i
n_{esd}	Electro-osmotic drag coefficient
N_i	Flux of species i

P	Operating pressure
P_{sat}	Saturation pressure of water
R	Gas constant
R_i	Reaction rate of species i
s	Liquid fraction
S_i	Source term for species i
S_i	Surface area of electrode i
T	Operating temperature
v_i	Diffusion volume of species i
x_i	Mole fraction of species i
$\alpha_{i,j}$	Charge transfer coefficient of electrode i, in the j direction
ε	Porosity of the GDL
η_i	Overpotential of electrode i
λ	Membrane water content
ρ_m	Membrane density
τ	Tortuosity of the GDL
ψ	“switch” function

Φ_i	Potential of species i

Subscripts

$()_{H2}$	Hydrogen
$()_{H2O}$	Water in the gaseous phase
$()_{H2O,l}$	Water in the liquid phase
$()_{H2Om}$	Water in the membrane
$()_{O2}$	Oxygen
$()_{ion}$	Ions
$()_{ele}$	Electrons
$()_R$	Reactants
$()_P$	Products
$()_a$	Anode
$()_c$	Cathode
$()_{a,a}$	Anode in the anodic direction
$()_{a,c}$	Anode in the cathodic direction
$()_{c,c}$	Cathode in the cathodic direction

$()_{ca}$	Cathode in the anodic direction
$()_{ref}$	Reference

Definitions and abbreviations

Anode: Electrode from which electrons are drawn externally out of the cell.

Bipolar Plates: Cell separation plates that supply reactants, provide electrical and thermal conduction, and provide structural support to the fuel cell. Both sides are channeled.

Cathode: Electrode to which electrons are supplied externally to the cell.

Flooding: Occurs when reaction sites are blocked by water, preventing the reactant from reaching the reaction sites.

GDL: Gas Diffusion Layer – Distributes reactant gas and enhances electrical conductivity between electrode and plate.

MEA: Membrane Electrode Assembly – Includes proton exchange membrane, anode, cathode, and two GDL's.

Nafion® Membrane: A Teflon®-like membrane that allows protons to be transported from anode to cathode, while preventing reactants and electrons from crossing.

PEM: Proton Exchange Membrane, most commonly a Nafion® membrane.

1 Introduction

The purpose of this thesis is to apply biomimetic design techniques to fuel cell challenges. First, the introduction presents a background of biomimetic design and PEM fuel cells. The next section is adapted from a paper written by Currie et al. (2009), which describes some preliminary biomimetic design concepts as well as compares biomimetic design to TRIZ (Theory of Inventive Problem Solving). Next, section 3 describes the problem that has been the focus of this thesis, achieving even current density distribution through flow field design. This section gives a background of common flow field designs and then moves on to describe the designs that biomimetic design techniques have inspired. The next section describes the method that was used to evaluate these concepts, a computer simulation using COMSOL Multiphysics. Then, the next section gives the results of these simulations. Experiments were also performed using a physical model of one of the flow field designs. The final section describes these experiments and gives the results.

1.1 Biomimetic design

Biomimetic design is a design methodology that uses analogical reasoning to solve engineering problems. Analogical reasoning uses imagery transfer from one domain to another to inspire a solution. It has been shown that using analogies as a design aid results in more creative concepts, where the most creative concepts come from completely different domains (Benami and Jin, 2002).

The biomimetic aspect of this design methodology is that the analogies are taken from the biological domain. Biology has been identified elsewhere as a rich source of analogies for inspiring design solutions (Vincent and Mann, 2002). According to Smith and Vincent (2002), biology offers great opportunity for inspiring solutions to design problems since there is a strong correlation between engineering design that seeks to optimize cost versus benefit, and biological systems that have evolved to optimize metabolic cost versus fitness.

The classic example of biomimetic design is the invention of Velcro. Velcro imitates the hook structures found on burrs that allow them to attach to animal fur and people's clothing. This idea was inspired by the designer's own experience with burrs and thus he could easily see an analogy

to a potential fastening problem. However, most designers may not have knowledge of all the useful biological phenomena that could be used to solve a given problem. This was addressed by Vakili and Shu (2001) who developed a systematic method to generate design solutions from biology. This method uses a plain language search of existing biological written knowledge to find relevant biological analogies. A keyword search of an undergraduate level biology textbook, *Life, the Science of Biology* (Purves et al. 2001), is used to find relevant biological phenomena. These keywords are verbs that describe the functionality of the device to be designed. The search returns biological phenomena that can be used either as direct inspiration for a design solution or as a starting point for further research into useful biological phenomena.

This design method has been successfully used to solve problems in design for remanufacture (Vakili and Shu, 2001, Hacco and Shu, 2002) and assembly of micro-parts (Shu et al., 2006). In addition, there has been work done to improve the technique by bridging the gap between the different lexicons used in engineering and biology so that more relevant keywords can be used (Chiu and Shu, 2005).

1.2 Fuel Cells

Fuel cells are attractive energy conversion devices. They provide energy at high conversion efficiency, typically 50% and higher, and are environmentally friendly. Fuel cells convert chemical energy directly into electrical energy. This means that more chemical energy is directly converted into electrical energy when compared to heat engines that involve intermediate conversions between thermal and mechanical energies. Besides the high energy conversion efficiency, fuel cells can produce electricity with a minimal amount of environmental pollution. For example, PEM fuel cells that run on hydrogen gas and air will only produce water, electricity, and heat as their products. Of course, the lowest pollution possibilities will be realized when the hydrogen gas for fuel can be generated from renewable energy sources, such as solar and wind energy. With these two attractive attributes, fuel cell technology is one of the most promising energy conversion devices for the future.

A fuel cell consists of many cells that are connected in series. Each cell is mainly composed of two electrodes, an anode and a cathode, separated by an electrolyte. Fuel is supplied and oxidized at the anode and electrons are produced during the reaction. The electrons flow through an external circuit, while the reaction intermediates (for example, hydrogen ions in a PEM fuel

cell) complete the current path through the electrolyte to the cathode side. At the cathode, an oxidizing agent reacts with the ions and the electrons, which return from the external circuit, to form the final products. The power output, and specifically the usable electric potential, that is generated from a single cell is insufficiently low. Therefore, many of these cells are connected together electrically in series to form a stack that can produce sufficient power for practical applications.

1.2.1 PEM Construction

Proton exchange membrane fuel cells are one of the fuel cell types that are presently available. Hydrogen gas and air are typically the two reactants that are fed to the cell to generate the electrical power in a PEM fuel cell. For example, in a two-cell stack PEM fuel cell as shown Figure 1.1, hydrogen gas enters the anode through channels on one side of a bipolar plate and air enters the cathode through channels on the other side of the bipolar plate. The term 'bipolar plate' is used due to the fact that anode and cathode plates of adjacent cells are connected together and can, in many cases, be one common component to the two adjacent cells, with both anode and cathode functionalities. Liquid coolant flows through intermediate channels within the bipolar plate to remove the heat energy that is produced from the electrochemical reaction and to maintain the operational cell temperature between 60°C and 80°C to prevent membrane degradation at higher temperature.

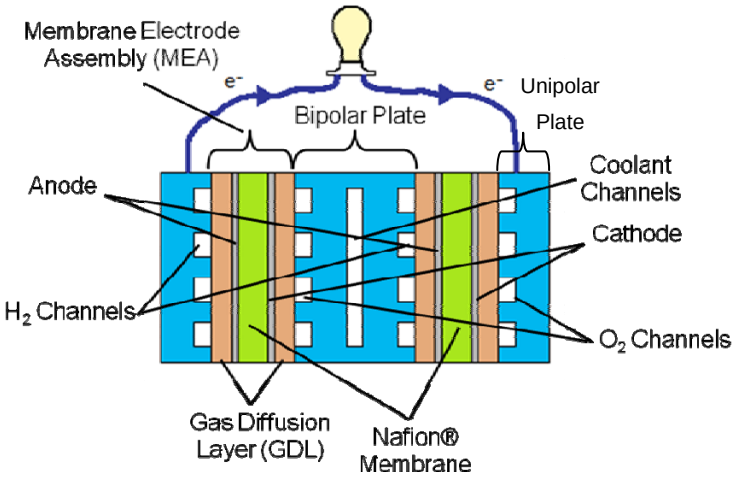

Figure 1.1 Fuel cell cross section detail – two cells in series

Part of the hydrogen gas will diffuse through the gas diffusion layers (GDL) toward the anode electrode on the surface of the proton exchange membrane, typically Nafion®, which constitutes the electrolyte in PEM fuel cells. At the anode, a precious metal catalyst, typically platinum, disassociates the hydrogen and assists the oxidation, or electron removal from the dissociated hydrogen, to produce the protons that will flow through the Nafion ionomer. Protons travel through the membrane, across the ion exchange sites, toward the cathode carrying water molecules along with them. Typically, one to five water molecules are associated with each proton and are carried across the membrane by the process of electro-osmotic drag (Zawodzinski et al., 1993).

On the catalyst sites at the cathode, the protons, the oxygen in the air and electrons that have passed through the external electrical circuit from the anode combine to produce water, thereby completing the electrochemical reaction. Because the operating temperatures of the PEM fuel cells are typically below the boiling point of water at the operating pressures, liquid water results as the reaction product. The product water, along with the water that was carried across from the anode, evaporates and is carried away from the reaction sites by the air in the cathode channels. Figure 1.2 illustrates this process.

The two electrodes are typically made from an extremely fine dispersion of platinum catalyst on a nanoparticulate carbon black support. The resultant carbon black powder is coated onto the ion exchange membrane. A gas diffusion layer (GDL) can be found on the outer surface of each electrode to provide proper distribution of reactant gas and to provide electrical connection to the external circuit. The ion exchange membrane, with the two electrodes coated on it, and a GDL immediately adjacent to each catalyst layer are often preassembled. This assembly is referred to as the membrane electrode assembly (MEA). Then the MEA is placed between two bipolar plates to form a complete cell in a stack. The first and last cells of a fuel cell stack have one bipolar plate and one unipolar plate to contain the MEA. The functions of unipolar and bipolar plates include supplying reactants, providing electrical and thermal conduction, providing structural support to the cell, as well as offering an easy stack connection.

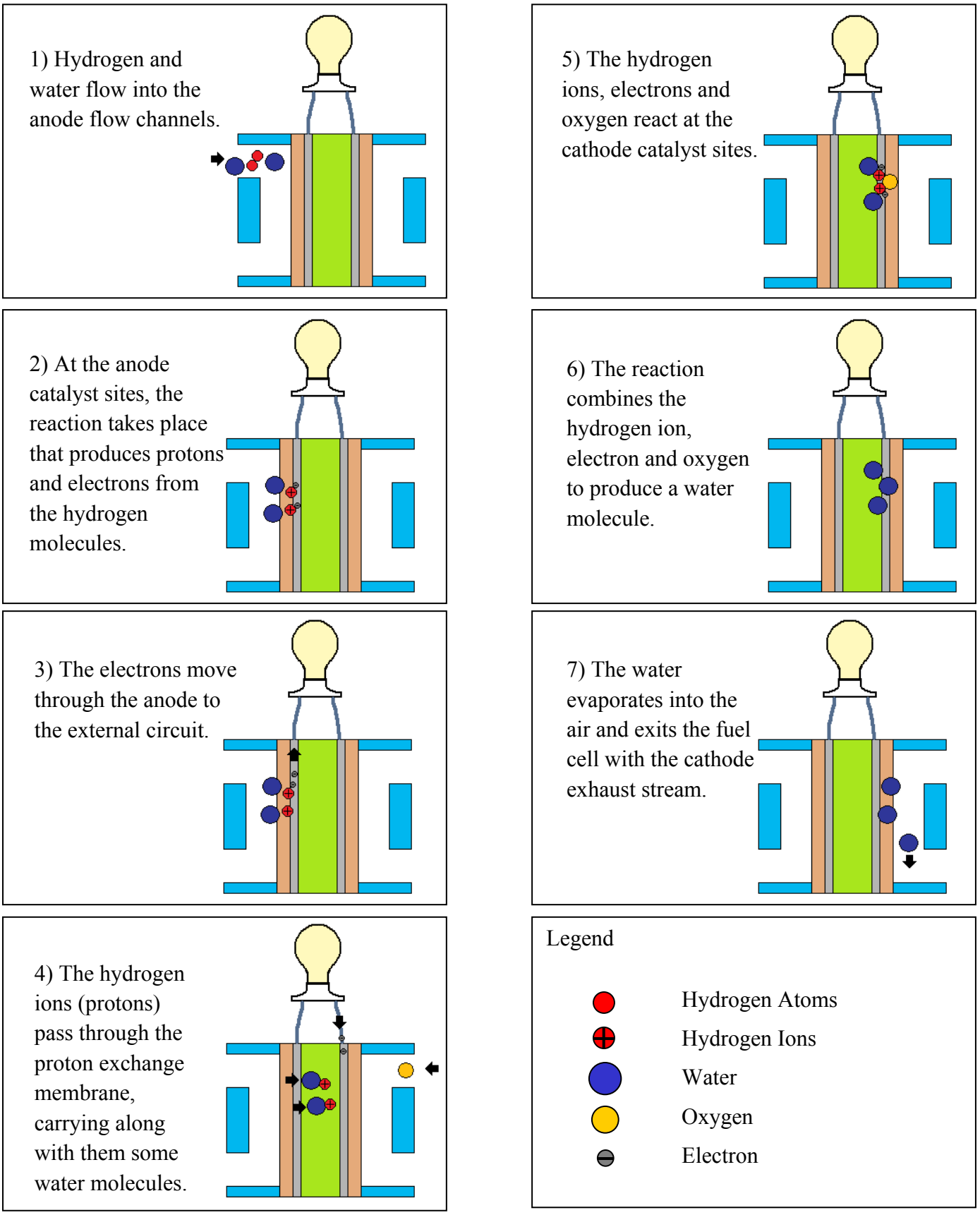

Figure 1.2 Progression of materials in a fuel cell

2 Preliminary Concepts and Biomimetic Design /TRIZ Comparison

The following section is adapted from a paper written by Currie et al. (2009). The paper is an investigation of two different design methodologies, Biomimetic design and TRIZ (Theory of inventive problem solving), applied to fuel cell redesign. Biomimetic design is design by analogy and TRIZ is design by identifying and improving a contradiction. The focus of this paper is on the problem of water management in a PEM fuel cell. Each methodology produced two design concepts. Using these concepts, the differences and similarities between the two methodologies are identified.

2.1 Problem definition – Water Management

Water management in a fuel cell is a most important factor in the design of a fuel cell for two reasons. The membrane needs water to function properly. Although water is a product of the reaction and is needed for the membrane to conduct protons, an excess of liquid water can seriously limit the flow of reactant air/oxygen to the cathode catalyst sites. These two major considerations in water management will be addressed through membrane hydration and cathode flooding.

2.1.1 Membrane Hydration

Nafion® has a Teflon®-like fluorocarbon backbone (repeating unit of $-CF_2-CF-CF_2-$) with a negatively charged hydrophilic site, SO_3^{2-}, at the end of each side chain as shown in Figure 2.1 below. SO_3^{2-} provides a temporary site for H^+ to move across the membrane. Owing to the nature of Nafion®, the presence of water is necessary for movement between sites, that is, the membrane must be hydrated. For each H^+ that moves across the membrane, several water molecules are, as mentioned earlier, carried across to the cathode side by electro-osmotic drag.

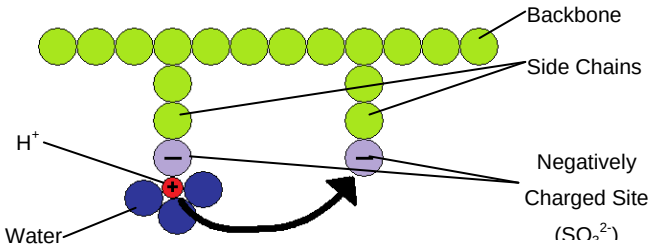

Figure 2.1 Nafion® membrane

If the membrane is not adequately hydrated, proton transport will be compromised due to an increased internal ohmic resistance that is caused by a lack of water which is required to facilitate the movement of H^+. Therefore, it is important to continuously hydrate the membrane in order to reduce this loss of water and thus loss of electrical potential due to an increase in the internal resistance. Hydration of the membrane is often accomplished by humidifying the feed hydrogen gas to provide extra water in addition to that produced electrochemically to the membrane. However, uniform water distribution cannot easily be obtained by simply humidifying the gas at the inlet. The hydrogen feed loses water to the membrane as it flows through the hydrogen flow fields at a faster rate than hydrogen is consumed in the reaction. This leads to lower relative humidity for the hydrogen gas at the anode exhaust, which causes a lower membrane hydration at this location.

It is also possible for water to enter the anode compartment through the membrane from the cathode compartment. This can occur if the concentration of water is greater on the cathode side than on the anode side. The resulting concentration gradient causes diffusion of water from the cathode side to the anode side. However, this will likely and effectively happen only where the membrane is fully hydrated.

2.1.2 Cathode Flooding

Water is present at the cathode surface due to two phenomena; it is produced by the cathode-side reaction, and it is carried by the H^+ molecules from the anode side as described above.

Flooding occurs when the water removal rate from the cathode surface is slower than the water production rate. The excess water prevents the oxidant from reaching the reaction sites.

Water removal is accomplished by the evaporation of water to the cathode reactant gas, either at the surface of the cathode or in the GDL. The GDL can allow water to be drawn from the cathode surface for effective removal and subsequent evaporation. The GDL is often coated with a hydrophobic substance, and sometimes immediately at the electrode/GDL interface, to improve water rejection at the cathode (Larminie and Dicks, 2003). However, at higher current the water removal rate may still be insufficient (Yamada, 2006).

Flooding of the cathode can occur at two locations, either at the inlet and/or at the outlet areas. At the inlet, the oxidant is at its highest concentration and the reaction rate as determined by the reaction kinetics would be at its highest. Ideally, a uniform reaction rate throughout the cathode compartment is desirable. It is common practice to provide a high flow rate through the cathode compartment to help ensure that an excess of reactant oxygen is supplied throughout the cathode compartment so that the depletion of oxidant due to reaction is minimized. However, this is rarely attained, even at the highest practical cathode stoichiometric ratios. There will always be a net reduction of reactant oxygen throughout the cathode compartment. At the cathode outlet, there will always be a net accumulation of water in the vapour phase and, hence, a decreased ability to evaporate water vapour at the cathode outlet. As a result, flooding can occur at some point upstream of the cathode exhaust because of a compromised capacity to take up water into the gas phase.

2.2 Biomimetic Design Concepts

This section describes two biological analogies that were identified with the biomimetic techniques. For each analogy, a description of the biological phenomenon is given, as well as how the phenomenon can be related to fuel cells. Moreover, a potential solution to the fuel cell water management problem is presented.

2.2.1 Keyword Generation

The first step in the biomimetic method is to generate a list of keywords that describe the problem. In this case we have chosen the water management problem. The initial keywords were identified from descriptions of the function of the bipolar plate related to water

management. These functions are, distribute gas (reactants and water), and remove water. The keywords are the verbs in these functions, i.e. distribute, and remove.

To produce a larger set of keywords to be used to search the biology textbook, the initial keywords were expanded using WordNet. WordNet is and online lexical database that can be used to find word relations, such as troponyms, a more specific form of a word and hypernyms, a more general form of a word.

Remove and distribute were expanded to give the words shown in Figure 2.2 below. The higher words are more general and break down into more specific forms.

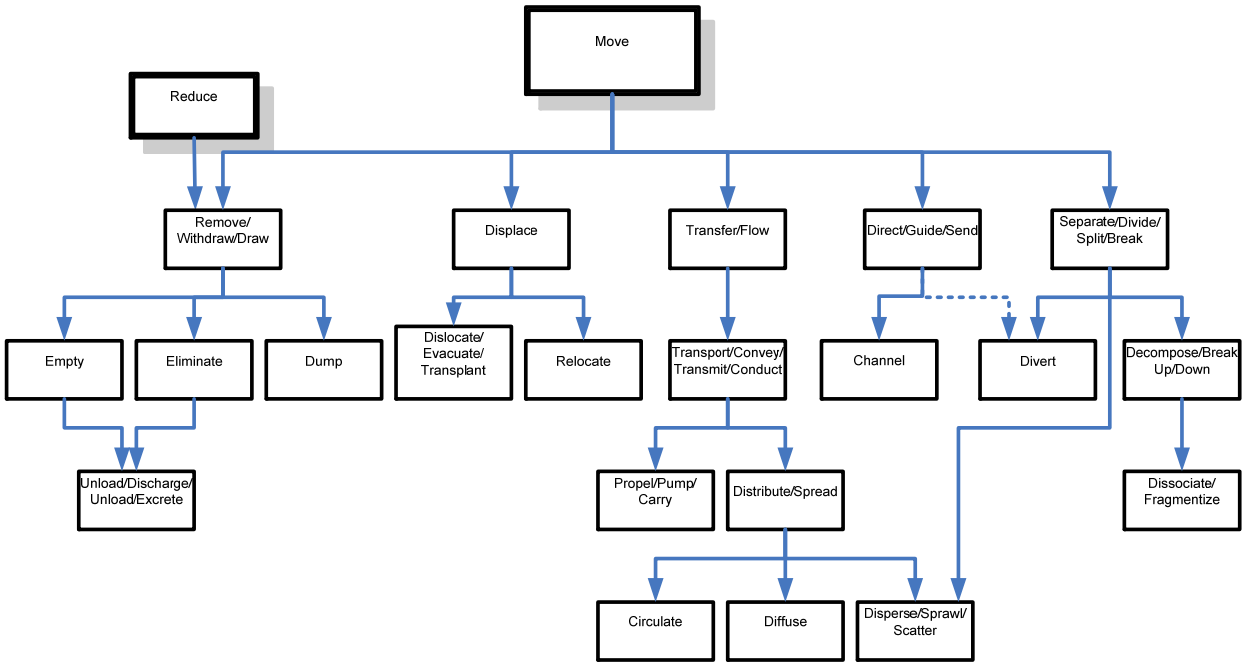

Figure 2.2 WordNet expansion of the keywords remove and distribute

2.2.2 Reproduction in Mushrooms

The initial keyword, ‘distribute’, was generated from the problem statement of distributing water to hydrate the membrane at the anode side. Through a series of troponym (a more specific form of a verb) relationships found using WordNet®, the keyword ‘discharge’ was used to search the biology text. The sequence that produced ‘discharge’ started with ‘distribute’ and led to ‘spread’

then to ‘discharge’, all of these being troponyms of the previous. With the keyword ‘discharge’, the biomimetic search tool returned the following excerpt describing a biological phenomenon:

> “The sexual reproductive structure of basidiomycetes is a basidium: The basidia *discharge* their spores into the air spaces between adjacent gills, and the spores sift down into air currents for dispersal and germination as new haploid mycelia.” (Purves et al., 2001, italics added)

A brief explanation of the reproduction mechanism of the basidiomycetes, a family of fungi, which has a special reproductive structure, is described below.

2.2.2.1 Biological Phenomenon

One of the most commonly known groups of fungi under the class of basidiomycete is the mushroom. The structure of a basidiomycete consists of a cap, with gills on the underside, sitting on a stalk, as shown in Figure 2.3. The gills take the shape of layers of thin strips of tissue that run in the radial direction. The spores of basidiomycetes are called basidiospores. Spores of a mushroom are equivalent to the seeds of a plant, which are the reproductive bodies that can grow into new organisms. On the surface of the gills are tiny protruding stalks called basidia. Approximately two to four basidiospores can be produced on a basidium. Once the basidiospores are mature, they are dispersed down into the air current to a different area for germination as new young mushrooms. (Purves et al., 2001)

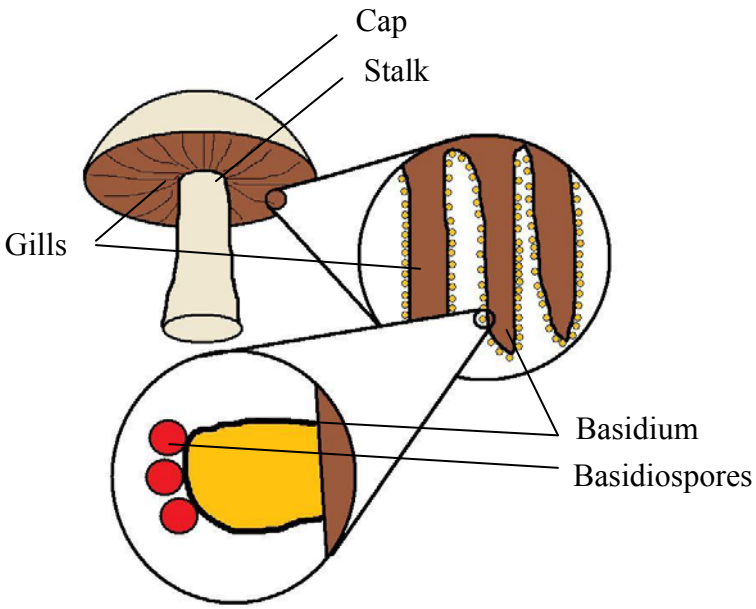

Figure 2.3 Mushroom detail

2.2.2.2 Domain Mapping

The analogy between the engineering problem, membrane hydration, and the biological phenomenon, reproductive structure of mushroom, is related through the idea of how the basidiomycete discharges its basidiospores through the air spaces between the gills into the air current to carry to suitable germinating sites. In a similar manner, the anode bipolar plate can be made porous to allow the discharge of water through the pore openings into the moving hydrogen gas. The water is evaporated into the flowing hydrogen gas because of the concentration gradient between the water on the surface of the bipolar plates and the relative humidity of the hydrogen gas. This configuration could provide sufficiently hydrated hydrogen gas throughout the flow field channels to hydrate the membrane.

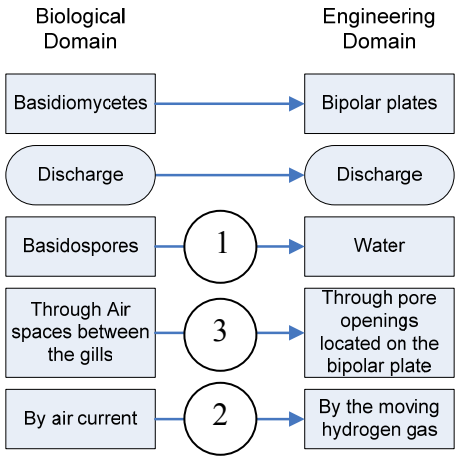

Figure 2.4 Biomimetic mapping - Bacidiomycetes

Bipolar plates are typically made from graphite and rendered impermeable (even though they are inherently porous) to avoid fuel crossover from anode to cathode (Li, 2006). They are kept thick and/or sealed with polymer fillers to prevent mixing of the different substances. By retaining the porosity in the graphite, and given that water is used as the coolant, one can supply water to the anode channels from the coolant water through the pores in the anode plate. The evaporated liquid water will replace the water in the hydrogen gas stream that was lost to the membrane.

The analogy was formed directly from the match that was returned by the biomimetic search tool and without further investigation of the biological details. The phenomenon was initially simplified to "discharge spores to air current through air spaces". The mapping sequence, shown in Figure 2.4 as numbered circles, was as follows, first the spore was mapped to water, and then air was mapped to hydrogen gas. By knowing that graphite, the material that is used to make bipolar plates, is inherently porous, a connection was made between air spaces and pore openings on the anode side of the bipolar plate. The resulting concept was then expressed as "discharge water to hydrogen gas through pore openings in anode side of the bipolar plates". Lastly, bipolar plates were mapped to basidiomycetes.

2.2.2.3 Limitations and Advantages

Minimizing hydrogen leakage into the coolant is desired. Two-phase flow, hydrogen gas and liquid water, will lead to greater pumping power required and also damage the coolant pump.

Higher coolant pressure will limit but not eliminate hydrogen diffusion into the coolant due to the concentration gradient. However, the rate of diffusion may be offset by the coolant flow rate from the coolant side to the anode side. It should also be noted that the plate on the anode side will be different from the plate on the cathode side, due to the fact that water is removed at the cathode. As a result, the cathode plate must be kept impermeable. The thickness of the anode plate may have to be adjusted to achieve the desired water flow rate to the anode from the coolant. For example, when the required flow rate is very high, the plate can be made thinner, giving the water a shorter and easier path to the hydrogen channels. In the extreme case where the anode plate must be very thin to allow higher water flow rate, it may be too thin to allow anode channels to be formed in the plate without compromising the structural stability. In this case the channels can then be formed on the GDL instead (Li, 2006).

Another advantage of the anode plate humidification system is that evaporative cooling may reduce the overall cooling demand of the fuel cell. When liquid water is evaporated from the surface of the plate, heat is absorbed into the water to facilitate the phase change. Moreover, evaporative cooling is several times more effective than a liquid coolant with no phase change. This could lower the coolant flow rate requirement. Since the functions of humidification and cooling are coupled, control of the cooling rate and humidification would need to be done very carefully.

2.2.2.4 Existing solution

After the concept was formulated using biomimetic design, a literature search was performed and a related idea by Peter Schütz (1989) was found. His idea also utilizes the porosity in the bipolar plate to humidify the hydrogen gas. He conducted experiments and confirmed that the system indeed was able to humidify the hydrogen gas. The results by Schütz support that the concept formed using biomimetic design is feasible.

2.2.3 Solute Excretion in Plants

The same initial keyword as in Section 2.2.2, ‘distribute’, was expanded using WordNet®. However, the situation was changed to distribute water away from the membrane to avoid flooding. Hypernyms, more general forms of the word, like ‘transport’ and ‘conduct’ were found and used for the search for biological phenomena. These searches returned many general biological phenomena that relate to the transport of sap and solutes in plants. Though a particular analogy was not found that inspired a solution in the initial search, it did inspire further research into the more specific mechanisms of plant sap and solute transport. This further research confirmed the relevance of solute excretion in plants.

2.2.3.1 Biological Phenomenon

The sap of plants may contain solutes such as salts or heavy metals that enter the plant through the roots from the soil. These can be very harmful to the plant in large quantities. Therefore it is necessary to remove excess solutes. The mechanism of solute excretion involves directing solutes by means of relative resistances in the vessels. In some plant leaves, including maize and eucalyptus leaves, the outermost vein consists of one very large vessel. A combination of low resistance due to its large size and rapid evaporation from the surface of the leaf causes solutes to be drawn there. There is no vein sheath (protective layer of cells) on this vessel, so solutes can easily be removed by excretion, dissolved out by rain, and pushed out by positive pressure that exists in the xylem at night time. (Atwell et al., 2001)

2.2.3.2 Domain Mapping

The fuel or oxidant gas can be considered analogous to the sap in the plant veins. Likewise, the water in the fuel cell channels can be considered analogous to the solutes in the plant veins. This relationship is illustrated in Figure 2.5 below. Since solutes can be removed from plant veins by directing them to the area where removal is easily accomplished, by analogy, water could be removed from fuel cell channels by directing it away from where it can do harm. Excess water, i.e., flooding, can do harm to a fuel cell because it can block the pathways for the oxidant to reach the catalyst, which hinders the reaction and decreases the power output.

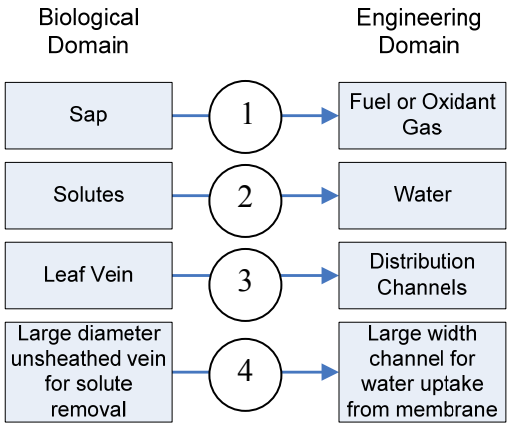

Figure 2.5 Biomimetic mapping – Solute excretion

In plants, the unprotected large diameter vein provides a large surface area where solutes can be removed from the vein. A similar concept can be used in the fuel cell; however, the phenomenon would take place in the opposite direction because to remove water it must be evaporated into the channels as opposed to out of the channels as is the case for plants. In a fuel cell, a wide channel can provide a large surface area for water to be evaporated into the channel from the membrane.

In addition, the larger channel diameter plant vein provides lower resistance to direct the sap, containing solutes, to this location where solutes can be removed. In a fuel cell, lower resistance due to larger width channels could direct oxidant gas to the locations of the fuel cell where water removal is desired.

On the cathode side of the fuel cell, two areas that could benefit from greater water removal rates are the inlet and the outlet. The inlet will be susceptible to flooding because of the high rate of water production. The outlet will also be at high risk of flooding because the oxidant gas will already have high water content and will be less able to remove any additional water. Incorporating wide channels near the inlet and outlet on the cathode side would help remove some of this excess water, allowing the fuel cell to operate more efficiently.

2.2.3.3 Limitations and Advantages

Increasing the width of the channels implies that the inter-channel contact area between the GDL and the bipolar plate will be decreased. This could have the effect of decreasing current collection. In addition, the membrane is fragile and needs to be supported. This contact area is important for structural support. A design using this solution would need to take this into consideration and ensure that there is sufficient support for the membrane.

An important advantage to this solution is that it does not require any additional energy input into the fuel cell.

2.3 TRIZ Concepts

This section describes two solutions to the fuel cell water removal problem that were found using TRIZ. For each solution, the contradictions and the principle used and how it is applied to the fuel cell are described.

2.3.1 TRIZ

TRIZ, the Russian acronym for "Theory of Inventive Problem Solving" has been shown to significantly increase the number of unique solutions compared to traditional methods such as brainstorming (Okudan, 2006). To develop TRIZ, Genrich Altshuller et al. (Altshuller, 1988) studied over 1.5 million patents to identify 39 engineering parameters as commonly improved attributes in innovative designs. Forty principles were generated based on methods used to solve engineering problems in these patents. Many tools are proposed for TRIZ, but the classical contradiction table remains as one of the more powerful tools (Ross, 2006).

To use the contradiction table, a given problem is expressed in terms of the 39 engineering parameters. Pairs of parameters, one of which is degraded in the process of improving the other, are used to identify principles that have been observed to overcome this contradiction. These principles are examined to generate ideas. The contradiction table, parameters, and descriptions of the principles used in this paper are from the text, *Product Design Techniques in Reverse Engineering and New Product Development* (Otto & Wood, 2001). Although examples for each principle are provided in the text, we did not use these examples as potential analogies, only the

description of the principles themselves. We did this to reduce the potential for design by analogy in TRIZ, as we intended to perform design by analogy using biomimetic design, and compare the two approaches.

2.3.2 Principle 19: Periodic Action

In a fuel cell, a high power output is desired. However, as the power increases, more water is produced by the cathode side reaction. This becomes a problem when the oxidant flow rate is not sufficient to carry it away, which causes flooding. When this occurs, the reaction cannot take place and the power decreases rapidly. Therefore there is a conflict between increasing the power and the amount of water that is produced through this increase.

This contradiction can be represented by the TRIZ Generic Engineering Parameters. When we improve power, Parameter 21, the result is an undesired quantity of substance created, Parameter 26. On the TRIZ relationship matrix, this contradiction leads to Principle 4: Asymmetry, Principle 34: Discarding and regenerating parts and Principle 19: Periodic action. A type of asymmetry was already used in the potential solution given in Section 4.2, asymmetry of channel diameter. As for Principle 34, the only part of the fuel cell that this would be applied to is the water, which we would like to evaporate after it is used to bring hydrogen ions across the membrane. Since this concept is the general goal for any of the potential design solutions, this principle will not be used on its own. For this solution, Principle 19 was used: The principle of periodic action.

2.3.2.1 Concept Generation

The principle of periodic action states: “Use periodic or pulsed actions, change periodicity.” (Otto and Wood, 2001 based on Altshuller, 1988). The “periodic action” in this description led to the idea of periodically reversing the flow of air to the cathode side of the fuel cell. Pulsing was also considered as a possible solution, such as a pulse of the current load. However, it is desired to have a smooth current so this type of pulsing would not be useful.

On the cathode side of the fuel cell, the further along the channel, the more water is contained in the oxidant. This decreases its ability to draw more water out and can cause an accumulation of water at the reaction site and subsequently flooding of the fuel cell near the outlet.

Periodically reversing the flow of air to the cathode side of the fuel cell, especially when a high power output is required, could help remedy this situation. When the air near the outlet becomes unable to carry more water, the flow direction of the air can be reversed, allowing the water to evaporate into the dry incoming air.

2.3.2.2 Limitations and Advantages

The hydrogen supply can either be left as is or reversed when the air is reversed. This would depend on whether concurrent or countercurrent flow is desired. In either case, the two gas pressures must be carefully controlled to ensure that they are equal. Equal pressure is required across the membrane because the membrane itself is fragile and could easily rupture if the pressure on one side is much higher than on the other.

The duration of the reversed flow can also be varied depending on the water removal requirement.

An added benefit to this solution is that it refreshes the concentration of fuel/oxidant in the fuel cell. This will ensure that the power will not decrease due to the depletion of reactants at the reaction sites.

This solution may cause fluctuation in the power output due to a brief stagnation of the fluid flow during the flow reversal. To ensure that the stack supplies a constant power, a hybrid system, including ultracapacitors or storage batteries, may be required. The ultracapacitors or batteries can be recharged by the fuel cell after the flow reversal.

A possible drawback of this solution is that additional energy is required to reverse the flow of the gas. This loss may be acceptable when weighed against the benefits of reduced flooding.

2.3.3 Principle 40: Using Composite Materials

Flooding on the cathode's reaction sites becomes more severe as current output increases. Water is present at the cathode by two modes; water is produced in the reaction, and water molecules are carried across the membrane from the anode by hydrogen ions. The effect of each of these modes is increased when there is an increase in the current output. Since producing more current and protons are desired, these can be considered the parameter to be improved, which can be represented by Parameter 26, quantity of substance. The deterioration of the performance due to

flooding, on the other hand, can be represented by Parameter 31, harmful side effect. This contradiction leads to the recommendation of Principles 3: Local quality, Principle 35: Changing the aggregate state of an object, Principle 39: Using an inert atmosphere, and Principle 40: Using composite materials. Since the fuel cell is already heterogeneous, the principle of local quality did not suggest new ideas. As for Principle 35, it can be applied to either water or the electrolyte. Water already changes between liquid to vapour states at various times. A change from solid electrolyte to liquid electrolyte is possible, but this will change the nature of the PEM fuel cell technology. Principle 39 did not lead to new ideas because the atmosphere of the fuel cell is already as inert as possible; the water itself contributes highly to corrosion of the fuel cell. In addition, measures are already taken to minimize this corrosion. Finally, a concept was formed from Principle 40.

2.3.3.1 Concept Generation

The resulting concept involves changing the GDL into a composite material. The concept was based on fibre reinforced material, where the fibres' function is to strengthen the material. Similarly, wicks may be applied to GDLs to increase their water removal rate. In this case, wicks are similar to the fibres where their placement and orientation are predetermined to maximize their effectiveness.

GDLs are usually made of carbon paper or cloth. They have randomized pores to allow oxygen to diffuse to the surface of the reaction sites and also provide a means for water to be removed by capillary effects and evaporation. Even though GDLs may have been coated with a hydrophobic substance to improve water removal, at higher current output the rate of water removal is insufficient. In order to enhance the cathode GDL's ability to draw water away from the reaction site, wicks can be placed strategically throughout the GDL (See Figure 2.6 below). The material and dimension of the wicks will be chosen to maximize capillary action and the absorption of water. The cathode GDL composite will draw water from the reaction site to the flow field channels in the bipolar plate. Then, water is evaporated to the air as it passes through the channels. Water evaporated at the channels will provide a more effective means of water removal than water evaporation at the reaction sites and relying on the diffused air to remove it.

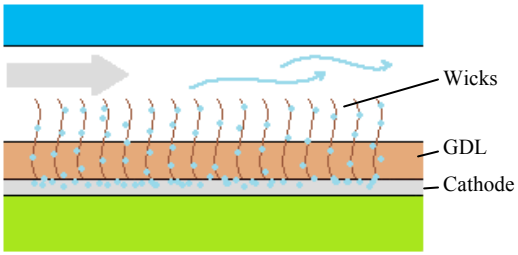

Figure 2.6 GDL with wicks

2.4 Comparison of Biomimetic Design and TRIZ

This section compares the two design methodologies used to find a solution to the water management problem. The two design methods are compared first in terms of the design processes, and then in terms of the specific solutions that were presented in this paper that were found by each of the methods.

2.4.1 Comparison of the Design Methods

Biomimetic design and TRIZ are compared in terms of the approaches to design used, the stimuli that inspired the designs and how preconceptions can affect the two methods.

2.4.1.1 Approaches to Design

There are variations to how biomimetic design was used in this study. Two different approaches were shown to be successful in finding a potential solution. In the mushroom case, the match that was found using the keyword search was sufficient to generate the mapping between the biological domain and the engineering domain. It is not always possible to generate concepts directly from the passages returned from the biomimetic search tool. Sometimes, it is possible to detect a trend in the phenomena found through the matches that leads to a strong analogy, but not an immediate solution. Recognizing these trends can lead to further research on the phenomenon. This was the case in the solute excretion concept. A trend was identified and further research into the plant distribution system was used to find the mapping that led to the solution presented.

While there are other variations to TRIZ, we chose to use only one of the design tools available. Both of the potential solutions found through TRIZ used only the contradiction tables.

2.4.1.2 Design Stimuli

With biomimetic design, the solutions came about as a result of mapping, i.e., identifying possible analogous items in the engineering domain that correspond to those existing in the biological domain. Biomimetic design began with the "solution" system where components that can be visualized, and those visualized components were transposed into the engineering system.

With TRIZ, because principles were given, there was less imagery to transfer to the solution. However, this, in fact, was not the case for the composite solution. The visualization of the reinforcing fibres in a composite material was transferred to the solution.

The mapping in biomimetic design tended to be more structured and specific to the part of the fuel cell that was being considered. That is, a given biological phenomenon could not be mapped to different parts of the fuel cell to provide different solutions. TRIZ, on the other hand, has very general principles that can be applied to many different parts of the fuel cell. For example, the periodic action could be applied to the reactant gas flow rate or pressure, the coolant flow rate or pressure or the current draw from the fuel cell.

2.4.1.3 Risk of Preconceptions and Biases

In biomimetic design, preconceptions and biases can play a major role in the process of selecting biological analogies. For example, with the solute-excretion inspired design, it was obvious that there was a similarity in function between the plant sap distribution system and the fuel cell reactant distribution system. It was this observation that motivated further research into plants. In this case, a useful analogy was found, and so the initial bias was helpful. However it is quite possible that this type of bias can also work against the designer. Having a preconceived idea about whether or not a specific biological phenomenon is useful could conceivably lead to the premature dismissal of potentially useful phenomena. When sorting through the biological matches it is easy to reject certain phenomena because they do not obviously lead to design solutions, particularly when there are a great number of matches. Therefore, there is a chance that perhaps looking more deeply into the mechanism would, in fact, return a useful analogy. When one is somewhat familiar with particular biological phenomena, it is easy to have a bias

for or against this or other phenomena. Therefore, the designer must take care to not be overly influenced by such biases. We found this type of bias to be less likely when using TRIZ, as we found the design principles are very abstract and allow the designer to think creatively without being influenced as much by preconceived ideas.

2.4.2 Comparison of the Generated Concepts

The biomimetic technique led to concepts that were 'passive'. That is, both of the biomimetic designs that were presented here allow improvements to the fuel cell without requiring any additional energy input, aside from the initial energy required to create the new design. Biological systems are generally optimized to function with as little energy input as possible. Therefore, it is intuitive that these types of solutions would arise from biomimetic design.

TRIZ also led to a passive solution, but it led to an active solution as well. The periodic flow reversal design requires additional energy input to reverse the flow as well as to control the periodic reversals.

2.4.2.1 Observed Overlap of Biomimetic Design and TRIZ

The plant analogy contained additional information about solute excretion that was not used in the proposed solution. That is, at the location of the large vessel there is no protective layer of cells, allowing solutes to be easily removed by excretion, dissolved out by rain, or pushed out by positive pressure at night. Each of these attributes is actually relevant to one of the other solutions presented in this paper. Lacking a protective layer of cells and allowing removal by excretion is analogous to the "unprotected" porous plate in Section 2.2.2 that allows water to "excrete" through the pores of the bipolar plate. Also, forced convection along a positive pressure gradient is suggested in Section 2.3.2, where forced flow reversal is used to remove water. These observations were made after all the concepts were developed independently, so the other concepts were not influenced by this particular biological analogy.

TRIZ also identified principles that could have been used to generate some of the other proposed solutions. For example, in Section 2.3.2 where the principle of periodic action was used to find a solution, Principle 4, asymmetry could also have been used. Asymmetry can be considered the principle used in Section 2.2.3. In that section, it was proposed that the diameter of the fuel cell distribution channels be made larger in certain sections to facilitate water removal. Also, in that

section, different bipolar plates were proposed for anode and cathode, in order to provide hydration to the membrane from the anode side and not on the cathode side. Both concepts involve asymmetry in the fuel cell design.

2.5 What Became of the Concepts

The four previous concepts were developed by the authors of the paper as a group and are considered starting points for individual research. The solute excretion in plants analogy led to further research into flow field design. The remainder of this thesis will focus in flow field design.

3 Biomimetic Flow Field Design

The main focus of this thesis is flow field design for the purpose of achieving an even current density across the surface of the electrodes. This section starts by giving a description of the problem that has been addressed. This includes an overview of flow fields that are currently being used and investigated. Next is a description of the concepts that have been identified using Biomimetic design techniques.

3.1 Problem Definition

In a fuel cell, there are situations which cause the current density to be uneven. One of those is an uneven flow distribution. The flow field must be able to distribute the gasses evenly such that there are no great gradients in fluid velocity or pressure. The velocity is related to how quickly reactants can be replenished as well as the gas stream's ability to remove water from the GDL. When the pressure is very high in one location and low in another, there will be a difference in the rate at which the reactants will be able to travel into the GDL and catalyst surface. This will cause a difference in the reaction rate and a difference in the current density.

Insufficient water management can also cause uneven current density distribution. Water management involves providing enough water to the membrane such that it is able to conduct protons effectively and removing water from the cathode to ensure a clear path to the reaction sites for the reactants. As a membrane dries, its ability to conduct protons is reduced, which means that the rate of electrochemical reaction occurring on the cathode side is reduced, thus decreasing the current density. Likewise if there is a local excess of water and the reactants are not able to get to the reaction sites, there will also be a local decrease in the current density.

An even current density distribution is desired in a fuel cell for many reasons. First of all, local "cold spots", i.e. sites where the rates of reaction and associated heat release are lower than average, decrease the performance of the cell. Similarly, a "hot spot" is a site where the rates of reaction and associated heat release are higher than average. An uneven current density causes low fuel utilization, low power density and an inefficient usage of the platinum catalyst. But

most importantly, uneven current density, especially local “hot spots” can significantly decrease the lifetime of the cell (Hwnag et al., 2008).

Many of the problems that lead to uneven current density can be solved with proper bipolar plate flow field design. Following is an overview of some different flow fields that have been found in the literature.

3.1.1 Flow Field Design

Many different types of bipolar plate flow field designs have been proposed and investigated in the literature. This review identifies the various types that have been studied, and discusses the effects of design on fuel cell performance.

The most common types of flow patterns are parallel, serpentine, pin or grid type, and interdigitated (See Figure 3.1 below). Other types have been made by combining some of the features of two or more of the common types, as well as by using completely different concepts.

Some studies have investigated the differences in performance between different types of flow patterns, while others have focused on the effects of varying the dimensions or attributes of one particular type.

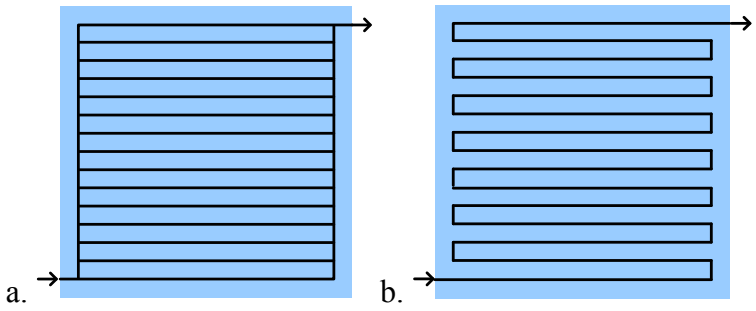

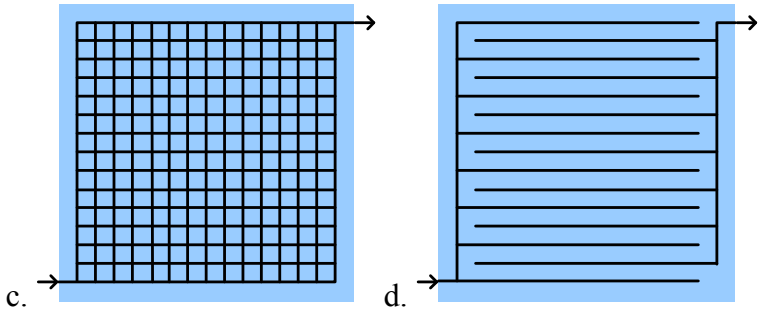

Figure 3.1 Common flow pattern designs. a. Parallel, b. Serpentine, c. Pin or grid type, d. Interdigitated

3.1.1.1 Parallel flow field

Parallel flow patterns are usually characterized by having a low pressure drop and reasonably uniform current distribution. Low pressure drop is desired for a fuel cell because it minimizes parasitic losses from external equipment. It can achieve an even current density distribution because the channel lengths are relatively short, so the reactant concentration is higher at the outlet than would be for a long serpentine channel. It is also common for parallel flow fields to suffer from flooding because of low water removal. Water removal is low because if a channel is blocked, the gas stream will simply take the path of least resistance, therefore there will not be sufficient pressure behind the blocked channel to force the water out.

3.1.1.2 Serpentine flow field

Serpentine flow fields tend to have high water removal but high pressure drop. High water removal is achieved because there is only one path of the reactant gas to flow so pressure forces out any water blocking the channels. However it has been found that water tends to build up in the bends of the serpentine patters, causing local reductions in current density (Hwnag et al. 2008; Turhan et al., 2008). Pressure drop is high because of the long channel. When there is a high pressure drop, a higher pressure is needed to feed the reactants, increasing in turn the fan or compressor power required, which causes higher parasitic losses. Also a high pressure drop causes uneven diffusion into the GDL (Kloess et al., 2009). A pressure difference between channels, however, is useful to drive flow between channels under the lands, causing convective mass transfer in the GDL.

One way to combat the high pressure drop is to have shorter, parallel serpentine flow designs. This combines the water removal abilities of the serpentine design with the low pressure drop of the parallel design.

Jeon et al. (2008) developed a computer simulation to investigate the effect of different configurations of serpentine flow fields. They looked at four different types: single channel, double channel, cyclic single which consisted of multiple short serpentine channels with the outlet to one adjacent to an inlet to the next, and symmetric single which also consisted of multiple short channels that in this case have the outlet to one adjacent to the outlet to the next. They looked at high humidity and low humidity operation. At high humidity the double channel gave the most even current density distribution. At low humidity, they all gave similar performance, however, the cyclic and symmetric had the lowest pressure drop which makes them a better choice.

Kim and Hong (2007) performed experiments on a single cell with different serpentine flow fields. They investigated the effect of channel length and width. The channels with the smaller width had a larger rib contact area. They found that the longer channels gave better performance because they had a higher pressure drop which helps remove water. However, the contact area had a greater effect on performance. Greater contact area gave better performance because it decreases contact resistance.

3.1.1.3 Interdigitated flow field

In interdgitated flow field designs, the inlet is not directly connected to the outlet. The reactant gases must pass through the GDL under the channel landings. This causes an increase in the mass flow close to the catalyst, which improves the reaction rate and thud the current flow. However, forcing the gas flow through the GDL requires a high pressure. Thus, interdigitated flow fields have better mass transfer but very high pressure drop.

Wang et al. (2008) investigated the effect of channel aspect ratio (ratio of height to width) and cross sectional area for parallel and interdgitated flow patterns. A 3D computational model was used. The anode flow channels were kept constant while only the cathode channels were varied. All of the channel changes had very little effect at voltages higher than 0.7 V. Aspect ratio had little effect on interdigitated flow fields, but for parallel flow fields, a shallower channel is best

because there are larger inlet velocities (for the same flow rate) that increase water removal. Their simulations showed that for parallel flow fields, a smaller cross sectional area is better and for interdigitated flow fields, a cross section of 1 mm x 1 mm is best, with a smaller and larger cross section giving worse performance. In all cases the interdigitated flow field gives better performance than the parallel flow field.

3.1.1.4 Pin-type flow field

A pin-type flow field consists of a uniform array of square or circular pins. Flow fields of this type have low pressure drop, but since the reactant gasses can take the path of least resistance they are prone to channelling (bypassing areas of liquid water accumulation instead of forcing the water out), areas of stagnation, and recirculation zones. Thus pin-type flow fields tend to have uneven current density distribution and low water removal.

3.1.1.5 Tapered or constricted channel flow field

Weng et al. (2008) developed a flow field design that uses contracted channels. The depth of the channel is decreased near the outlet to increase the pressure of the exiting gas so that the transport of reactants into the GDL will be greater. The purpose of this is to combat the pressure and reactant losses that occur as a result of the length of the channel and the reaction rate. They tested this design using a 3D numerical simulation of a straight channel, including anode gas channel, GDL and catalyst layer, membrane, and cathode catalyst layer, GDL and gas channel. They found a significant improvement in performance when operating at voltages lower than 0.7 V. However the constricted channel design did increase pressure drop compared to a straight channel with no constriction.

Similar to the contracted channels, Liu et al. (2006) developed a tapered channel flow field design. The channel height is decreased in a gradient towards the outlet. Again, a numerical simulation was used to evaluate the effectiveness of this design. They also found that the tapered channels improved the performance of the fuel cell at low operating voltages, which is the high power operating region of the fuel cell. For low power operation (high voltages) performance remained the same. The same group investigated the effectiveness of channels tapered both in height and in width (Yan et al., 2006). Again, performance of the new designs was determined by numerical simulation. As with tapered channel height, when the channel was tapered in

height to decrease towards the outlet, there was better fuel utilization and performance. However, when looking at the width of the channel, an increase towards the outlet gave better performance. This happened because there was more contact area between the channel and the GDL.

3.1.1.6 Serpentine interdigitated flow field

Debe and Herdtle (2006) developed a flow pattern that combines the concepts of interdigitated and serpentine flow fields, and uses a zig-zag serpentine channel design to achieve uniform flow over the membrane. In this design, the land width varies, so the distance that the gas has to travel under the land through the GDL also varies causing a difference in flow resistances along the channel. The angle of the land was also varied from large near the inlet to small near the outlet. They also decreased the depth of the channel from inlet to outlet. Computer simulations of the flow showed that these modifications improved the uniformity of the velocity in the GDL. Uniformity in velocity was assumed to correlate to uniform current density in the cell.

A flow field design that combines serpentine and interdigitated design concepts was developed by Wang et al (2007). It uses a traditional triple-serpentine flow field but includes blockages, or baffles, that change the pressure distribution and increase convection of the reactant gasses under the land as in an interdgitated flow field. This new design resulted in greater performance at low voltages (high power), and similar performance at high voltages (low power) compared to a standard triple-serpentine flow field. They also found that the compressor power needed for the increased pressure drop of the baffled cells is not significant compared to the power output of the cell.

3.1.1.7 Biomimetic

Morgan fuel cells (US patent 7,067,213) developed a biomimetic flow field design modeled after a leaf. This design includes branching and tapered channels that lead to very small capillaries. This design gives a smaller pressure drop than a standard serpentine flow field and can achieve an even current density distribution (Li and Sabir, 2005).

Kloess et al. (2009) combined the concepts of serpentine and interdigitated with biomimetic design to create an interdigitated leaf and lung flow field design. Each of the biomimetic designs gave a lower pressure drop and higher power density than the standard serpentine or

interdigitated flow field. CFD was used to show pressure distribution and pressure drop. The GDL was made more permeable and thicker than normal so that they could visualize flow better. Thus their results are not representative. They also conducted physical experiments to show the performance of the cells in terms of power output.

3.1.1.8 Experimental measurement of fuel cell performance

Hwnag et al. (2008) used an array of current collectors on the cathode side, a total of 16 sensors for a 25 cm^2 cell, to map the current distribution for different flow pattern designs. Serpentine, parallel, interdigitated and biomimetic interdigitated flow fields were investigated. As voltage was increased, the current was found to become more even across the flow field. It was found that the serpentine flow field has the most even current distribution among those tested.

Barreras et al. (2008) used laser-induced fluorescence to characterize the flow in parallel diagonal, serpentine and branching cascade flow fields. They also used a numerical simulation to evaluate flow characteristics. They found that the parallel diagonal flow field gave an uneven flow distribution with the majority of the flow going through the middle channels. The serpentine flow field had a very large pressure drop, which is characteristic of a serpentine flow field. The cascade design had the best performance; it had more even pressure and flow distributions than the other two designs.

Neutron imaging was used by Turhan et al (2008) to compare liquid water accumulation in different flow field designs. They used multi-channel serpentine flow field designs and varied the land and channel dimensions and investigated the effects of land to channel ratio, land size and channel size. They found that water tends to accumulate under the landings, and it is best to have land to channel ratios lower than 2:3. Water accumulation is dependent on the number of channel wall GDL interfaces. There is more accumulation of water when there are more interfaces, as in the corners of a serpentine flow field. Fewer corners mean that less liquid water will accumulate.

Hsieh and Huang (2008) performed in-situ measurements of current density for four different flow patterns: mesh (pin-type), serpentine, parallel and interdigitated. The 5 cm^2 cell was divided into four segments, with current lead wires to measure the current density for each segment. Water accumulation was measured visually by taking photographs of the anode and

cathode. They found that the interdigitated flow field gave the most even and highest current density compared to the others. All of the flow fields reached a near steady-state condition after about 30 min of operation, but after about 3 hours, the current density decreased due to flooding. Liquid water could not be seen until after 5 min of operation.

Using this knowledge of existing flow field design and the techniques of biomimetic design, several relevant biological phenomena are identified and expanded to concepts for low field designs.

3.2 Bipolar Plate Flow Field Concepts

This section describes the biomimetic design process and the concepts that were identified.

3.2.1 Keyword Generation

The important function for achieving an even current density is to distribute the reactant gasses. Distribute was one of the keywords that was expanded for the water management problem, described in section 2.2.1, so the expanded keywords identified there will be used again in this section.

3.2.2 Solute Excretion in Plants

This first concept is one of the preliminary biomimetic design concepts that were identified to solve the water management problem. Many keywords, for example, ‘distribute’, ‘transport’ and ‘conduct’ returned biological phenomena related to the transport of sap and solutes through plants. While this did not return an immediate solution, further research into the mechanisms of this transport returned the biological phenomena of solute excretion in plants.

Solutes such as salts or heavy metals can build up in plants and cause them harm. Some plants, like maize and eucalyptus, have a mechanism to remove these solutes which involves directing the solutes by relative resistances to an area where they can be removed. In the leaves of these plants, the outermost vein is a large unprotected vessel. Low resistance due to its size and rapid evaporation from its surface causes sap containing solutes to be drawn there. Since it is unprotected, the solutes can be easily removed (Atwell et al., 2001).

The fuel or oxidant gas can be considered analogous to the sap in the plant veins. Likewise, the liquid water in the fuel cell channels can be considered analogous to the solutes in the plant veins. Since solutes can be removed from plant veins by directing them to the area where removal is easily accomplished, by analogy, liquid water could be removed from fuel cell channels by directing it away from where it can do harm.

In plants, the unprotected large diameter vein provides a large surface area where solutes can be removed from the vein. In a fuel cell, a wide channel can provide a large surface area for water to be evaporated into the channel from the membrane.

In addition, the larger channel diameter plant vein provides lower resistance to direct the sap, containing solutes, to this location where solutes can be removed. In a fuel cell, lower resistance due to larger width channels could direct oxidant gas to the locations of the fuel cell where liquid water removal is desired.

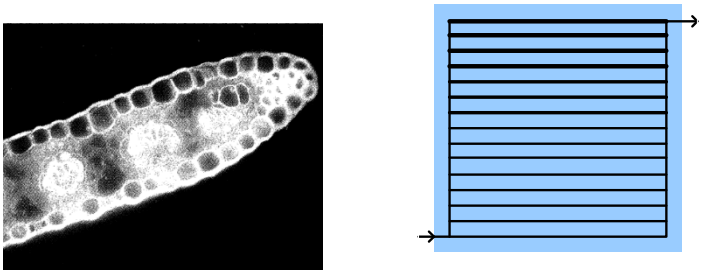

Figure 3.2 Plant leaf cross section showing large outer vein and conceptual sketch of how this can be applied to flow field design

3.2.3 Cell Connections in Plants

This concept comes from the keyword ‘channel’, however it is not used in the traditional biomimetic method, because in the biological phenomenon identified, this keyword is used as a noun. Traditionally, only verbs should be used in this technique. The biological phenomenon was cell connections in plants. In plants, cells are connected laterally as well as axially to provide greater distribution of sap throughout the plant.

In a fuel cell flow field design this concept can be used to help mix the gasses between channels such that internal gradients are minimized.

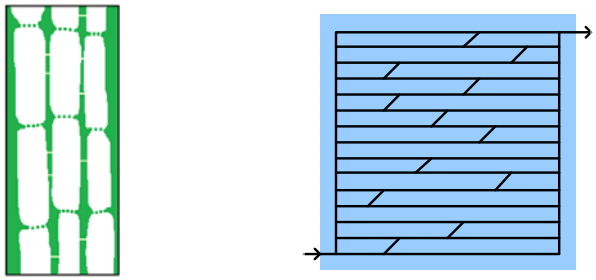

Figure 3.3 Lateral connections in plant cells and a conceptual sketch of how this can be applied to flow field design

3.2.4 Lymph System

The keywords ‘disperse’ and ‘conduct’ lead to the biological phenomena of the human lymph system. In the human body, lymph is distributed throughout the body through lymph ducts. The lymph circulates through the body and through lymph nodes. Lymph nodes supply white blood cells with antigens so that they can fight pathogens in the body. They act as sources of white blood cells which can then be transported to the body where they are needed.

In a fuel cell flow field design lymph nodes can be considered analogous to pure sources of fuel or oxidant. A flow field can be designed such that there are multiple inlets and more sources of pure gas to ensure high current density. When there is only one inlet, the reactants can become depleted towards the end of the channel. In this concept, more sources of pure gas can keep the concentration high over a greater area of the cell.

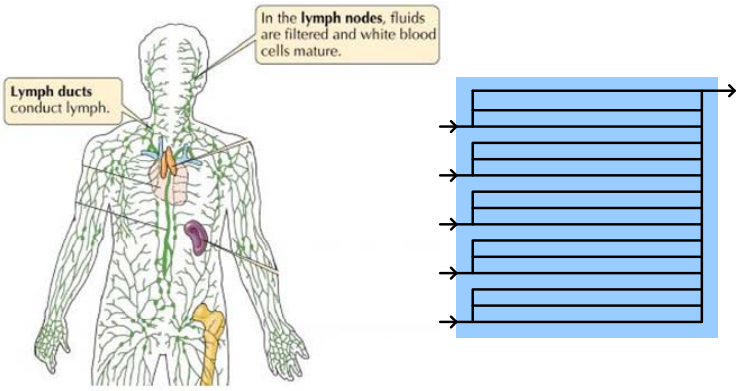

Figure 3.4 Diagram of human lymph system and a conceptual sketch of how this can be applied to flow field design

3.2.5 Murray's Law of Branching

A final concept that comes from further research into plant transport systems as well as animal blood transport systems is Murray's law of branching.

Murray's Law states that in branching vessels, the cube of the radius of the parent vessel is equal to the sum of the cubes of the radii of the daughters. This law is also obeyed for blood vessels. In plants it only applies to vessels that do not function as support. In obeying this law, the hydraulic conductance of the vessels is maximized (resistance is minimized). This relation can also be derived mathematically assuming that the metabolic power requirement must be minimized (Sherman, 1981). However, this metabolic power term can also be considered to represent pumping power to supply fuel and oxidant gasses in a fuel cell.

In a fuel cell this relation could be applied to almost any flow pattern, from a standard parallel flow field to a leaf-inspired flow field. It could help to minimize the work needed to supply the fuel and oxidant gasses, reducing parasitic losses.

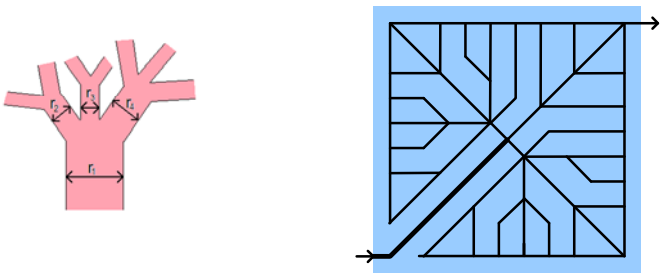

Figure 3.5 An illustration of Murray's law in a blood vessel and a conceptual sketch of how this can be applied to flow field design

3.3 Bipolar plate flow field designs

The above concepts led to seven different designs. All flow fields have an active area of 25 cm, and are 5 cm by 5 cm. Two designs were developed using the first concept of using large channels as a means of water removal. The first one, seen in Figure 3.6 below usues larger channels near the outlet since there would tend to be more water near the outlet. We would generally expect more water near the outlet due to generation by electrochemical reaction along the channel accumulating. The large channels at the end will provide more surface area for water removal. In addition, the larger channel area will provide more surface area for reaction, which may help increase the electrochemical reaction rate in this area which would contain a lower ccentration of reactant, causig the electrochemical reaction rate over the entire cell area to be more uniform. This design is a parallel type, and includes nine channels 1 mm in width, seven channels 1.5 mm in width and five channels 2 mm in width closest to the exit of the flow field. The side channels are 2 mm wide.

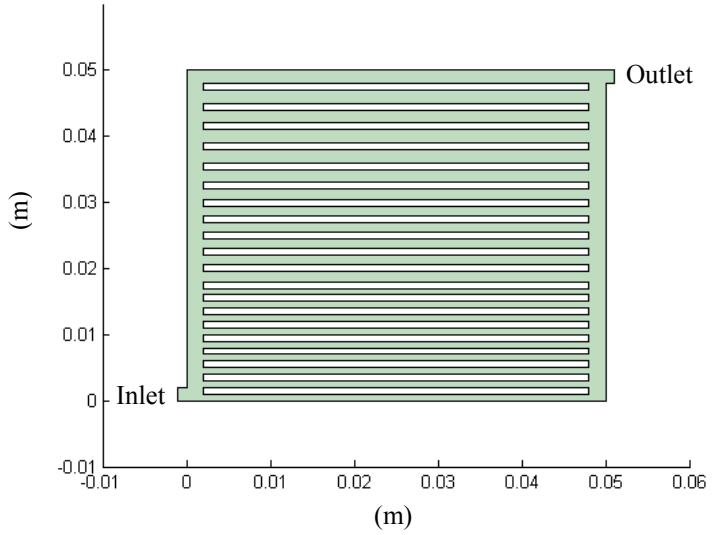

Figure 3.6 Parallel flow field with large channels near the outlet

The second design that came from this concept uses the same premise that more water removal is needed near the outlet. In this case the side channel on the inlet side is increased towards the inlet and on the outlet side is increased towards the outlet. It increases from 1 mm at the narrow end to 2 mm at the wide end. All parallel channels are 1 mm wide.

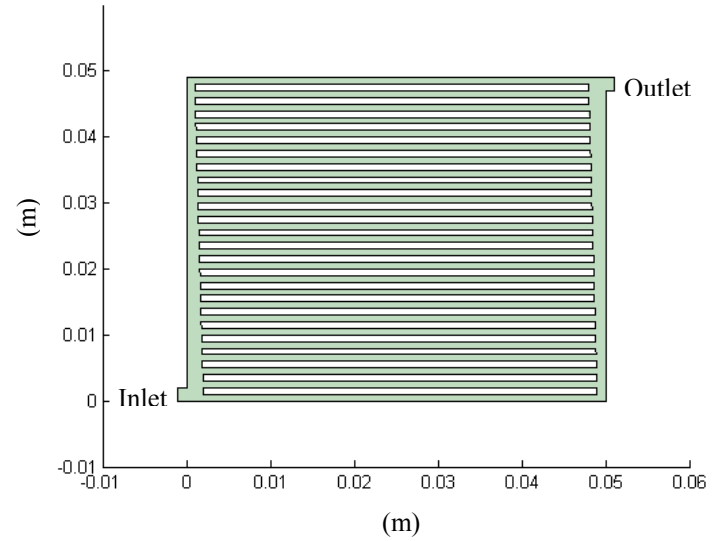

Figure 3.7 Parallel flow field with decreasing/increasing side channels

The next design comes from the concept of connections between parallel channels. This design starts with a standard parallel flow pattern with 1 mm channels and a 2 mm inlet and outlet.

Connections were made between adjacent channels measuring 1 mm wide and at an angle 45 degrees to the parallel channels. The connections are placed in three different locations along the parallel channels. The pattern repeats itself every three channels. The position and number of channels was chosen to maximize the connections while avoiding too many connections, which would in the limiting case approach a pin-type flow field.

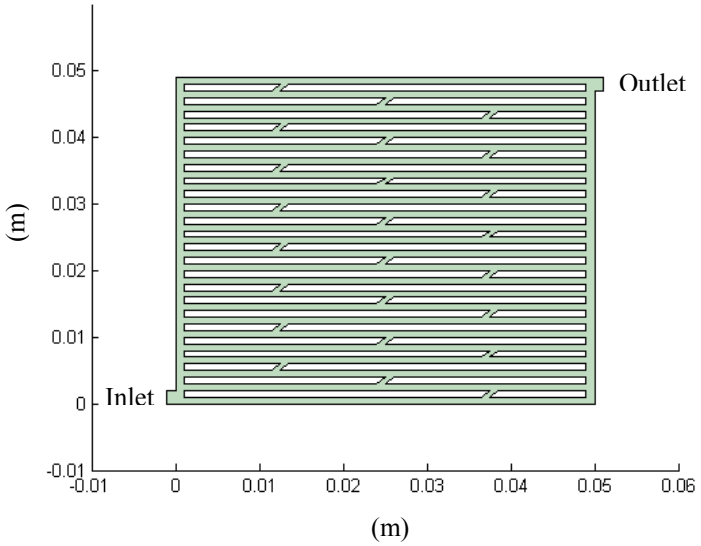

Figure 3.8 Parallel flow field with connections

The third design came from the concept of multiple inlets. In this case there are five 1 mm inlets that each branch to five parallel channels. All the parallel channels are connected at the outlet side channel which is 3 mm wide.

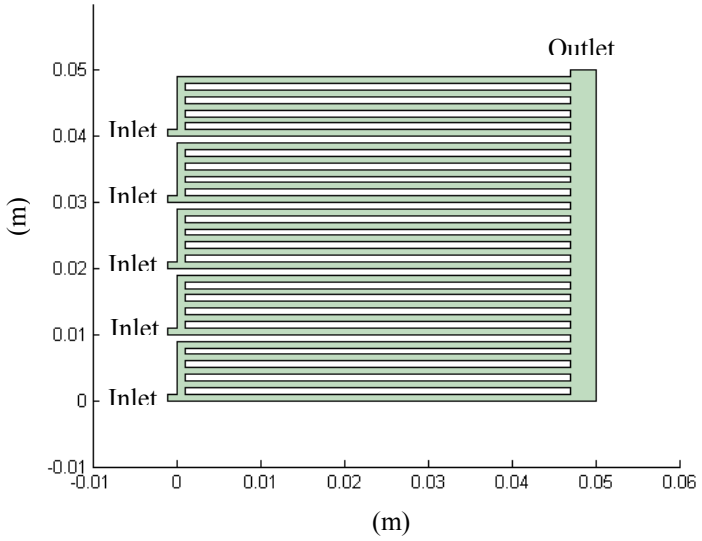

Figure 3.9 Parallel flow field with multiple inlets

The fourth concept is branching in plants and animals using Murray's law of branching. The first design, shown in Figure 3-10, uses a pattern that starts at the inlet as a main branch. The inlet is 2 mm wide and branches into three daughter branches. The middle branch is twice the width of the two side branches, and each of their widths is calculated by Murray's law. The middle branch is the next parent branch and is divided as before. This procedure is done from the outlet as well and meets in the middle.

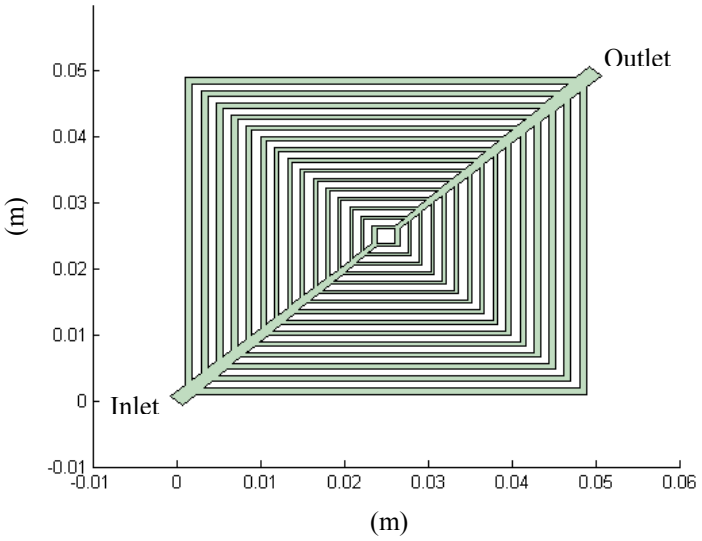

Figure 3.10 Murray's law 1 flow field design

A second Murray's law design was created using a similar branching pattern. In this design, shown in Figure 3.11, the side branches connect straight to a side channel that increases in width as more branches are attached according to Murray's law. The inlet channel is 4 mm. It is larger in this design because the small branches near the outlet would be much too small if the inlet was only 2 mm.

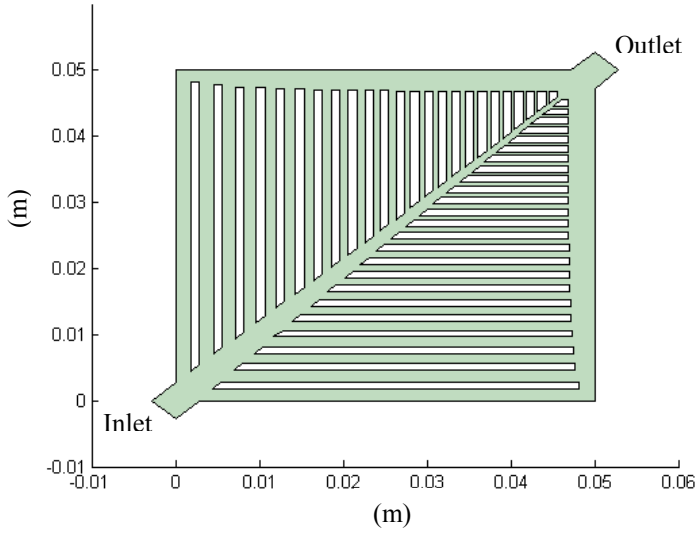

Figure 3.11 Murray's law 2 flow field design

The final design that was based on the Murray's law (Murray's law 3) takes the standard parallel design and applies Murray's law of branching. As shown in Figure 3.12, the inlet is first branched into two channels, with the channel on the left (the side channel) twice the size as the channel on the right (the parallel channel). The left channel is then the new parent branch and is divided in the same way.

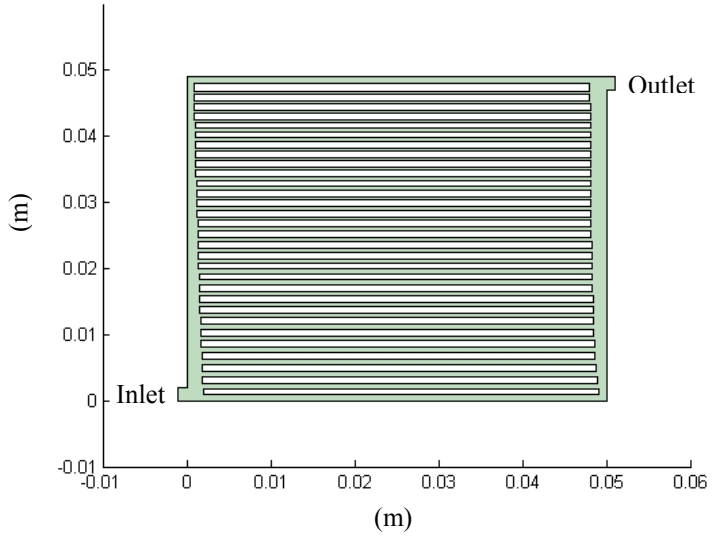

Figure 3.12 Murray's law 3 flow field design

3.4 Concept Validation

To validate these concepts and determine the best design, the goal is to show that the designs produce an even current density over the surface of the electrodes. In order to do this a numerical model was developed. This model represents an entire fuel cell with as much detail as was feasible and necessary to evaluate the designs accurately. A 3D model is called for since it will be necessary to show the changes along the channel from the flow and into the membrane electrode assembly (MEA) and how this changes with different flow patterns. The next section describes this model and the process that was used to develop it.

4 Numerical Model Concept Validation

A numerical model was used to validate the flow field design concepts that were identified using biomimetic design. The numerical model started as a one dimensional model of a membrane electrode assembly (MEA), which consists of two gas diffusion layers (GDL), two catalyst layers and a membrane. Next the model was extended into two dimensions. The two dimensional model included the flow channels as well as the MEA. Finally, the two dimensional model was extended into three dimensions. This chapter starts by giving an overview of fuel cell models and then describes the models that were used for concept validation.

4.1 Overview of Fuel Cell Models

Many fuel cell models have been presented in the literature. An adequate model must account for a number of processes, including transport to the membrane, transport through the membrane, and the electrochemical reactions. In addition to these processes, it is also useful to account for the presence of liquid water, though this is not always considered.

These different processes can be represented in 1D, 2D or 3D. Many 1D models represent the variables as a function of the length of flow channel in the bipolar plate. In this case it is assumed that there are uniform gradients in the membrane, GDL and/or flow channel. Examples of models of this type are those by Van Nguyen and White (1993) and Hung et al. (2007).

Amphlett et al. (1995) created a type of 1D model that is based on a Ballard fuel cell. It is a parametric model to describe the fuel cell performance, where regression is used to fit some of the parameters. The model returns cell voltage when given operating and inlet conditions.

Some 2D models assume that the membrane can be represented in 1D since the aspect ratio is low. In the case of Fuller and Newman (1993), the fluid composition in the channel is assumed uniform in the direction straight above the membrane so the fuel cell model is a combination of two 1D models. Yi and Van Nguyen, (1998) also make a 2D model using the same techniques.

Some true 2D models were done by Van Bussel et al. (1998) and Siegel et al. (2004). These account for gradients in the membrane and in the channels.

The 3D models include those by Sinha et al. (2007), Lin et al. (2004), and Ye and Van Nguyen (2007).

4.1.1 Transport to the Membrane

Transport to the membrane can involve simple diffusion through the GDL, porous medium flow through the GDL or transport through gas channels to the GDL followed by either or both of the previous. Diffusion is usually represented by the Stefan-Maxwell equation for multi-component flow, and there are many simplifications to this equation that have been used. (e.g. Fuller and Newman, 1993; Van Bussel et al., 1998 (binary); Siegel et al., 2004). Sometimes, as in the case of Sinha et al. (2007), diffusion is assumed to be constant in the gas channels and GDL, and is expressed by binary diffusion coefficients. In the model by Sigel et al. the species equations include movement by advection (by bulk flow).

Many models use Darcy's law of flow through a porous medium to represent the transport of gasses through the GDL (e.g. Sinha et al., 2007; Siegel et al., 2004; Akbari and Rismanchi, 2008). These models use an extra term in the momentum equation to account for the extra drag term due to flow through the porous medium.

4.1.2 Modeling the Membrane

When making a model of a PEM fuel cell one of the most important aspects is modeling the membrane. Any complete model must describe and account for the transport of both water and ions through the membrane. Researchers have used many different approaches to represent these transport processes in polymer membranes.

Water content is very important to the transport of ions and water through the membrane. The water content of a membrane is characterized by the number of water molecules per sulfonic acid group in the membrane. Springer et al. (1991) originally developed a third order polynomial equation for the water content of the membrane in terms of the activity of the water vapour outside the membrane based on experiments. In addition they also developed an equation for the electro-osmotic drag coefficient in terms of this water content. The electro-osmotic drag (eod) coefficient is the number of water molecules that are dragged through the membrane for each

hydrogen ion. These two equations are widely used in fuel cell models. (e.g. Yi and Van Nguyen, 1998; Van Nguyen and White 1993; Siegel et al., 2004) Water diffusivity and ionic conductivity are also dependant on water content of the membrane. Another group (Hinatsu et al., 1994), performed their own measurements of water content, and found a relation that is very similar to that found by Springer et al. (1991). Van Bussel et al. (1998) used this measurement for their model. Some models use a simplified linear equation for water content (i.e. Yi and Van Nguyen, 1998; Van Nguyen and White 1993) or assume that the membrane is fully humidified and use a constant value for the water content (e.g. Akbari and Rismanchi, 2008; Bernardi and Verbrugge, 1991). This number for a fully humidified membrane is usually taken to be 22 water molecules per sulfonic acid group, which is based on the measurements done by Springer et al. (1991). It represents a fully humidified membrane in the presence of liquid water at 80°C.

Some models represent the transport of ions as a function of the ionic potential gradient, and the transport of water as a function of the concentration gradient and the ionic potential gradient (e.g. Van Bussel et al., 1998; Siegel et al., 2004). However, Van Bussel et al. (1998) describe the transport of water through the membrane using two separate equations for diffusion and electro-osmotic drag. Some models also include a term in the water transport equation for convection (e.g. Yi and Van Nguyen, 1998; Hung et al., 2007). Sinha et al. (2007) do not account for transport of water by ionic potential through the membrane, but as a source term at the catalyst layer.

Yi and Van Nguyen, (1998), Van Nguyen and White (1993) have an expression to describe the amount of water that is transferred through the membrane per proton. The expression is a function of the eod, diffusion and pressure driven convection, based on properties at the of the anode and cathode surfaces. This number is used in the water flow channel equations.

Another method of modeling the membrane was used by Bernardi and Verbrugge (1991, 1992). This method focuses on ionic transport, which is modeled using the Nernst-Planck equation. The Nernst-Planck equation is used to describe the transport of ionic species and is written in terms of the charge-based ionic potential and the concentration of the ionic species. Water transport through the membrane is based on the velocity form of the Schlogl equation, which relates the pore velocity of the water in the membrane to the ionic potential gradient and the pressure gradient. In this case water is assumed not to diffuse by concentration gradient.

Fuller and Newman (1993) used concentrated solution theory to describe transport in the membrane, where the driving force for transport is described by frictional forces and velocities and used in the form of the Stefan-Maxwell equation. The gradient of electrochemical potential is described in terms of gradient of electrical potential and gradient of mole fraction of the ionic species.

4.1.3 Electrochemical Reactions

The electrochemical reactions are always described by some form of the Butler-Volmer equation (e.g. Bernardi and Verbrugge, 1992; Bernardi and Verbrugge, 1991; Akbari and Rismanchi, 2008; Siegel et al.,2004). The Butler-Volmer equation describes the reaction rate of the electrochemical reaction. Activation overpotential in the Butler-Volmer equation is related to the difference between the electrical potential in the solid catalyst particles and in the membrane. Butler-Volmer is also dependant on the concentration of the gaseous reactants, which decreases in the channel direction by the reaction rate.

Many modellers choose to model only the cathode side of the fuel cell, as a means of simplifying the computations (e.g. He et al, 2000; Lin et al., 2004). This is usually a valid assumption since the cathode reaction is slower than the anode reaction.

Akbari and Rismanchi (2008) include contact resistance in their model. The contact resistance exists between the GDL and the bipolar plate which is used to collect the electrical current.

4.1.4 Liquid Water

Accounting for the effect of liquid water in the model is not a straightforward task. Various methods have been used to do this. Many models assume that liquid water exists only on the surface of the electrode where it is formed and immediately evaporates into the pores of the GDL where it can diffuse out (e.g. Fuller and Newman, 1993; Yi and Van Nguyen, 1998; Van Nguyen and White 1993). This is the simplest way to model water in the system, but it can be an oversimplification and lead to an underestimation of mass transfer limitations. Flooding of the GDL and gas channels with liquid water causes an added resistance to mass transfer for the gaseous fuel and oxidant species which decreases the performance of the cell.

The model by Fuller and Newman (1993) does not account for the limitations caused by liquid water, and as a result overestimates the cell current density. The limiting current density was 5 A/cm^2, which is much higher than the value around 1.2 A/cm^2 that most experimental results give (Siegel et al, 2004; Akbari and Rismanchi, 2008).

Some models (e.g. Sinha et al., 2007; Yi and Van Nguyen, 1998; Van Nguyen and White 1993) account for liquid water by quantifying the amount present, but do not account for the resulting effects. As above, this will cause an underestimation of the mass transfer limitations.

Baschuk and Li (2000) created a model to represent the effects of flooding. They allow liquid water to be present by setting the amount of flooding. This model is based on the parametric model by Marr and Li (1999). It is set up as a series of resistances, and diffusion resistances are modified to account for the presence of water. Hung et al. (2007) also set the amount of flooding to account for liquid water. They use a diffusion layer thickness to account for resistance due to the presence of liquid water.

Siegel et al. (2004) account for the effect of liquid water by introducing a correction factor into the Butler-Volmer equation and in the diffusion coefficients. They assume that the water is created by the electrochemical reaction, and through condensation from the vapour water. The Butler-Volmer equation is modified by an effectiveness factor that accounts for the structure of the catalyst layer. They assume diffusion through a spherical shell to represent mass transfer resistance through a layer of liquid water that forms on the surface of the catalyst and use the Thiele modulus to calculate the effectiveness of the reaction at the surface. The Thiele modulus describes the effect of reaction rate constant and diffusion coefficient on the concentration profile in the liquid water layer. The diffusion coefficients also include a correction factor using the fraction of liquid water present to account for the catalyst sites being blocked by liquid water.

Lin et al. (2004) use a similar method to Siegel et al. (2004), but their catalyst pellets are modelled as a cylindrical geometry. Liquid water exists on the surface of these pellets which is used as a ‘film’ resistance to mass transfer. The Thiele modulus is used to calculate an effectiveness factor, which is the ratio of the observed reaction rate to the ideal reaction rate with no mass transfer limitations.

Water transport through the GDLs can also be described by Darcy's law, where the flow of water is driven by the pressure gradient in the GDL (Singh et al., 1999).

Ye and Van Nguyen (2007) account for capillary forces in the GDL using experimentally measured capillary pressure functions.

A study by Sui et al. (2008) considers evaporation/condensation, capillary diffusion and gravity when accounting for liquid water in the fuel cell. They consider liquid water to be central to all the coupled processes in the fuel cell, since it affects transport across the membrane, electrical properties of the membrane and cell electrical potential.

Many of the concepts described here were used in the fuel cell model developed in this thesis. The following section describes the development of the numerical model.

4.2 One Dimensional Model

The 1D model is a steady state, isothermal, isobaric representation of a proton exchange membrane (PEM) fuel cell. It is modeled using COMSOL Multiphysics, a finite element modeling software, which runs on a Dell Precision T400 desktop computer with and 8 core Intel Xenon 2.66 GHz processor and 32.0 GB of RAM. The model includes mass transport and charge transport. Mass transport includes movement of the gaseous reactants and product on the anode and cathode sides of the fuel cell and of water through the electrolyte membrane. Charge transport includes the ionic transport of H^+ ions through the membrane and electrical transport from the electrodes to the external circuit.

The model consists of three regions, the anode gas diffusion layer (GDL), the polymer membrane, and the cathode GDL as shown in figure 1 below. The anode and cathode GDL's are 200 μm and the membrane is 25 μm. The catalyst layers are assumed to be thin enough that they can be considered to be points. In the model, the catalyst layer will be treated as boundary conditions.

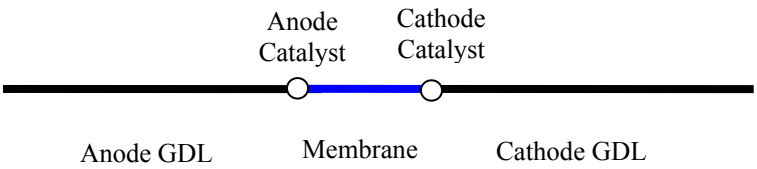

Figure 4.1 Schematic of PEM fuel cell model

Before describing the model, this section will introduce the dependant variables in the model, give details on the mechanisms of electro-osmotic drag, and describe the electrochemical reactions occurring in the cell.

4.2.1 Model Dependant Variables

The following are the dependant variables in the model. They are the key variables in the governing equations of the model.

c_{H2}	Concentration of hydrogen
c_{H2O}	Concentration of water vapour
$c_{H2O,m}$	Concentration of water dissolved in the membrane
$c_{H2O,l}$	Concentration of liquid water
c_{O2}	Concentration of oxygen
Φ_{ion}	Ionic potential
Φ_{ele}	Electrical potential

The concentration of nitrogen will be given by the continuity equation since it does not participate in any reactions or transport.

Please refer to the List of Nomenclature for definitions of all other variables.

4.2.2 Electro-Osmotic Drag and Water Content of the Membrane

As H^+ ions move across the membrane, water molecules move along with them, in a process called electro-osmotic drag. The electro-osmotic drag coefficient, n_{drag}, represents the number of water molecules that are transferred per ion. This value is dependent on the water content of the membrane.

Water content, λ, is defined as the number of moles of water per sulfonic site in the electrolyte membrane (1). It can be described using the properties of the membrane, including the sulfonic capacity, Cap_m, and the density, ρ_m.

$$\lambda = \frac{c_{H2O,m}}{\rho_m Cap_m} \tag{1}$$

The electro-osmotic drag coefficient, n_{eod}, is defined using the membrane water content (2).

$$n_{eod} = \frac{2.5\lambda}{22} \tag{2}$$

4.2.2.1 Equilibrium Water Content in the Membrane

The water in the membrane is assumed to be in equilibrium with the gaseous water present in the gas channels of the fuel cell. The equilibrium water content is dependent on the activity of the gaseous water present in the gas channels of the fuel cell as described by equation (3) (Springer et al., 1991). Activity is defined by equations (4) and (5) (Springer et al., 1991). Equation (3) allows for activities greater than 1 as an artificial way to represent liquid water. Experiments showed that when saturated gas was used to hydrate the membrane, the water content of the membrane was 14, but when liquid water was used they obtained a value of 16.8 (Springer et al., 1991). Equation (3) is an attempt to represent this phenomenon. In the present model, the water content will be represented by vapour water only, so it will not be necessary to use the second part of equation (3).

$$\lambda = 0.043 + 17.81a - 39.85a^2 + 36.0a^3 \quad \text{for } 0 \leq a \leq 1 \tag{3}$$

$$\lambda = 14 + 1.4(a - 1) \quad \text{for } 1 \leq a \leq 3$$

$$a_{H2O} = \frac{x_{H2O}P}{P_{sat}} \tag{4}$$

$$log_{10}P_{sat} = -2.1794 + 0.02953(T - 273.15) - 9.1837E^{-5}(T - 273.15)^2 + 1.4454E^{-7}(T - 273.15)^3 \tag{5}$$

When describing the transport of water in and out of the membrane, activities will be used. Equation (3) above is converted to an equation for the activity of water expressed in terms of water content of the membrane (6). In this case the water content is described by the concentration of water in the membrane as in equation (1) above.

$$a_{H2Om} = -0.12 + 1.76E^{-6}\lambda^4 + 2.17E^{-4}\lambda^3 - 0.0088\lambda^2 + 0.16\lambda - 0.12 \quad \text{for } \lambda < 14 \tag{6}$$

$$a_{H2Om} = -9 + \frac{3\lambda}{7} \quad \text{for} \lambda \geq 14$$

4.2.3 Butler-Volmer Equations

The Butler-Volmer equations describe the production and consumption of ions by electrochemical reaction at the anode and the cathode. The general form of the Butler-Volmer equation is given by equation (7) below. The formats of the specific anode and cathode equations are determined by the specific electrochemical half-reaction occurring at each electrode.

$$i = i_0\left[\frac{c_R}{c_R^{\,o}}exp\left(\frac{\alpha_{i,a}F}{RT}\eta\right) - \frac{c_P}{c_P^{\,o}}exp\left(\frac{-\alpha_{i,c}F}{RT}\eta\right)\right] \tag{7}$$

4.2.3.1 Anode

The electrochemical half reaction occurring at the anode is as follows:

$$H_2 \rightarrow 2H^+ + 2e^- \tag{8}$$

The Butler-Volmer equation for the anode side is as follows in equation (9) where the over-potential is defined by equation (10).

$$i_a = i_{0,a}\left[\frac{c_{H2}}{c_{H2}^{\ref}} exp\left(\frac{\alpha_{a,a}F}{RT}\eta_a\right) - exp\left(\frac{-\alpha_{a,c}F}{RT}\eta_a\right)\right] \tag{9}$$

$$\eta_a = \Phi_{ele} - \Phi_{ion} \tag{10}$$

4.2.3.2 Cathode

The cathode half reaction is as follows:

$$\frac{1}{2}O_2 + 2H^+ + 2e^- \rightarrow H_2O \tag{11}$$

Using this, the cathode side Butler-Volmer equation is as follows in equation (12) where the over-potential is described by equation (13). It should be noted that the cathode side over-potential includes a reference potential (14), which is the theoretical thermodynamic open circuit cell potential. This term does exist for the anode side over-potential, however, it is equal to zero.

On the cathode side, the Bulter-Volmer equation includes a correction factor, $(1-s)$, where s is the fraction of liquid water in the pores (Siegel, 2004). This accounts for catalyst sites that are blocked due to the presence of liquid water.

$$i_c = i_{o,c}\left[\frac{c_{H2O}}{c_{H2O}^{\ref}}\exp\left(\frac{\alpha_{ac}F}{RT}\eta_c\right) - \frac{c_{O2}}{c_{O2}^{\ref}}\exp\left(\frac{-\alpha_{cc}F}{RT}\eta_c\right)\right](1-s) \tag{12}$$

$$\eta_c = \Phi_{ele} - \Phi_{ion} - \Phi_{ref} \tag{13}$$

$$\Phi_{ref} = E^{\ref} + \frac{RT}{2F}\ln\left(\frac{P_{H2O}}{P_{H2}P_{O2}^{1/2}}\right) \tag{14}$$

This equation (12) will return a negative value because it is the second term that dominates. This means that when we use this equation to describe reaction rates, we must remember to assign the signs correctly.

4.2.4 Mass Transport

Mass transport in the fuel cell includes the movement of hydrogen and water at the anode, and water, liquid water and oxygen at the cathode. For the electrolyte membrane, only diffusion of water will be considered, we will assume that it is impermeable to all other species for simplicity. Movement of water through the membrane is determined by ionic movement of H^+ ions as well as by the concentration gradient.

In the mass balance the unsteady and convection terms are zero so we are left with only a diffusion and source term as follows:

$$\nabla(N_i) = S_i \tag{15}$$

This equation applies for all diffusing species in the fuel cell (H_2, H_2O, and O_2). The diffusion flux and source terms for each species and for each different part of the fuel cell are described in Sections 4.1.4.1, 4.1.4.2 and 4.1.4.3 below.

4.2.4.1 Hydrogen and Water at the Anode

The diffusion flux is determined for each species through Fick's law of diffusion with the diffusion coefficients based on an approximation of the Maxwell-Stefan equation (16) (Gurau et al, 1998).

$$D_i - \frac{(1 - x_i)}{\sum_{j \neq i}(x_j / D_{ij})} \tag{16}$$

Inserting the appropriate values, the diffusivities of hydrogen and water turn out to be equal to the binary diffusivities and, since there is only hydrogen and water present at the anode, $x_{H2} + x_{H2O} = 1$. The binary diffusion coefficients in these effective diffusivities are described in Section 1.6.

However, in the GDL, effective diffusivities also must include corrections for porosity (ε) and tortuosity (τ) as shown in equations (17) and (18).

$$D_{H2,eff} = \frac{\varepsilon}{\tau} D_{H2,H2O} \tag{17}$$

$$D_{H2O,eff} = \frac{\varepsilon}{\tau} D_{H2,H2O} \tag{18}$$

Therefore the fluxes of these two species are as follows in equation 19 and 20.

$$N_{H2} = \left(-\frac{\varepsilon}{\tau} D_{H2,H2O}\right) \nabla c_{H2} \tag{19}$$

$$N_{H2O} = \left(-\frac{\varepsilon}{\tau} D_{H2,H2O}\right) \nabla c_{H2O} \tag{20}$$

For hydrogen there is no source term within the GDL, since there is no reaction occurring in the GDL, only transport. A flux boundary condition at the interface of the GDL and membrane represents the reaction at the catalyst. This boundary condition is described in equation (21). It is negative because the hydrogen is being consumed by the electrochemical reaction at the anode. The reaction rate is proportional to the current, i_a, which is described by the Butler-Volmer equation (9).

$$R_{H2} = \frac{-S_a i_a}{2F} \tag{21}$$

The water also has no source term. The membrane interface flux boundary condition (equation 22) represents the transfer of water into the membrane due to electro osmotic drag, and the transfer between the gas phase of the anode channel and the electrolyte phase of the membrane. The mass transfer coefficient, h_m, between the gas phase water and the water dissolved in the electrolyte is described by equation (23) (Majsztrik et al., 2007).

(22)

$$R_{H2O} = -\frac{n_{eod} S_a i_a}{F} + h_m (a_{H2O,m} - a_{H2O,g})$$

$$h_m = 8 * 10^{-6} \exp(0.034T) \quad (23)$$

The complete equations for the anode can be summarized as follows:

	Anode GDL	Catalyst Interface
c_{H2}	$\nabla(-D_{H2,eff} \nabla c_{H2}) = 0$	$-D_{H2,eff} \nabla c_{H2} = \frac{-S_a i_a}{2F}$
c_{H2O}	$\nabla(-D_{H2O,eff} \nabla c_{H2O}) = 0$	$-D_{H2O,eff} \nabla c_{H2O} - -\frac{n_{eod} S_a i_a}{F} + h_m (a_{H2O,m} - a_{H2O,g})$

4.2.4.2 Oxygen, Gaseous Water and Liquid Water at the Cathode

Determining the diffusion fluxes on the cathode side is done similarly to those on the anode side. The species diffusivities are determined using the approximation to the Maxwell-Stefan equation (16). The diffusivities for oxygen and water are as follows on equation 24 and 25.

$$D_{g2} = \frac{(1 - x_{O2})}{\left(\frac{x_{N2}}{D_{O2,N2}} + \frac{x_{H2O}}{D_{O2,H2O}}\right)} \quad (24)$$

$$D_{H2O} = \frac{(1 - x_{H2O})}{\left(\frac{x_{N2}}{D_{H2O,N2}} + \frac{x_{O2}}{D_{O2,H2O}}\right)} \quad (25)$$

In the GDL, these diffusivities also must include corrections for porosity (ε) and tortuosity (τ).

On the cathode side, since there may be liquid water present, there is also a correction $(1-s)$ to account for the blockage of the pores with liquid water. The binary diffusion coefficients in these effective diffusivities are described in Section 1.6.

$$D_{O2,eff} = (1-s)\frac{\varepsilon}{\tau}\left(\frac{(1-x_{O2})}{\left(\frac{x_{N2}}{D_{O2,N2}}+\frac{x_{H2O}}{D_{O2,H2O}}\right)}\right) \tag{26}$$

$$D_{H2O,eff} = (1-s)\frac{\varepsilon}{\tau}\left(\frac{(1-x_{H2O})}{\left(\frac{x_{N2}}{D_{H2O,N2}}+\frac{x_{O2}}{D_{O2,H2O}}\right)}\right) \tag{27}$$

The diffusion coefficient of liquid water is based on a correlation for capillary flow in gas diffusion media (28) (Siegel, 2004 , Natarajan and Van Nguyen, 2001) The diffusion coefficient is defined by the fraction of liquid water present in the pores, s (29).

$$D_{H2O,l} = 0.0118s^3 - 0.0162s^2 + 0.0068s + 0.001 \tag{28}$$

$$s = \frac{\frac{c_{H2O,l}M_{H2O}}{\rho_{H2v}}}{a_{3DL}} \tag{29}$$

Oxygen has no source term within the GDL. The reaction rate is also represented by a flux boundary condition (30) as with hydrogen on the anode side. Oxygen is consumed by the

electrochemical reaction (11), in which the current, i_c, is described by the Butler-Volmer equation for the cathode (12). Note that even though oxygen is being consumed by the reaction, the term is positive here because i_c is negative on the cathode side.

$$R_{O2} = \frac{S_c i_c}{4F} \tag{30}$$

Since gaseous water is assumed to be in equilibrium with the membrane phase water, any equilibrium-based transport between the membrane and the GDL will be assumed to be in the gaseous phase. We will assume that all water formed at the catalyst by electrochemical reaction is formed as liquid water. All water leaving the membrane due to electro osmotic drag will also be in the liquid form. All of these forms of transport will be represented as flux boundary conditions at the membrane GDL interface. The transport between gaseous water in the GDL and dissolved water in the membrane will be represented by equation (31) where the mass transfer coefficient, h_m, is represented by equation (23) as on the anode side. The first term in equation (32) represents the formation of water by electrochemical reaction and the second term represents the water dragged along by electro-osmotic drag. Both terms are negative because i_c is negative.

$$R_{H2O} = h_m(a_{H2O,m} - a_{H2O,g}) \tag{31}$$

$$R_{H2O,l} = -\frac{S_c i_c}{2F} - \frac{n_{sod} S_c i_c}{F} \tag{32}$$

It will also be assumed that there will be a transfer of water between the liquid and the gaseous phase in the form of condensation or evaporation. This will be represented by a source term in

each of the water equations (33, 34) (Ye and Van Nguyen, 2007). The evaporation or condensation rate is proportional to the driving force, which is the difference between the partial pressure of the gaseous water and the saturation pressure of water. The symbol ψ can be thought of as a "switch" function, where it takes a value of 1 for water activities lower than 0.98, and a value of 0 otherwise. This means that if the water activity is low, the first term will be active, thus water will evaporate from the liquid phase into the gas phase. If the water activity is high, meaning that the water vapour is saturated, the second term will be active and water will transfer from the vapour phase to the liquid phase. The liquid fraction, s, is included in the condensation/evaporation terms to ensure that water only evaporates when liquid water is present (Siegel et al., 2004).

$$S_{H2O} = -\psi s h_e \varepsilon_{GDL} (x_{H2O} P - P_{sat}) \frac{\rho_{H2O}}{M_{H2O}} - (1-\psi)(1-s) h_c \varepsilon_{GDL} \frac{(x_{H2O} P - P_{sat})}{RT} \quad (33)$$

$$S_{H2O,l} = \psi s h_e \varepsilon_{GDL} (x_{H2O} P - P_{sat}) \frac{\rho_{H2O}}{M_{H2O}} + (1-\psi)(1-s) h_c \varepsilon_{GDL} \frac{(x_{H2O} P - P_{sat})}{RT} \quad (34)$$

The evaporation and condensation mass transfer coefficients, h_e and h_c, were chosen to be large enough to ensure equilibrium.

$$h_e = 1 s^{-1} \quad (35)$$

$$h_c = 5 * 10^{-5} Pa^{-1} s^{-1} \quad (36)$$

The complete equations for the cathode can be summarized as follows:

	Cathode GDL	Catalyst Interface
c_{O2}	$\nabla\left(-D_{O2,eff}\nabla c_{O2}\right) = 0$	$-D_{O2,eff}\nabla c_{O2} = \frac{S_c i_c}{4F}$
c_{H2O}	$\nabla\left(-D_{H2O,eff}\nabla c_{H2O}\right) = -\psi s h_e a_{GDL}\left(x_{H2O}P - P_{sat}\right)\frac{\rho_{H2O}}{M_{H2O}} - (1-\psi)(1-s)h_e a_{GDL}\frac{\left(x_{H2O}P - P_{sat}\right)}{RT}$	$-D_{H2O,eff}\nabla c_{H2O} = h_m\left(a_{H2O,m} - a_{H2O,g}\right)$
$c_{H2O,l}$	$\nabla\left(-D_{H2O,eff}\nabla c_{H2O}\right) = \psi s h_e a_{GDL}\left(x_{H2O}P - P_{sat}\right)\frac{\rho_{H2O}}{M_{H2O}} + (1-\psi)(1-s)h_e a_{GDL}\frac{\left(x_{H2O}P - P_{sat}\right)}{RT}$	$-D_{H2O,eff}\nabla c_{H2O} = -\frac{S_c i_c}{2F} - \frac{n_{eod} S_c i_c}{F}$

4.2.4.3 Water Transport through the Electrolyte

The flux of water through the polymer electrolyte membrane depends on diffusion driven by a concentration gradient and on electro osmotic drag. Electro-osmotic drag is driven by the flux of ions through the electrolyte, which is represented by the second term in equation (37).

$$N_{H2O,m} = -D_{H2O,m}\nabla c_{H2O,m} - \frac{n_{eod} k_{ion}}{F}\nabla\Phi_{ion} \tag{37}$$

The diffusion coefficient of water through the electrolyte, $D_{H2O,m}$, (38) is also dependant on the electro-osmotic drag coefficient, and through that, on water content.

$$D_{H2O,m} = n_{eod} D_q \exp\left[2416\left(\frac{1}{303} - \frac{1}{T}\right)\right] \tag{38}$$

where, $D_o = 5.5 * 10^{-7}\ cm^2/s$ (Nguyen and White, 1993)

The rate of water entering or exiting the membrane phase is represented by the flux boundary condition shown in equation (39) below. The first term represents the water that is brought along with the ions by electro osmotic drag and the second term represents the transfer from the gas phase to the electrolyte phase.

$$R_{H2O,m} = \frac{n_{eod} S_{a/c} i_{a/c}}{F} - h_m\left(a_{H2O,m} - a_{H2O,g}\right) \tag{39}$$

The complete equations for the membrane can be summarized as follows:

	Anode Catalyst Interface	Membrane	Cathode Catalyst Interface
$c_{H2O,m}$	$-D_{H2O,m}\nabla c_{H2O,m} - \frac{n_{eod} k_{ion}}{F}\nabla\Phi_{ion}$ $= \frac{n_{eod} S_a i_a}{F} - h_m\left(a_{H2O,m} - a_{H2O,g}\right)$	$\nabla\left(-D_{H2O,m}\nabla c_{H2O,m} - \frac{n_{eod} k_{ion}}{F}\nabla\Phi_{ion}\right) = 0$	$-D_{H2O,m}\nabla c_{H2O,m} - \frac{n_{eod} k_{ion}}{F}\nabla\Phi_{ion}$ $- \frac{n_{eod} S_c i_c}{F} - h_m\left(a_{H2O,m} - a_{H2O,g}\right)$

4.2.5 Charge Transport

Charge transport consists of transport of hydrogen ions (H^+) across the electrolyte membrane and of electrons from the electrodes, through the gas diffusion layer and to the external circuit.

4.2.5.1 Ionic Transport

Equation 40 below is the steady state charge balance for H^+ ions in the cell. The variable i_{ion} represents the current density and can be related to potential gradient via Ohm's law (Gazzarri and Kesler, 2007).

$$\nabla\cdot(i_{ion}) = S_{ion} \tag{40}$$

$$i_{ion} = -k_{ion}\nabla\Phi_{ion} \tag{41}$$

The ionic conductivity of the membrane depends on its water content (λ_m) and temperature according to the following equation.

$$k_{ion} = exp\left[1268\left(\frac{1}{303}-\frac{1}{T}\right)\right](0.005139\lambda_m - 0.00326) \tag{42}$$

The reaction rate is represented by a flux boundary condition and is given by the current density multiplied by the electrochemically active surface area of the catalyst. The current density in this term is described by the Butler-Volmer equation (12). At the anode, the reaction rate term is positive because ions are being produced. The term will be negative at the cathode because i_c will be negative, which means that ions are being consumed.

$$S_i = S_a i_a \text{ (at the anode)} \tag{43}$$

$$S_i = S_c i_c \text{ (at the cathode)} \tag{44}$$

The complete equations for the membrane can be summarized as follows:

	Anode Catalyst Interface	Membrane	Cathode Catalyst Interface
Φ_{ion}	$-k_{ion_m}\nabla\Phi_{ion_m} = S_a i_a$	$\nabla(-k_{ion_m}\nabla\Phi_{ion_m}) = 0$	$-k_{ion_m}\nabla\Phi_{ion_m} = S_c i_c$

4.2.5.2 Electronic Transport

The transport of electrical charge can be described in a similar way to ionic charge using a steady state charge balance and Ohm's law as shown below (45, 46).

$$\nabla(i_{ele}) = S_{ele} \tag{45}$$

$$i_{ele} = -k_{ele}\nabla\Phi_{ele} \tag{46}$$

The reaction rate for electronic transport is represented by a flux boundary condition at the membrane-GDL interface by the following equations (47, 48). These have the opposite sign of the ionic transport since conservation of charge requires equation 49 to hold true.

$$S_i = -S_a i_a \text{ (at the anode)} \tag{47}$$

$$S_i = -S_c i_c \text{ (at the cathode)} \tag{48}$$

$$\nabla i_{ion} + \nabla i_{ele} = 0 \tag{49}$$

The complete equations for the membrane can be summarized as follows:

	Anode Catalyst Interface	Membrane	Cathode Catalyst Interface
Φ_{ele}	$-k_{ele}\nabla\Phi_{ele} = -S_a i_a$	$\nabla(-k_{ele}\nabla\Phi_{ele}) = 0$	$-k_{ele}\nabla\Phi_{ele} = -S_c i_c$

4.2.6 Material Properties and Constants

The material properties used in the model are calculated, taken from manufacturer's specifications or taken from previous studies.

4.2.6.1 Binary Diffusion Coefficients

In the effective diffusivity coefficient equations (17, 18, 26, 27), the diffusion coefficients are represented by a combination of mole fractions and binary diffusion coefficients. These binary diffusion coefficients are calculated using the Fuller-Schettler-Giddings method (Fuller et al., 1966).

$$D_{A,B} = \frac{0.001T^{1.75}\left(\frac{1}{M_A}+\frac{1}{M_B}\right)^{0.5}}{P\left[(\Sigma v)_A^{1/3}+(\Sigma v)_B^{1/3}\right]^2} \quad (50)$$

The variable v represents the diffusion volume of the particular species.

$v_{O2} = 16.6$

$v_{H2O} = 12.7$

$v_{N2} = 17.9$

$v_{H2} = 7.07$

The result of applying equation 53 is the following binary diffusion coefficients.

$D_{H2,H2O} = 1.220\,cm^2/s$

$D_{O2,H2O} = 0.2665\,cm^2/s$

$D_{N2,H2O} = 0.2661\ cm^2/s$

$D_{N2,O2} = 0.2091 cm^2/s$

4.2.6.2 Electrodes

The electrode/GDL conductivity is taken from the BASF gas diffusion electrodes specification sheet (BASF Gas Diffusion Electrode).

$$k_{ele} = \frac{1}{500\ m\Omega * cm}$$

Most of the other properties are taken from a study done by Siegel et al. (2004), including the porosity and tortuosity of the GDL and the composition fractions of the electrodes.

$\varepsilon_{GDL} = 0.375$

$\tau_{GDL} = 3.5$

The electrochemical properties are also taken from Siegel et al. (2004).

$S_a = 6990/mm$

$S_c = 6990\ /mm$

$i_{o,a} = 3 * 10^{-3}\ A/mm^2$

$i_{o,c} = 4.1 * 10^{-9}\ A/mm^2$

$c_{H2}^{\circ} = 2.66 * 10^{-8}\ mol/mm^2$

$c_{H2O}^{\circ} = 0.59 * 10^{-9}\ mol/mm^2$

$c_{O2}^{\circ} = 1.10 * 10^{-9}\ mol/mm^2$

$\alpha_{a,a} = 0.5$

$\alpha_{a,c} = 1.5$

$\alpha_{c,c} = 0.55$

$\alpha_{c,a} = 1.45$

The standard open circuit voltage is calculated using the equation below (51), where Δg_f° is the change in the standard Gibbs free energy of formation for the complete cell electrochemical reaction.

$$E_o = \frac{-\Delta g_f^{\circ}}{2F} = 1.23V \tag{51}$$

4.2.6.3 Electrolyte Membrane

The membrane preoperties are taken from the specification sheet for DuPont Nafion PFSA Membranes (Dupont Nafion PFSA Membranes, 2005).

$\rho_{m,dry} = 360\, g/m^2$

$Cap_{m,dry} = 0.95\, meq/g$

The thickness of the memebrane is given by Hydrogenics as a standard size for one of the membranes used in their fuel cells. (personal communication with Hydrogenics, August 15, 2008)

$t_m = 25\mu m$

4.2.6.4 Constants

Two constants uses in this model are Farraday's constant and the ideal gas constant.

$F = 96485\,C/mol$

$R = 8.314 m^3 Pa/molK$

4.2.6.5 Operating Conditions

The operating pressure of the fuel cell is set to 3 psig (122 000 Pa), which is the pressure used by Hydrogenics in their fuel cells. The temperature is set to 60°C (personal communication with Hydrogenics, August 15, 2008).

4.2.7 Boundary Conditions

The boundary conditions for the model are as follows:

Species	Outside Anode GDL	Anode GDL / Membrane	Membrane / Cathode GDL	Outside Cathode GDL
c_{H2}	$\frac{(P - P_{sat})}{RT}$	$N = \frac{-S_a i_a}{2F}$	-	-
c_{H2O}	$\frac{(P_{sat})}{RT}$	$N = -\frac{n_{eod} S_a i_a}{F} + h_m(a_{H2O,m} - a_{H2O,g})$	$N = h_m(a_{H2O,m} - a_{H2O,g})$	0
$c_{H2O,m}$	-	$N = \frac{n_{eod} S_a i_a}{F} - h_m(a_{H2O,m} - a_{H2O,g})$	$N = \frac{n_{eod} S_c i_c}{F} - h_m(a_{H2O,m} - a_{H2O,g})$	-
$c_{H2O,l}$	-	-	$N = -\frac{(1 + 2n_{eod}) S_c i_c}{2F}$	0
c_{O2}	-	-	$N = \frac{S_c i_c}{4F}$	$\frac{0.21P}{RT}$
Φ_{ion}	-	$N = S_a i_a$	$N = S_c i_c$	-
Φ_{ele}	0	$N = -S_a i_a$	$N = -S_c i_c$	V_{cell}

The anode side inlet gas concentration is set such that the hydrogen is fully humidified. The cathode contains dry air. Also, the cathode side potential is set to the operating voltage of the cell. This can be changed to investigate the performance at different voltages. At this point the outside boundary condition for liquid water is set to zero, for the 2D model, water will be allowed to leave the GDL and flow into the distribution channel. The flux boundary conditions

at the membrane/GDL interface represent reaction rates and rates of transport between the two phases. These are described in Sections 1.4 and 1.5 above.

4.2.8 Summary of Assumptions

The flowing table gives a list of significant assumptions that have been used in the 1D model. These also apply to the 2D and 3D models.

Table 4.1 Model assumptions and their impacts

Assumption	**Impact on Model**
Isothermal	Electrochemical reaction is exothermic, and is faster at higher temperatures, so has the potential to underestimate reaction rate.
Isobaric	For a small single cell, do not expect differences in pressure to have a large impact.
Catalyst layers as points/ interfaces	Catalyst layers are usually very thin (about 15 μm), but have a very high surface area, so this is a reasonable assumption if the surface area is accounted for (which it was in this model).
Membrane impermeable to gasses	This assumption was used to simplify the model; however, membranes are not impermeable to gasses. A phenomenon called fuel crossover will not be accounted for because of this assumption. Fuel crossover causes a decrease in the open circuit voltage in a fuel cell.
Liquid water – capillary flow correlation	A correlation for capillary flow was used instead of actual flow equations; this correlation was found to be a good representation of capillary flow in other models in the literature (Siegel, 2004, Natarajan and Van Nguyen, 2001).
Liquid water – fraction in pores used a correction factor for reactions and diffusion of gasses	Liquid water was converted into a volume to represent the fraction of pores blocked by liquid water. This number was then used to account for blocked catalyst sites and gas diffusion rates that would be lower due to the presence of liquid water. This assumption has a big effect on the model because it affects many of the processes present; however, it also has been shown to give a good approximation of the performance of a fuel cell in the

	literature (Siegel, 2004, Natarajan and Van Nguyen, 2001).
Forms of water – gas when equilibrium between membrane and GDL, liquid for eod and reaction	It is assumed that water forms as a liquid when it goes in or out of the membrane, as a gas when it is formed at the catalyst layer and as a gas when it comes through the membrane with a proton by electro-osmotic drag. Since the rate constant for evaporation/condensation was chosen to ensure equilibrium, the form that water initially takes has less of an impact.

4.2.9 1D Mesh Study

In order to generate an appropriate mesh for the model, different sized meshes were investigated. The goal was to generate a mesh that gave accurate results with a minimum number of elements to minimize computational time. First, a very fine mesh of 50 elements was assigned (20 in the anode and cathode GDL's and 10 in the membrane), this mesh is considered to be the 'correct' solution. The number of elements was decreased until it was very coarse and the results compared to the 'correct' solution. Variation in current density was compared as an indication of the 'wellness' of the model, since this variable is dependent on all aspects of the model and since it is the variable of interest in defining the performance of the fuel cell. The meshes were compared using a total percent error in the current density, which was the sum of the errors for various operating voltages ranging from 0.2 V to 1.2 V at 0.1 V intervals. Error was defined by subtracting the current density computed using the very fine mesh to represent the 'correct' solution. Seven elements in the GDL and 4 elements in the membrane gave a very close solution, with a total percent error over the voltage range of 0.0308%. In an attempt to reduce the mesh even further, the anode GDL had a simple linear trend for all operating conditions. This enabled the reduction of the anode GDL mesh to only 2 elements while still achieving the same total percent error as the model with 7 elements.

4.3 Two Dimensional Model

The 2D model, similarly to the 1D model, is a steady state, isothermal, isobaric representation of a proton exchange membrane (PEM) fuel cell. It is modeled using COMSOL Multiphysics, a finite element modeling software. The model includes mass transport and charge transport.

Mass transport includes movement of the gaseous reactants and product on the anode and cathode sides of the fuel cell and of water through the electrolyte membrane. Charge transport includes the ionic transport of H^+ ions through the membrane and electrical transport from the electrodes to the external circuit.

The model consists of five regions, the anode gas channel, the anode gas diffusion layer (GDL), the polymer membrane, the cathode GDL and the cathode gas channel as shown in Figure 4.2 below. The GDL's and membrane are the same thickness as in the 1D model and the channel depth is 1 mm. The catalyst layers are assumed to be thin enough that they can be considered to be the interface between the GDL and the gas channel. The length of the channel is 10 cm.

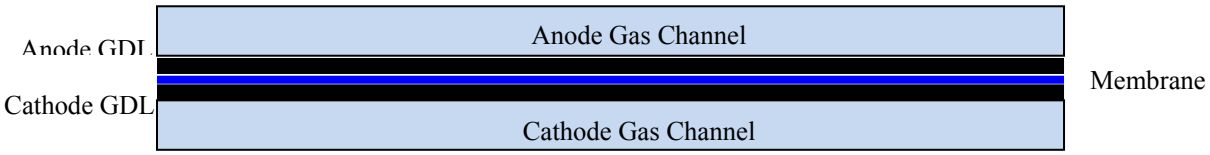

Figure 4.2 2D Schematic of model

Much of the 2D model remains the same as the 1D. The difference is that the 2D model now accounts for momentum transport. Also, a 2D model allows identification of the changes in the current density along the channel.

4.3.1 Momentum Transport

The incompressible Navier-Stokes equations are used to account for momentum transport in the gas channels. The gasses can be assumed to be incompressible because the velocity of the gasses is much lower than the speed of sound, making the Mach number much less than 1 (it was calculated to be 0.008). For simplicity, the model does not include momentum transport in the GDL, the gasses are assumed to flow by diffusion only. A study by Shi and Wang (2007) compares Darcy's law, the Brinkman equation and the modified Navier-Stokes equation to diffusion alone. They found that Darcy's law, the Brinkman equation and the modified Navier-Stokes equation all give very similar results which correlate to experimental results. However diffusion alone predicted slightly lower than experimental measured current density, so they recommend using the Brinkman equation. When applying that to my model I found that using

these other equations made the model unstable and so was not able to converge to a solution. I decided to sacrifice a bit of accuracy for the sake of stability and also to reduce the number of degrees of freedom to be solved for. Thus the Navier-Stokes equation was used in the channels only and in the following form (equation 52).

$$-\nabla \cdot \left[\eta\left(\nabla \mathbf{u} + (\nabla \mathbf{u})^T\right)\right] + \rho(\mathbf{u} \cdot \nabla)\mathbf{u} + \nabla p = 0 \tag{52}$$

where **u** is the velocity field, p is the pressure, η is the viscosity and ρ is the density of the fluid. Viscosity and density are constants based on inlet conditions. All walls, including the GDL/channel interface, are set to a no slip boundary condition where the velocity field is set to 0 m/s on the boundary. The inlet is a velocity which is based on the flow rate assuming a particular cross section of the inlet. The flow rate can be set to correspond to a certain fuel/oxidant stoichiometric ratio. The outlet boundary condition is set to atmospheric pressure (101325 Pa) with no viscous stress.

4.3.2 Species Transport

The species that exist in the flow channels are almost the same as those that exist in the GDL. The exception is that electrical potential will not be considered in the flow channels. The boundary for electrical potential will remain at the surface of the GDL. The equations in the flow channels for those species that still exist there are similar to the species equations in the GDL. However, the equations now include an extra term for advection (the second term in equation 53), which describes the movement of the species due to the flowing fluid.

$$-D_i \nabla c_i + \mathbf{u} \cdot \nabla c_i = S_i \tag{53}$$

4.3.2.1 Hydrogen and Oxygen

The diffusivities are calculated in the same way as above in Section 4.2, however there is no need for the correction for porosity and tortuosity of the GDL, since they are no longer in the GDL. The source term, S_i, is equal to zero since there are no reactions occurring in the channels for hydrogen and oxygen.

$$D_{O2,eff} = (1-s)\left(\frac{(1-x_{O2})}{\left(\frac{x_{N2}}{D_{O2,N2}}+\frac{x_{H2O}}{D_{O2,H2O}}\right)}\right) \quad (54)$$

$$D_{H2,eff} = (1-s)\left(D_{H2,H2O}\right) \quad (55)$$

The channel equations for hydrogen and oxygen can be summarized as follows:

	Anode Channel	Cathode Channel
c_{O2}	-	$\nabla\left(-D_{O2,eff}\nabla c_{O2}\right)+\mathbf{u}\cdot\nabla c_{O2}=0$
c_{H2}	$\nabla\left(-D_{H2,eff}\nabla c_{H2}\right)+\mathbf{u}\cdot\nabla c_{H2}=0$	-

4.3.2.2 Liquid Water and Water Vapour

As with the hydrogen and oxygen, the diffusivities are calculated in the same way except that there is no correction for porosity or tortuosity. The source term used in the GDL is likewise the same, except it does not contain a correction for porosity.

$$D_{H2O,a,eff} = (1-s)\left(\frac{(1-x_{H2O})}{\left(\frac{x_{N2}}{D_{H2O,N2}}+\frac{x_{O2}}{D_{O2,H2O}}\right)}\right) \quad (56)$$

$$D_{H2O,a,eff} = (1-s)\left(D_{H2,H2O}\right) \quad (57)$$

The equations for water vapour and liquid water in the anode and cathode channels can be summarized as follows:

	Anode Channel	Cathode Channel
c_{H2O}	$\nabla\left(-D_{H2O,a,eff}\nabla c_{H2O}\right)+\mathbf{u}\cdot\nabla c_l=0$	$\nabla\left(-D_{H2O,a,eff}\nabla c_{H2O}\right)+\mathbf{u}\cdot\nabla c_l = -\psi s k_e(x_{H2O}P-P_{sat})\frac{\rho_{H2O}}{M_{H2O}} - (1-\psi)(1-s)k_c\frac{(x_{H2O}P-P_{sat})}{RT}$
$c_{H2O,l}$	-	$\nabla\left(-D_{H2O,eff}\nabla c_{H2O}\right)+\mathbf{u}\cdot\nabla c_l = \psi s k_e(x_{H2O}P-P_{sat})\frac{\rho_{H2O}}{M_{H2O}}$

		$\cdot + (1-\psi)(1-s)h_g \frac{(x_{H2O}P - P_{sat})}{RT}$

4.3.2.3 Boundary Conditions

All outside boundaries of the gas channels are set to no flux. The inlet is set to the inlet concentration of the species as they were defined in Section 4.2.7. The outlet concentration is convective flux. At the interface between the GDL and the channel there is a continuity boundary condition.

4.3.3 Solving Procedure

When solving this 2D model, a direct solver is used. To reduce the memory requirements, first the momentum equation is solved to obtain the velocity field of the channel. Next, all of the other equations are solved using the solution from the Navier-Stokes equations as inputs for the velocity field in the species equations. Thus, in this model the composition of the channel fluid does not affect the momentum equations.

4.3.4 2D Mesh Study

A mapped grid mesh is used for the 2D model. The same mesh size is used for the anode GDL, cathode GDL and membrane. However a mesh study was needed to determine the optimum mesh size for the anode and cathode flow channels and for the model length. As with the 1D mesh study, a fine mesh was used as the "correct" solution and subsequent meshes were compared to that one. It was found that the results from the 1D mesh study still hold. That is, there is no difference between 7 and 2 mesh elements in the anode GDL. It was also found that there is a relatively small difference between 6, 7 and 8 elements in the cathode GDL. The anode and cathode channels, like the cathode GDL, give a better solution for a larger number of elements. Twelve elements gave very good results (0.6 % difference from the "correct" solution), but in the interest of computational time, 6 elements in the channel depth were used (1.9 % difference from the "correct" solution). As for the length of the channel, it was found that 50 elements gave a very similar result to 200 elements.

4.4 Three Dimensional Model

The 3D model is an extension of the 2D model; all equations are the same and can be found in Sections 4.2 and 4.4 above. The 2D straight channel was first extended to a 3D straight channel. Next 3D models of the bipolar plate flow channel designs were created.

4.4.1 3D Straight Channel: Solving Procedure

Different solving methods were tested to determine how to solve the 3D problem using the least memory. A direct solver, an iterative solver and a segregated solver were used. Direct solvers tend to use a lot of memory, but can achieve a relatively robust solution. Iterative solvers tend to use less memory, but require a lot of tuning to get a stable and accurate solution. Segregated solvers are used with direct solvers to reduce the memory requirements of loosely coupled systems. (COMSOL AB, 2007) While this problem would be considered more than just loosely coupled, the segregated solver was investigated to see if it could save on memory while keeping the solution relatively accurate.

The segregated solver solves the problem in parts (groups), iteratively. For this solver the equations are split into three groups: hydrogen/oxygen, water/liquid water, and membrane water/ions/electrons. These groups are never solved all together, but are solved one group at a time, one step at a time, using the solutions from the previous step of all groups for the next step, until all groups converge.

A solver study was done in conjunction with the mesh study to determine the effect of using different solvers with various mesh sizes.

4.4.2 3D Straight Channel: Mesh Study

The initial 3D straight channel used a mapped mesh like in the 1D and 2D models. However, when making the flow patterns, it is difficult to produce a mapped mesh on subdomins that are not rectangular. For these a free mesh is a better choice. However, a free mesh alone tends to use many more elements than necessary in the small subdomains, making the memory requirements for solving the problem very high. Like the 2D model, fewer elements are required along the channel than are required through the GDL and membrane. A mesh strategy was used that uses a free mesh on the outer surface of the gas channels and maps this through each

subdomain. This method aims to enhance resolution in all subdomains in the in-plane direction. The number of elements in the mapped direction is the same as is used in the 2D model. A mesh with a maximum element size of 0.0005 m was the smallest mesh that allowed the flow and species equations to be solved using an error of 10^{-6}, and was able to be solved using the computer resources available. This element size was used in the flow channels for the 3D flow patterns. The same GDL and membrane mesh size as the 2D model was used.

The above mesh was used with the segregated solver, which allowed the simulation to solve using less memory than a direct solver. When comparing the accuracy of the two types of solvers, the average current density was used as the value to compare the quality of the solver. When the same maximum element size was used, the direct solver and the segregated solver gave the same value of average current density. Iterative solvers also require less memory, however, they require more tuning and appropriate values for the tuning parameters of the solver were not found for this simulation. Thus, the segregated solver was used.

4.4.3 3D Flow Patterns

3D flow patterns were created from each of the 2D flow pattern models. Using the mesh as described above proved to be insufficient to reduce the computational time required to solve the simulation with the complete flow pattern. The computer used to solve the simulation did not have enough memory to obtain a solution.

After repeated attempts to solve the 3D flow field model using different meshes and solvers, it became clear that another means was necessary to validate the biomimetic flow pattern designs. Thus, a physical model of a bipolar plate was created that can be tested on a single cell fuel cell. The following section gives the results of the simulations described above, and following that is a description of the experimental results.

5 Simulation Results

This section gives an overview of the results of the simulations. This includes the initial results of the 1D model including validation by comparison with other models in the literature. Preliminary flow pattern assessments using a 2D approximation are presented. Next the 2D model shows how current density would change along a straight channel. Finally the 3D results from the straight channel are compared to the 2D straight channel results.

5.1 1D Model

The results of the1D model are shown by a polarization curve. Figure 5.1 was produced for a cell operating at 60 °C, and 3 psig, and using hydrogen and air as the fuel and oxidant, respectively. The inlet humidity of the anode is 100% and of the cathode is 0% (dry air).

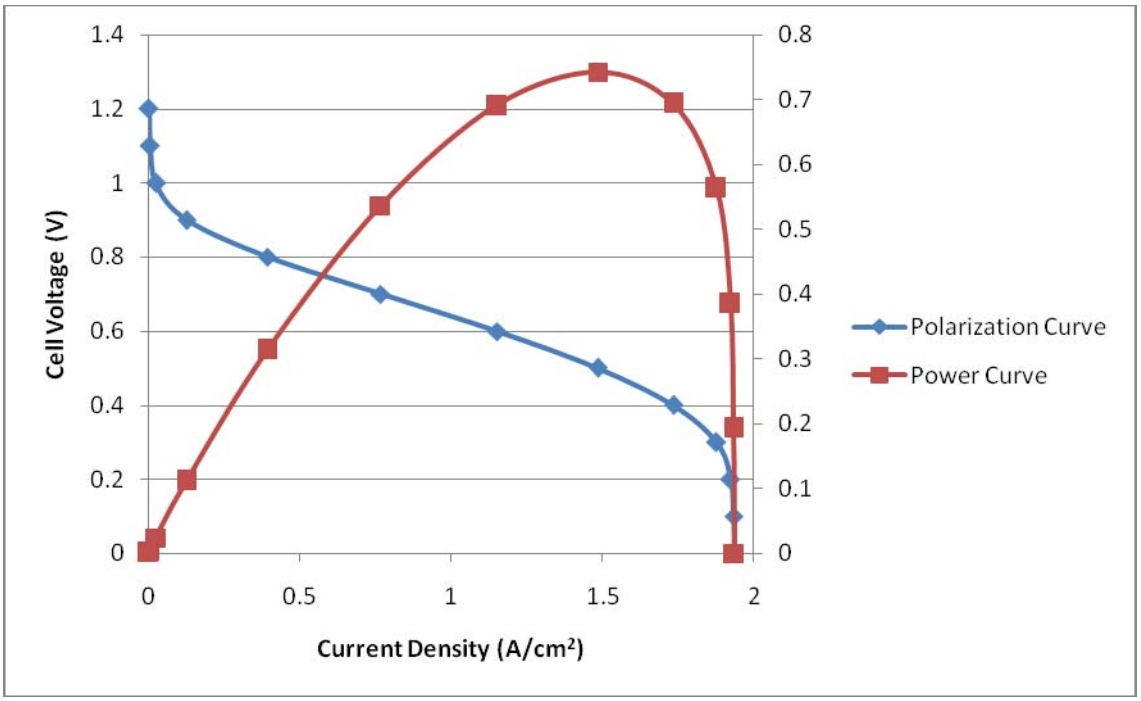

Figure 5.1 1D Polarization and power curve for dry cathode

In practice it is not feasible to use dry air for a fuel cell since it is common to use ambient air, which contains varying amounts of water depending on the location and time of year. Figure 5.2 below shows the effect of various cathode inlet humidities on the performance of the fuel cell modeled in 1D. It can be seen that the performance decreases as the humidity is increased. This is because water at the cathode side can block the path for reactants to reach the catalyst, thus increasing concentration polarization.

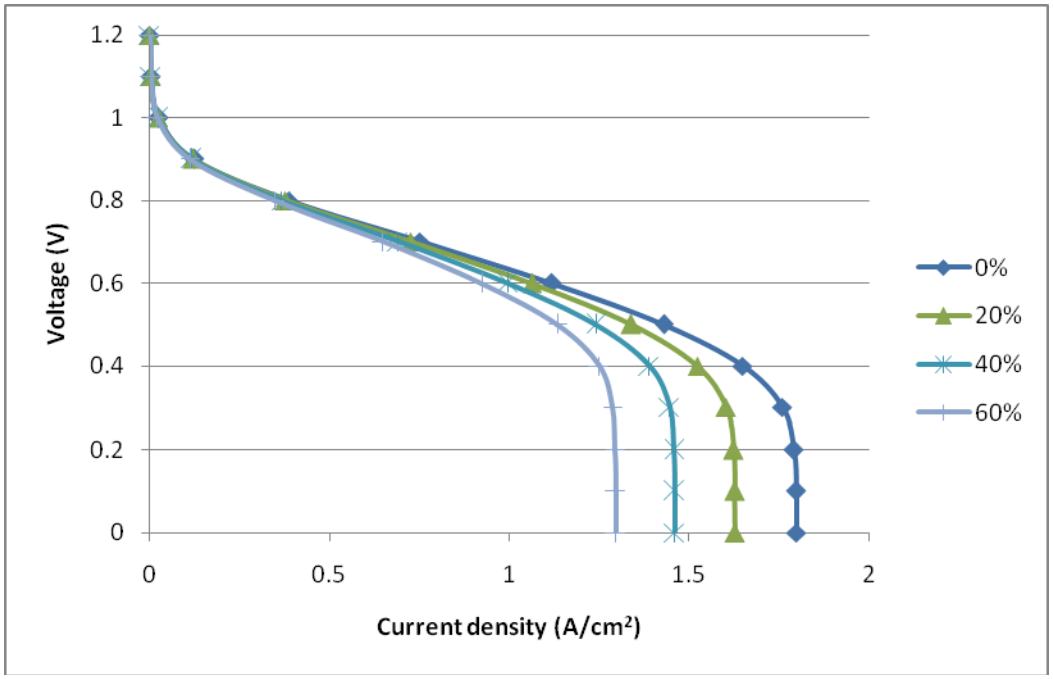

Figure 5.2 Polarization curves illustrating the effect of cathode inlet humidity

5.1.1 1D Model Validation

The 1D model was first validated by comparing the results with other models found in the literature. Figure 5.3 below is a polarization curve from a model by Weng et al. (2008). It shows very similar results to the above polarization curves generated from the 1D model.

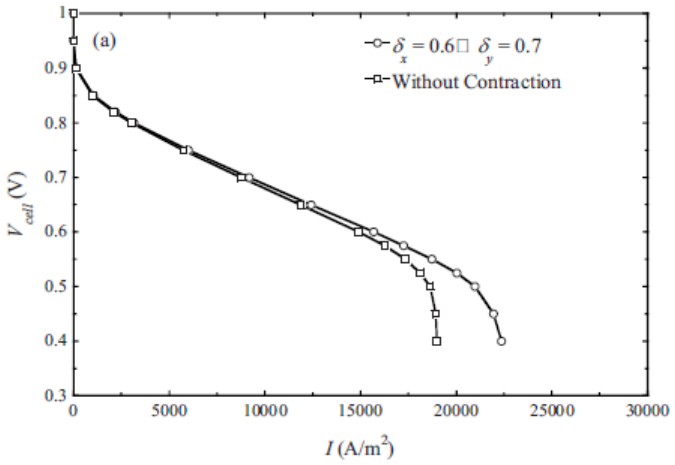

Figure 5.3 Polarization curve by Weng et al. (2008)

The model was also validated by comparing it to experimental results of a single cell. Having access to a cell allowed access to the fuel cell parameters that may not have been available from the literature, and control the operating conditions of the cell. The tests were performed on a single cell from Fuel Cell Technologies Inc. (FCT). This cell has a triple serpentine flow pattern with an active area of 25 cm^2. It uses a Nafion 115 membrane and an SGL 10BC GDL. This GDL has a microporous and a macroporous layer, however, the specification sheet gives only one value of porosity, so it will be assumed that this is an average property for the GDL. A polarization curve was produced for the operating conditions given in Table 5.1 below.

Table 5.1 Operating conditions for the FCT single cell

Cell Temperature:	60 °C
Anode Dew Point:	60 °C (100% RH)
Cathode Dew Point:	36 °C (30% RH)
Anode Flow Rate:	0.32 SLPM
Cathode Flow Rate:	0.75 SLPM

The cell was held at a constant current density while the voltage was measured for each of the points shown in Figure 5.4 below. The flow rates were chosen to correspond to an air stoichiometry of 1.5 when the test was at its highest current density.

The cell parameters and operating conditions were inputted into the 1D model and the result was the following figure.

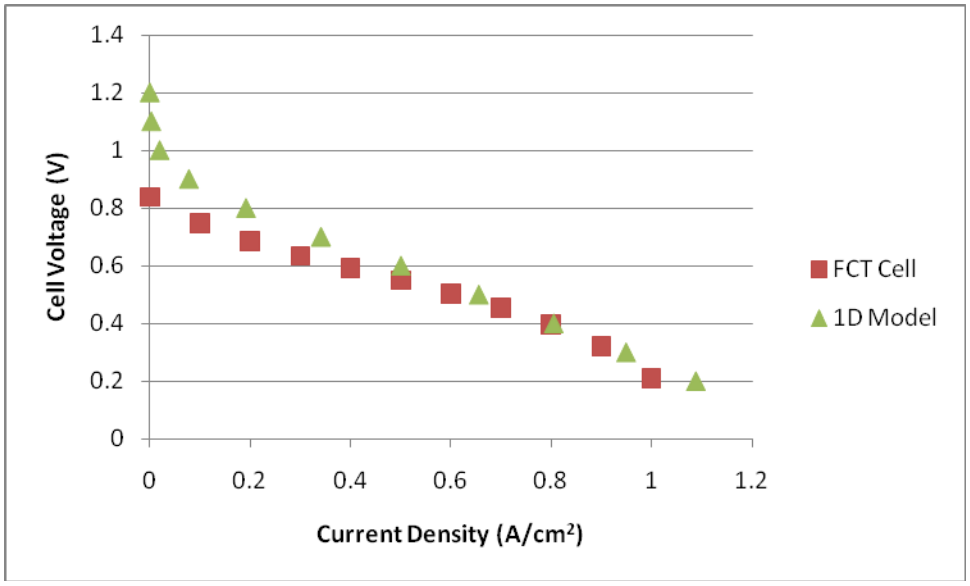

Figure 5.4 Comparison of Fuel Cell Technology cell and the 1D model used to represent it

The model gave relatively good agreement with the test cell. The open circuit voltage is lower in the test cell than in the model. This is because the model does not account for any non-idealities in the open circuit voltage such as fuel crossover. The model also does not predict the point of concentration polarization. However it is promising that the results are as similar as they are.

5.2 2D Flow distribution and current density approximation

As a first approximation, a 2D representation of the flow pattern with a reaction rate based on the concentration of oxygen was used to quantify the effectiveness of the bipolar plate flow pattern designs. Oxygen was chosen because the cathode is the limiting electrode in a PEM fuel cell. This method is not a completely accurate approximation since other variables also affect the current density, but it was found that the effect of oxygen concentration was the greatest.

Using values of oxygen concentration ranging from 0.25 mol/m^3 to 9.5 mol/m^3, current density was calculated using the 1D model, keeping all other variables constant. A cell voltage of 0.3 V was used since it is in the high power operating range where the fuel cell is most likely to be sensitive to fluctuations. A curve was fit to these data to describe the effect of oxygen concentration on the current density of the cell (See Figure 5.5 below). Equation (60) describes

the relationship between current density and oxygen concentration. Note that the intercept in the equation is very small relative to the scale.

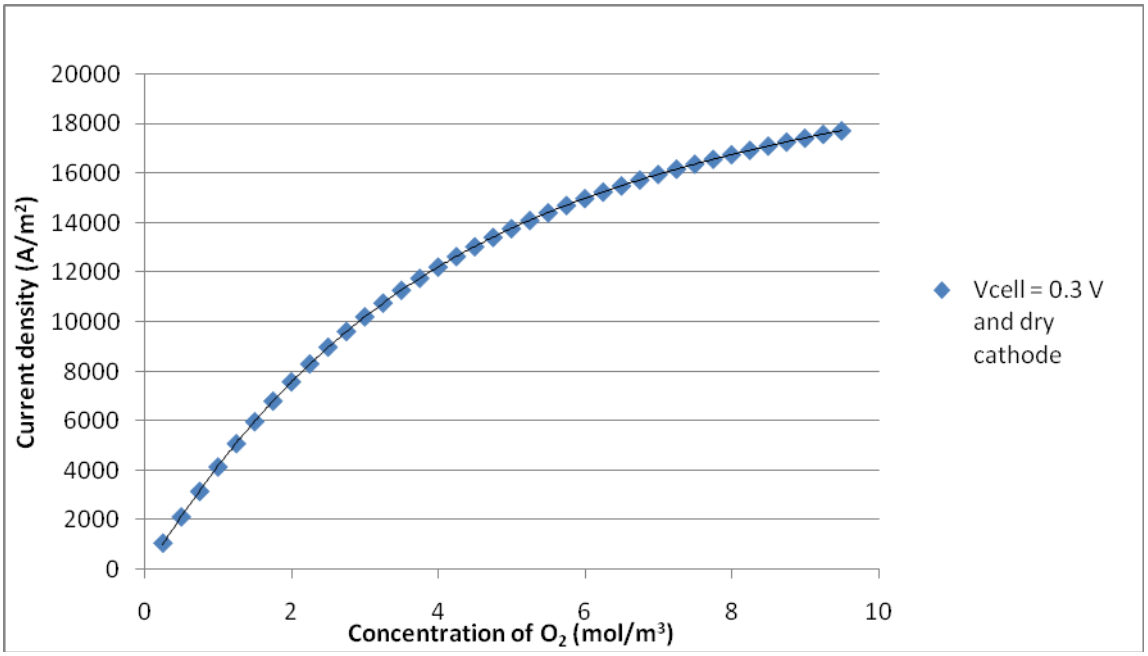

Figure 5.5 Graph of effect of oxygen concentration on cell current density

$$i_{approx} = -0.9258c_{O2}^4 + 36.508c_{O2}^3 - 579.76c_{O2}^2 + 4890.1c_{O2} - 156.66 \quad (60)$$

For the approximation, the Navier-Stokes equation is coupled with a species equation. The cathode was the only side considered for this approximation, and oxygen the only species. The species equation was as follows:

$$\nabla \cdot \left(-D_{O2N2}\nabla c_{O2}\right) + \mathbf{u} \cdot \nabla c_{O2} = -\frac{i_{approx}}{4F} \quad (61)$$

The binary diffusion coefficient was used in this case since the amount of liquid water was not quantified. Thus only oxygen and nitrogen are present. The second term on the left is the advection term, accounting for the movement of oxygen due to flow. Unlike the previous

models described, this one has a reaction term. This is because the 2D domain that is being modeled is a representation of the catalyst layer of the fuel cell.

5.2.1 2D Flow Pattern Comparison

All of the flow pattern designs are compared to a standard parallel flow pattern, with twenty-five 1 mm parallel channels connected by 1 mm channels on either side. They are also compared to a commercially available triple serpentine flow pattern; this is the flow pattern that is present in the single cell that was tested for comparison with the 1D simulation. The results using the triple serpentine pattern are not expected to be similar to what would be obtained with that cell since the approximation is based on initial parameters and conditions described in Chapter 4, not on the parameters and conditions of that cell. It is used only as an example of a serpentine flow field for comparison.

To quantify the effect of the different flow patterns, current density was used. The goal is to achieve an even current density over the surface of the catalyst. The minimum and maximum current density was calculated to give the range. In addition the average over the surface was also calculated as another measure of the quality of the flow pattern. Let us first take a look at the current density over the surface of the catalyst.

The following figures show the resulting current density across the flow field for each of the flow field designs. Each has been plotted with the same current density scale for ease of comparison. The inlet is at the bottom left and the outlet is at the top right. The first thing to notice is that the standard parallel design (Figure 5.6) has an area of relatively low current density. In fact, this trend has been observed before in a study by Jung et al. (2007) and by Barreras et al. (2005) who each numerically and experimentally investigated a standard parallel flow pattern that was commercially available. The triple serpentine flow field (Figure 5.7) has a much more even current density in this case due to the even velocity field. In this approximation, current density is highly dependent on velocity field.

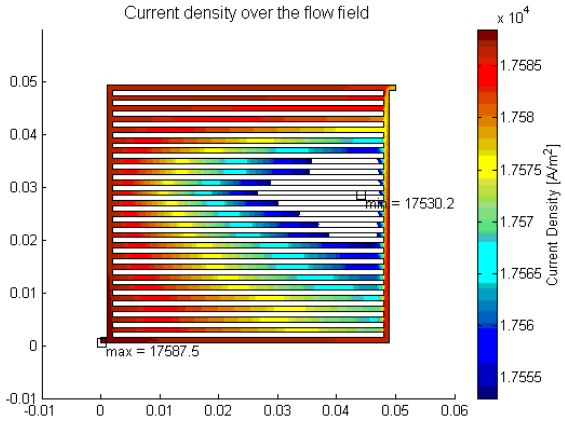

Figure 5.6 Standard parallel flow field

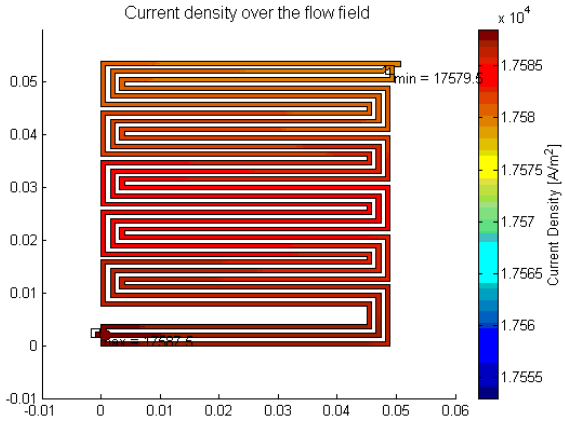

Figure 5.7 FCT triple serpentine flow field

The parallel designs that were inspired by solute excretion in plants (Figures 5.8 and 5.9) appear to have a similar problem to the standard parallel design in that that an even velocity field is not achieved and thus leads to an uneven current density distribution.

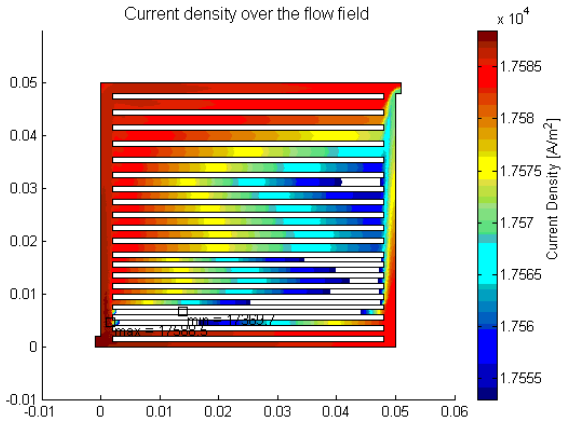

Figure 5.8 Parallel design large near outlet

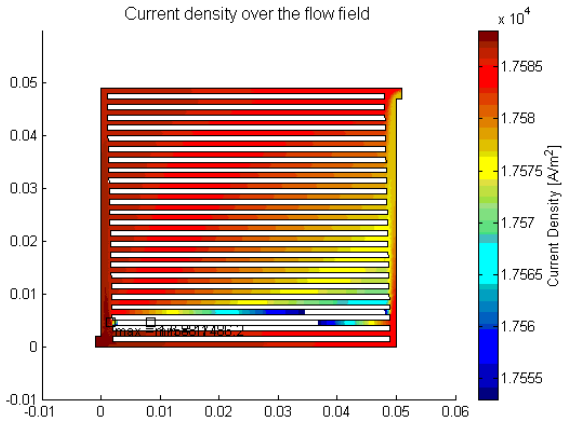

Figure 5.9 Parallel design increasing outlet

The design that is inspired by cell connections in plants (Figure 5.10) has a current density distribution that is much more even than the standard parallel, but still has areas of low current

density. The design with multiple inlets that was inspired by the lymph system (Figure 5.11) appears to be very even, keeping with the concept that multiple sources of pure gas will keep the reactant concentration high over the flow field.

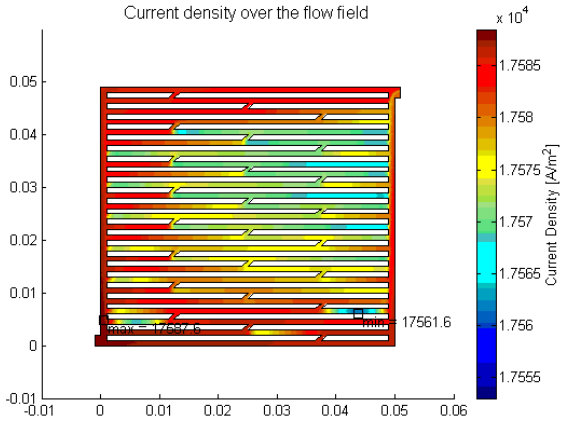

Figure 5.10 Parallel design with connections

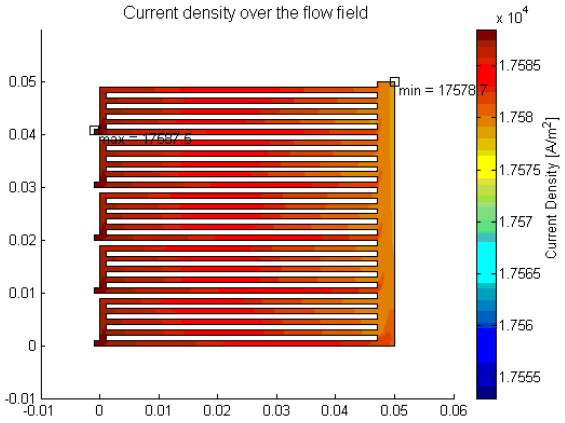

Figure 5.11 Parallel design with multiple inlets

All three of the designs that used Murray's law of branching (Figures 5.12, 5.13 and 5.14) produced relatively even current density across the flow field. Even the design that was modelled after a parallel flow pattern but using Murray's law for the branching strategy gave very good results.

After looking at all of the results, the designs with the most even current density appear to be Murray's law 1, Murray's law 3, Parallel with multiple inlets and the triple serpentine.

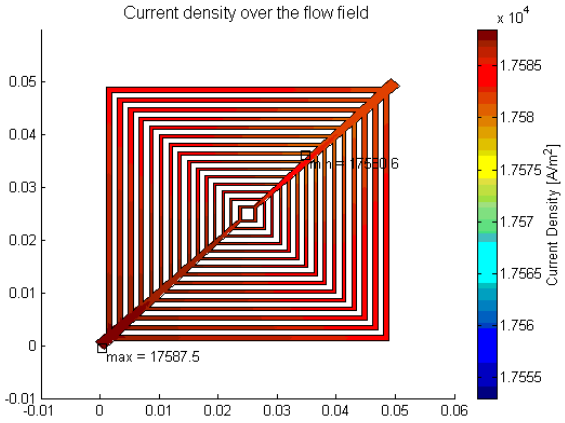

Figure 5.12 Murray 1 flow field

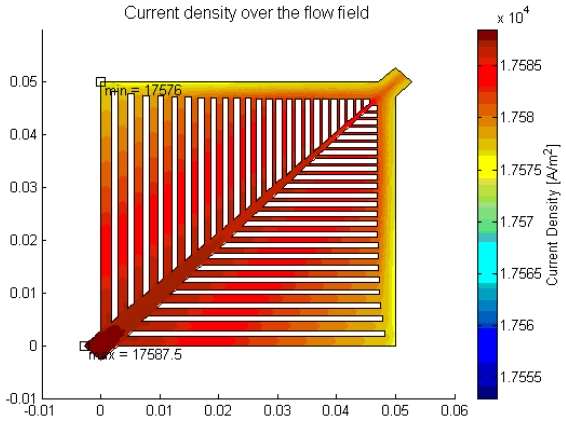

Figure 5.13 Murray 2 flow field

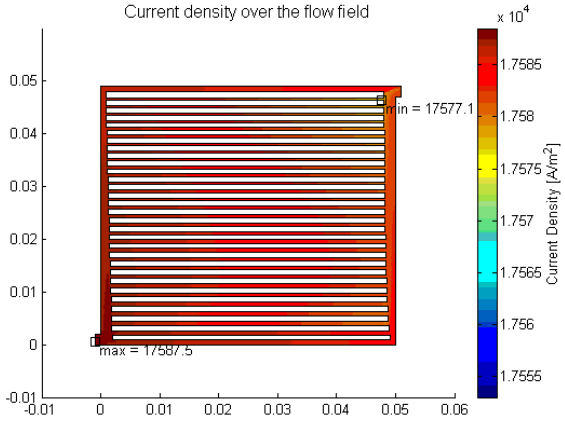

Figure 5.14 Murray 3 flow field

Table 5.2 below shows these results in numerical form, giving the maximum, minimum, range and average current density for each of the designs. These results quantify the visual results above and show that the flow pattern that gives the most even current density distribution is Murray's law 1 with an average current density of 17584.4 A/m^2. This one is followed closely by the triple serpentine and the multiple inlet design.

Table 5.2 Current density results of 2D approximation

Model	i_{MAX} (A/m^2)	i_{MIN} (A/m^2)	i_{RANGE} (A/m^2)	i_{AVG} (A/m^2)
Parallel Standard	17587.5	17530.2	57.3	17573.9
FCT Triple Serpentine	17587.5	17579.5	8.0	17583.6
Parallel Increasing	17588.1	17486.2	101.9	17579.8
Parallel Large Outlet	17588.5	17369.7	218.8	17571.3
Connections	17587.6	17561.6	26.0	17578.5
Multiple Inlet	17587.5	17578.7	8.8	17583.3
Murray 1	17587.5	17580.6	6.9	17584.4
Murray 2	17587.5	17576.0	11.7	17582.5
Murray 3	17587.5	17577.1	10.4	17584.2

5.3 2D Straight channel

The 2D model results show how the current density will change along the channel of a fuel cell. The following results are for a cell operating at 0.3 V and a dry cathode, with an inlet velocity of 0.5 m/s on both the anode and the cathode. Along a length of 10 cm the results show a significant drop in the current density, with the majority of this drop occurring at the beginning of the channel (See Figure 5.15 below). This trend has also been observed in models by Yi and Van Nguyen (1998) and by Siegel et al. (2004). The results of these models are shown in Figure 5.16.

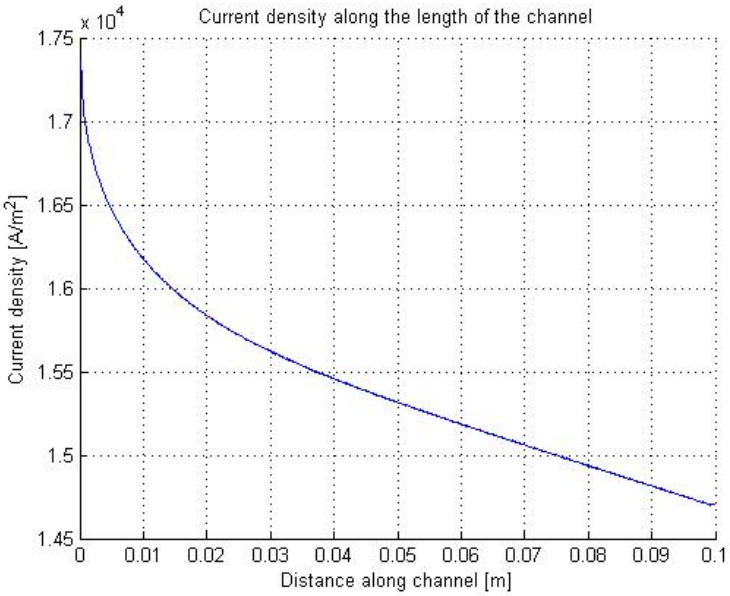

Figure 5.15 Current density along a 10 cm straight channel

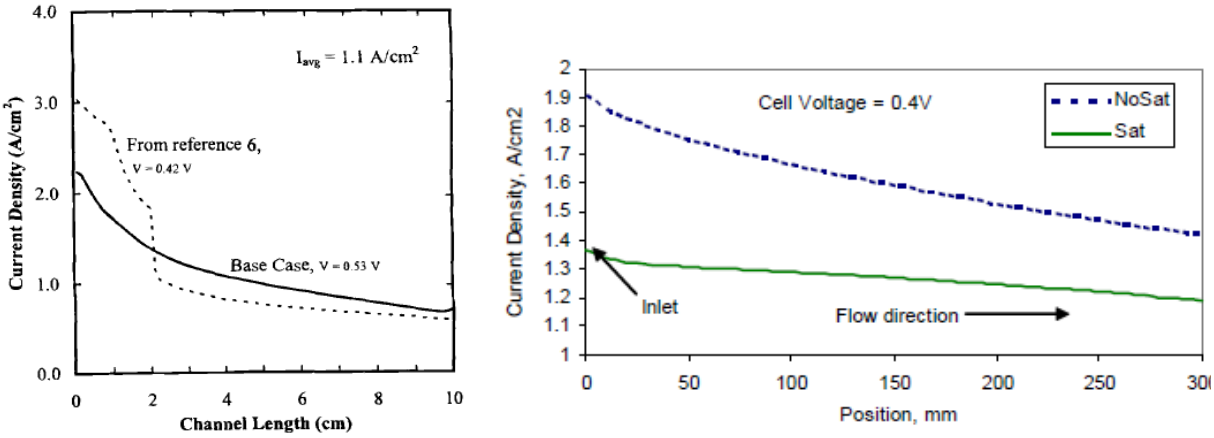

Figure 5.16 Current density along the channel from Yi and VanNguyen (1998) and from Siegel et al. (2004)

The figure below (Figure 5.17) shows the change in species along the channel of the fuel cell.

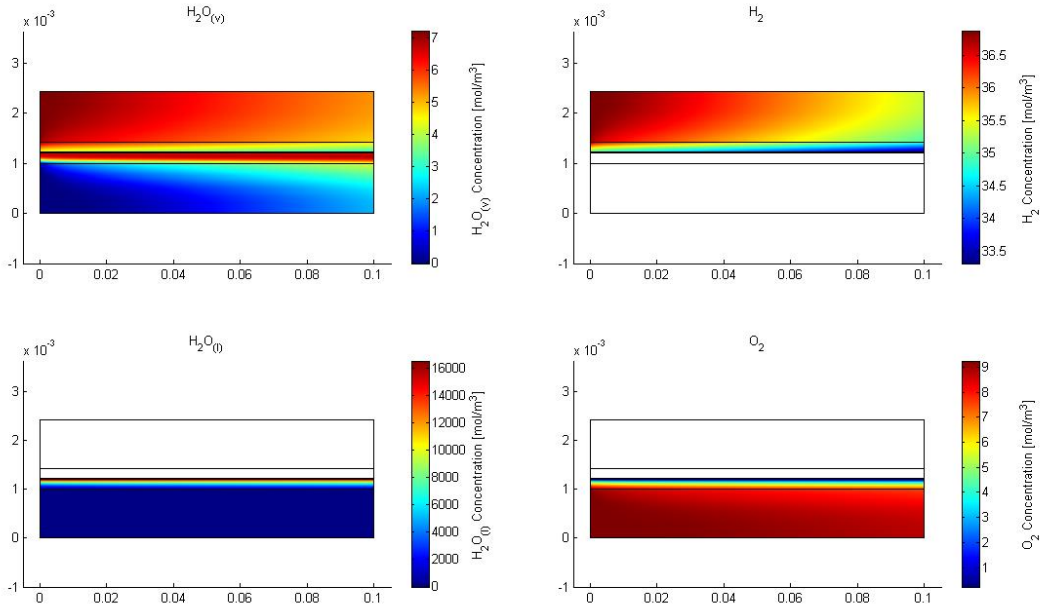

Figure 5.17 Water vapour, hydrogen, liquid water and oxygen profiles in a 10 cm straight channel

5.4 3D Model Results

The following section first gives a comparison between the 2D approximation and the 3D model. This evaluates the validity of the 2D approximation.

5.4.1 2D Approximation vs. 3D Model

The following two figures show the results of the 2D approximation in a straight channel and results from the 3D straight channel model. Looking at the two figures, it is clear that the 2D approximation does not adequately model the change in current density along the channel of a fuel cell. The 3D results, like the 2D results, show a sharp drop in current density followed by a more gradual drop until the end. The 2D approximation does not capture this feature, having a more linear variation in current density along the channel. It is possible that this could result in the false identification of a superior flow pattern design. Therefore, a full 3D model of the flow

fields is necessary to evaluate the flow pattern designs numerically. However, as stated above, solving the 3D flow field model is too computationally intensive for the resources that are available.

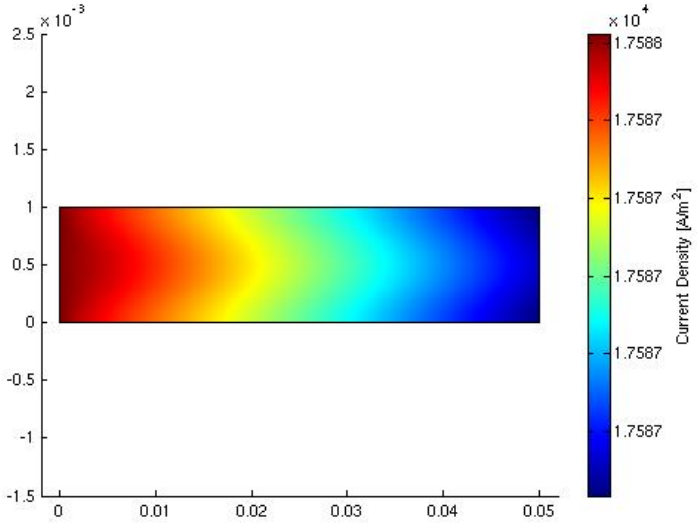

Figure 5.18 Current density along a 5 cm straight channel – 2D approximation results

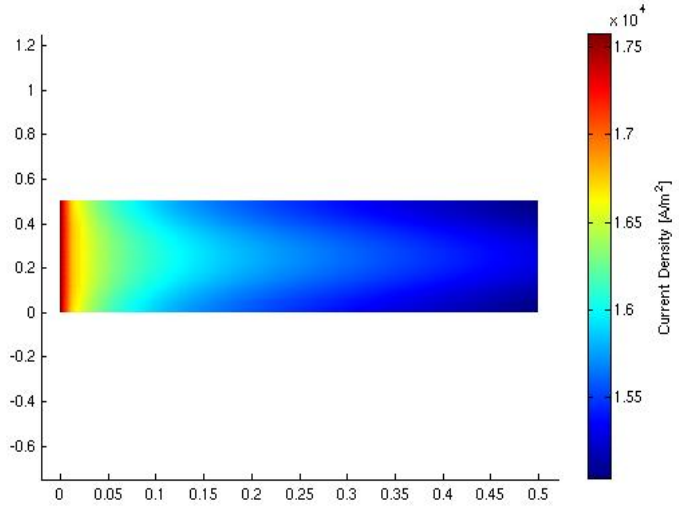

Figure 5.19 Current density along a 5 cm straight channel – 3D results

In order to evaluate the biomimetic flow field designs, a physical model was used. The following chapter gives a description of the flow field chosen for the physical model and the results of the testing.

6 Experimental Concept Validation

A 3D simulation could not be solved with the computing resources that were available. Experimental validation of the concept was chosen instead. This necessitated the construction of a bipolar plate incorporating the flow field of interest so that physical tests could be done to determine its performance.

While it has been determined that a 2D flow channel approximation is insufficient to determine the quality of the flow field, the 2D flow field comparison (Section 5.2.1) was revisited in order to determine which flow field to produce for the physical test,. In section 5.2.1, the flow fields were compared using an approximation of the current density across the flow field that consisted of a correlation based on the 1D model and a 2D flow simulation. It was found in that section that the biomimetic flow field that gave the most even current density was the Murray 1 flow field. This flow field was inspired by Murray's law of branching in plants and animals. Accordingly, the Murray 1 flow field was chosen for the experimental validation.

6.1 Test Fuel Cell

The test fuel cell is from Fuel Cell Technologies Inc.; it is a 25 cm^2 cell that originally came with a triple serpentine flow field. The membrane and GDL were purchased from Ion Power Inc. The membrane is a Nafion 115 catalyzed membrane electrode assembly, and the GDL is an SGL 10 BC carbon paper felt-type GDL.

6.2 Flow Field Comparison

As mass transfer limitations are most problematic on the cathode side, the flow field evaluation was carried out only on the cathode side. A new cathode side bipolar plate incorporating the Murray 1 flow field design was constructed by the same manufacturer that made the original triple serpentine plate, Entergis Inc. The plate material was AXF-5Q graphite and the Murray 1 flow field plate was pyrosealed after machining as was the original. Each flow field covers a 25 cm^2 active MEA area and has a 1 mm inlet and outlet. Figure 6.1 below shows the two bipolar plates that were used for this experiment (See Appendix A for a drawing of each of the bipolar plates, with dimensions). Both are cathode side bipolar plates.

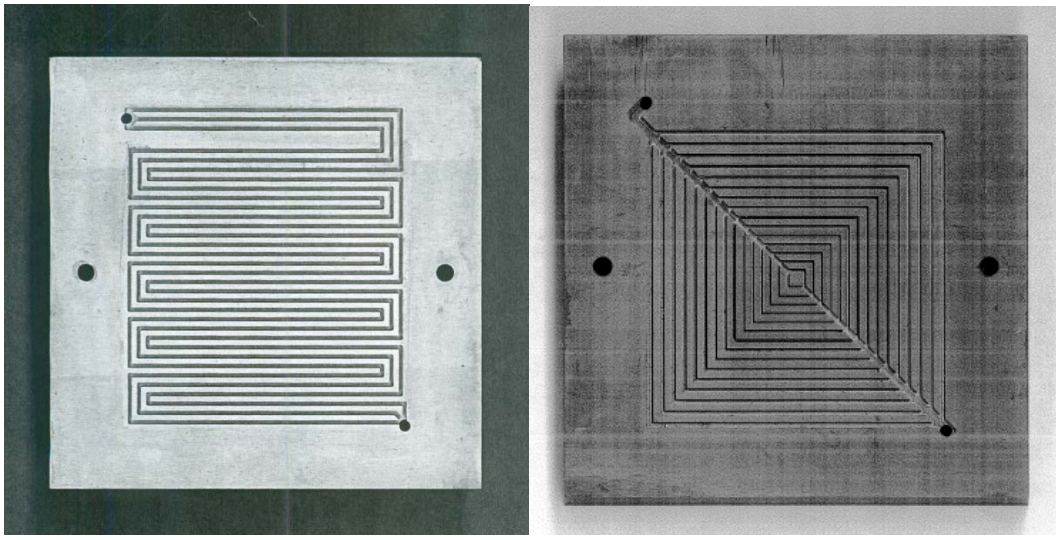

Figure 6.1 Triple Serpentine and Murray 1 bipolar plates

The channel to land ratio for the two cells is not equal. The triple serpentine flow field is 1176 mm^2 (channel:land = 0.89) and the Murray's law flow field is 1113 mm^2 (channel:land = 0.80). While the channel to land ratio has been shown in other studies to have an effect on performance (Akbari et al., 2008), it is mostly at very low ratios, around 0.5, that the effect is very great (See Figure 6.2 below). It is assumed that the differences in the design of the flow field will have a greater effect on the cell performance. This is a very conservative assumption since Figure 6.2 shows that the higher channel width/rib width will achieve a slightly higher current density at low voltages (high power), the advantage here would be to the triple serpentine flow field. Thus, any improvement shown by the Murray 1 flow field design will be significant. The red vertical line in Figure 6.2 shows the optimum channel to land ratio for each voltage.

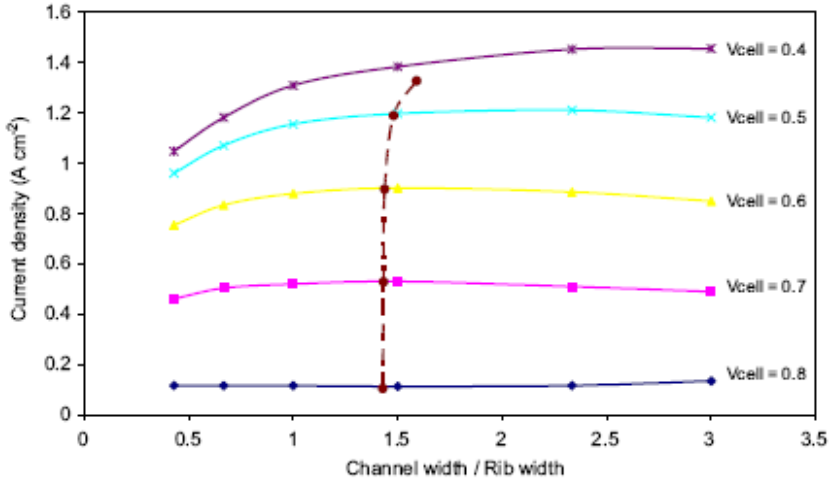

Figure 6.2 Current density versus channel width to land width ratio at several cell voltages (Akbari et al., 2008)

Another aspect of the flow fields that will be investigated is the pressure drop across the flow field. Murray's law exists in plants because it provides a low resistance to flow. Accordingly, the Murray 1 flow field should also provide a lower resistance to flow, a lower pressure drop. The 2D approximation model also predicts a lower pressure drop for the Murray 1 flow field when compared to the triple serpentine flow field.

6.3 Test Set-Up

The tests were performed using a test station from Scribner Associates Inc., model number 850e. This test station has the ability to supply reactant gasses at a desired temperature and humidity, and keep the cell at a desired temperature. The load can either set the current or the voltage. The test station does not take pressure readings. A 140 cm water manometer was used to measure the differential pressure across the flow fields. This range was enough for the tests at low flow rates, but a greater range was required for high low rates. For these tests, a 1-15 psi pressure transducer was used (Omega PX142-015D5V).

Each of the two flow field tests used a new membrane electrode assembly and GDL. Each time the cell was conditioned before testing at 70C and with 100% humidity on the anode and cathode for 30000s.

For each flow field five different tests were performed so that performance could be assessed under a range of conditions. Two parameters were varied, cathode flow rate and cathode humidity. Cathode flow rate was varied by changing the stoichiometric ratio of air that was fed into the cell. Stoichiometric air ratios of 1.5, 3 and 5 were used. These were done at a cathode relative humidity of 41%. Next, keeping the cathode flow rate constant at a stoichiometric air ratio of 5, the humidity was varied at 11%, 41% and 61%. Table 6.1 below lists the tests that were performed.

Table 6.1 Summary of conditions for the tests performed on the two flow fields

Test #	Fuel Conditions	
	Cathode Stoich ratio	Cathode Temperature Set Point
M9/TS1	5	34C (11% RH)
M13/TS2	1.5	59C (41% RH)
M11/TS3	3	59C (41%RH)
M10/TS4	5	59C (41% RH)
M12/TS5	5	68C (61% RH)

6.4 Results

Both flow fields were tested as described above. The results of these tests are presented below.

6.4.1 Murray 1 Flow Field

The Murray's law inspired flow field gives poor performance at low flow rates. Comparing the tests at a constant 41% cathode relative humidity and varying cathode stoichiometries, the high stoichiometries are seen to have better performance (Figure 6.3). The test done at a cathode stoichiometry of 1.5 is unable to perform when the current density drawn is higher than 0.4 A/cm^2; but as the stoichiometry is increased, higher current densities can be drawn.

This low performance at low stoichiometries is likely due to water, formed during the electrochemical reaction, blocking the channels and catalyst sites. As the current density increases, the rate of the reaction producing water increases, necessitating higher rates of water

removal. The Murray 1 flow field is a type of parallel flow field design, which is known to be less effective at water removal due to the presence of multiple paths. If one channel becomes blocked, the gasses can easily take another path, allowing the water to remain in the channel and block the reaction sites.

To further back up this theory, liquid water was observed during the testing at high current densities. Liquid water was seen in the outlet gas stream in the form of slugs that periodically were ejected from the cell. Also, the impact of these slugs forming and leaving could be seen in the cell voltage measurements. Looking at a graph of voltage versus time, decreases and increases in cell voltage were observed when the cell was operating at a constant current density. At the point of cell failure, it was these decreases in performance that finally brought the cell below its low voltage limit (0.1 V). Finally, upon disassembling the fuel cell, droplets of liquid water were observed in the flow channels.

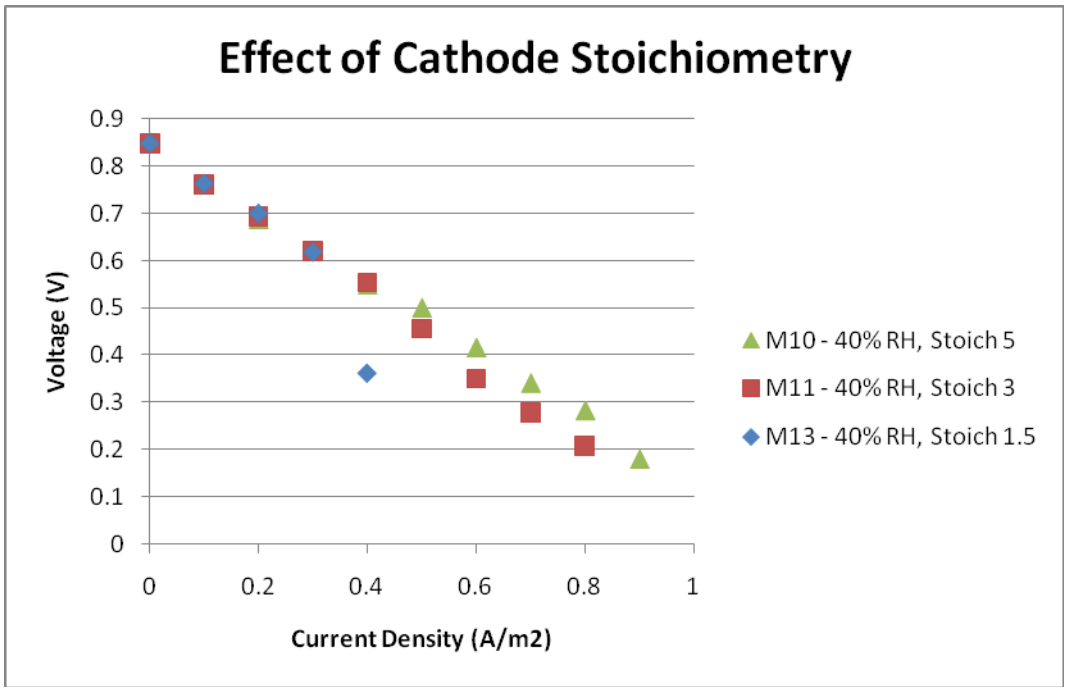

Figure 6.3 Effect of cathode air stoichiometry for the Murray 1 flow field

Cathode relative humidity also has an effect on the performance of the cell. Figure 6.4 shows that as the cathode relative humidity is increased, at a stoichiometric air ratio of 5, the performance improves. Specifically, this shows up as a decrease in the slope of the polarization curve, which indicates a decrease in the ohmic polarization (the resistance to either ionic or

electronic transport). In this case, it is likely the ionic resistance that is decreased since the more humidified the membrane, the easier ions transport though it. At this high stoichiometric air ratio it is likely that the inlet side of the membrane is dried when the relative humidity of the inlet air is low.

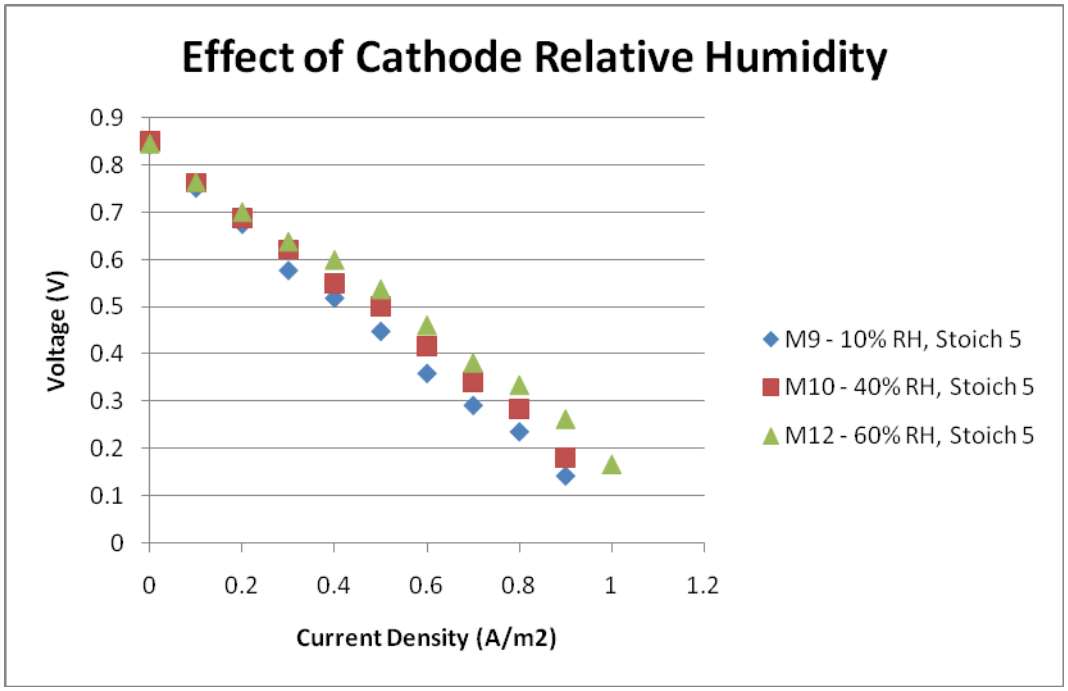

Figure 6.4 Effect of cathode relative humidity for the Murray 1 flow field

6.4.2 Triple Serpentine Flow Field

For the triple serpentine flow field, cathode air stoichometry does not seem to have a significant, if any, effect (Figure 6.5). At all the cathode air stoichiometries tested, the flow rate was high enough that the water was removed from the flow channels before it could cause a decrease in performance. The performance is slightly degraded at a cathode air stoichiometry of 5, suggesting that some drying of the membrane occurs at this high flow rate with only 40% relative humidity. Figure 6.6 shows the sensitivity of the triple serpentine flow field to relative humidity for a cathode air stoichiometry of 5.

In this case, liquid water was also observed in the cathode outlet gas stream. The cell voltage versus time also showed decreases and increases in performance. However, in this flow pattern,

the decreases were more easily overcome and did not seem to result in premature failure of the cell.

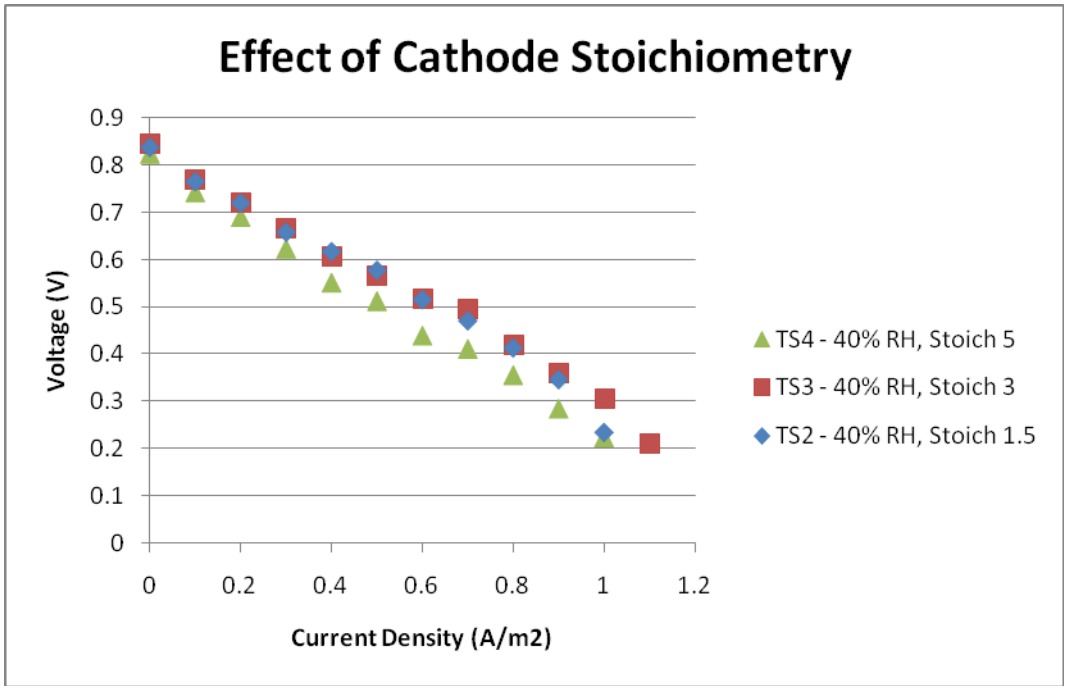

Figure 6.5 Effect of cathode air stoichiometry for the triple serpentine flow field

The triple serpentine flow field polarization curves (Figure 6.6) show a similar trend to those of the Murray flow field for cathode relative humidity. The slope of the polarization curve, indicating the ohmic polarization, decreases as the relative humidity is increased. However, the effect is greater for this flow field than for the Murray flow field. This may be a combined effect of the decreased resistance and the better ability of the triple serpentine to remove liquid water.

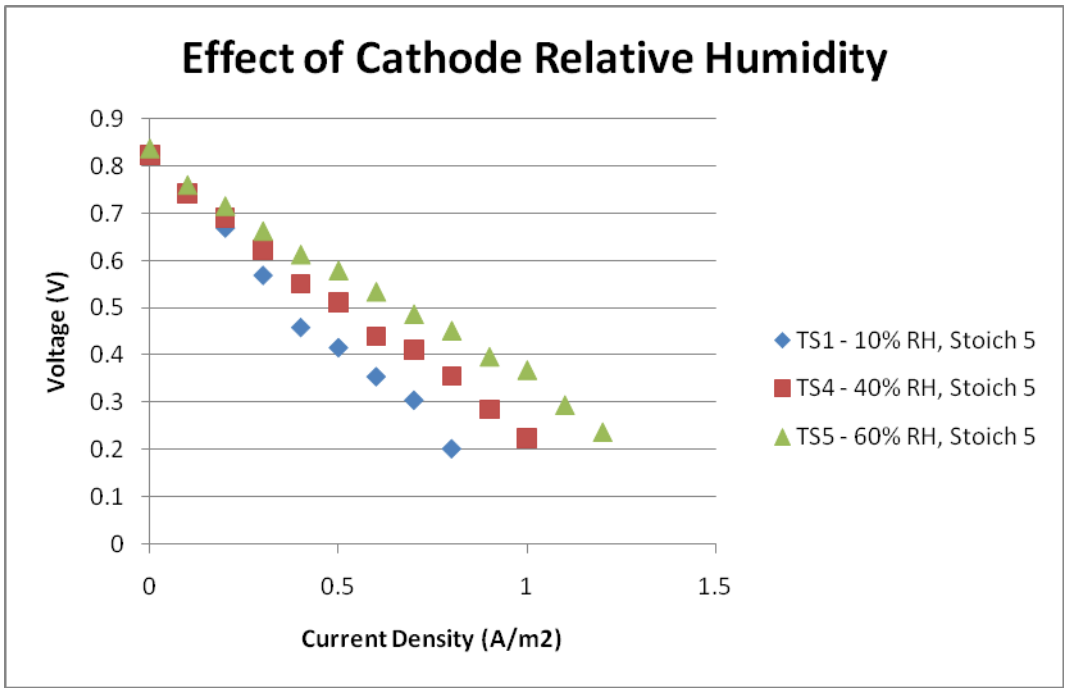

Figure 6.6 Effect of cathode relative humidity for the triple serpentine flow field

6.4.3 Comparison

For most of the tests performed on the two flow patterns, the triple serpentine performed better than the Murray inspired flow field in terms of the maximum current density and maximum power density that can be drawn from the cell (See Figures 6.8-6.11) . As discussed in previous sections, the poor performance of the Murray 1 flow field is believed to be due to the build-up of liquid water in the branches and the reduced pressure force available to remove liquid water once formed.

The low humidity test (10% relative humidity on the cathode side), however, gave different results (Figure 6.7). The Murray inspired flow field gives at least equal, and perhaps better performance at this low relative humidity. The two polarization curves almost completely overlap, except for at the high current density end (0.9 A/cm^2) of the Murray flow field curve, where the Murray flow field was able to give a voltage higher than 0.1 V (the test station cut-off voltage) and the triple serpentine was not. This indicates that there is less concentration

polarization for the Murray flow field, which means that there is a possibility that there is better oxidant distribution with the Murray flow field.

Looking at pressure drop across the flow field, the Murray inspired flow field consistently gives a lower pressure drop for all the tests performed. The triple serpentine flow field has long channels to flow the oxidant through, creating a large pressure drop. On the other hand, the defining feature of the Murray's law concept is low flow resistance due to its branching structure. A low pressure drop is very advantageous in a fuel cell because it reduces the parasitic load required to pump the fuel and oxidant gasses.

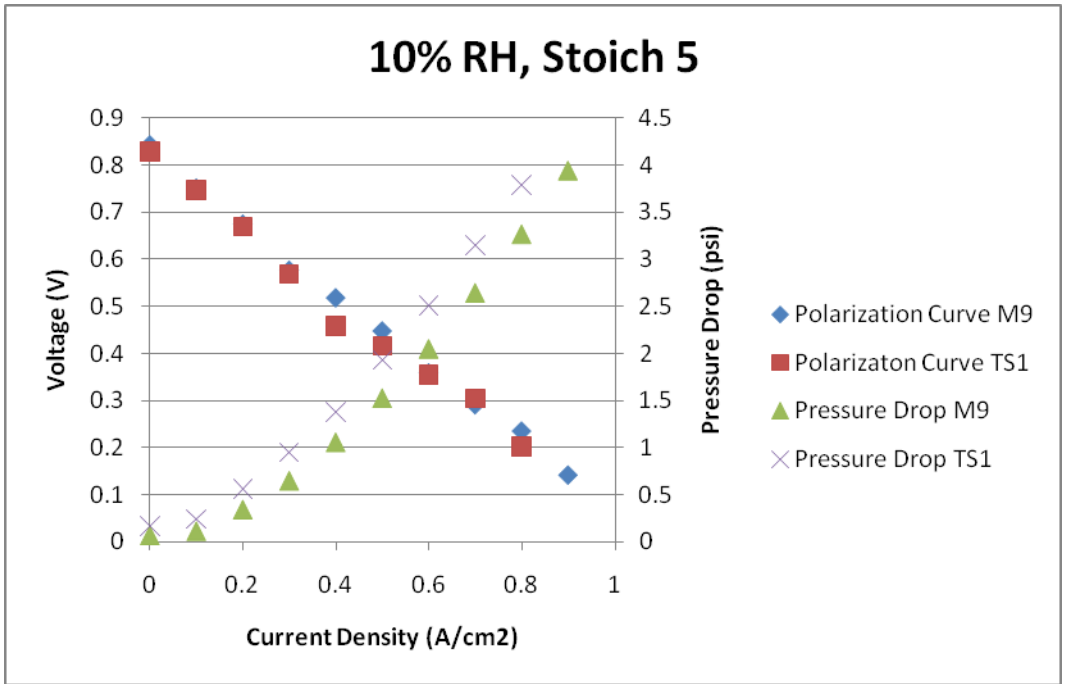

Figure 6.7 Comparison between the Murray 1 and triple serpentine flow fields at 10% cathode relative humidity and a cathode air stoichiometric ratio of 5

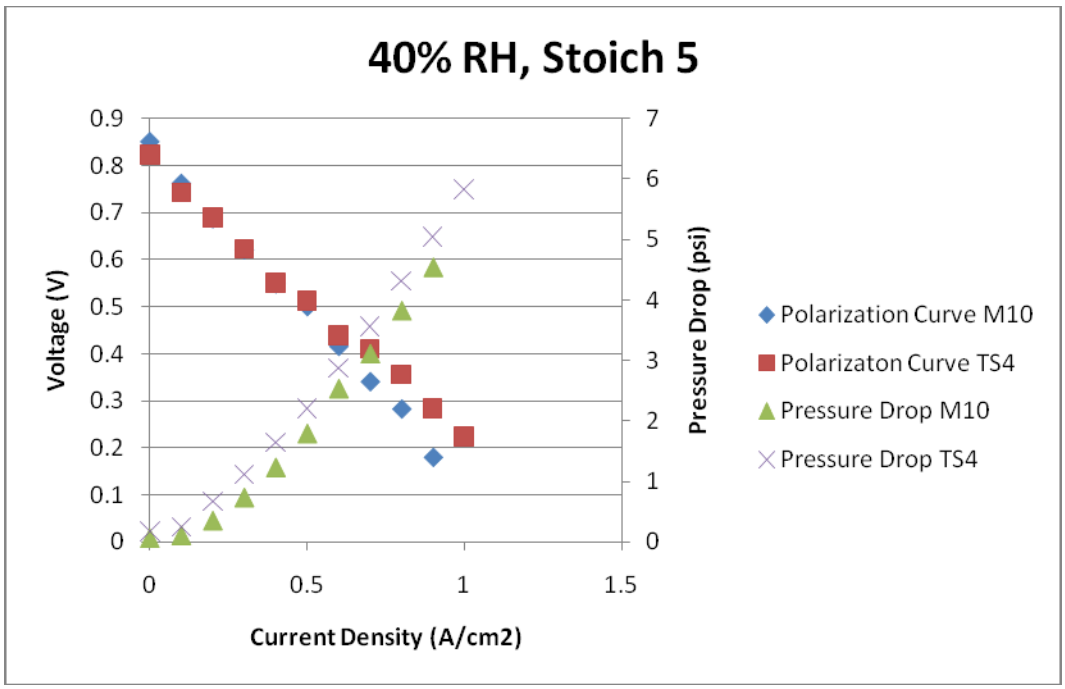

Figure 6.8 Comparison between the Murray 1 and triple serpentine flow fields at 40% cathode relative humidity and a cathode air stoichiometric ratio of 5

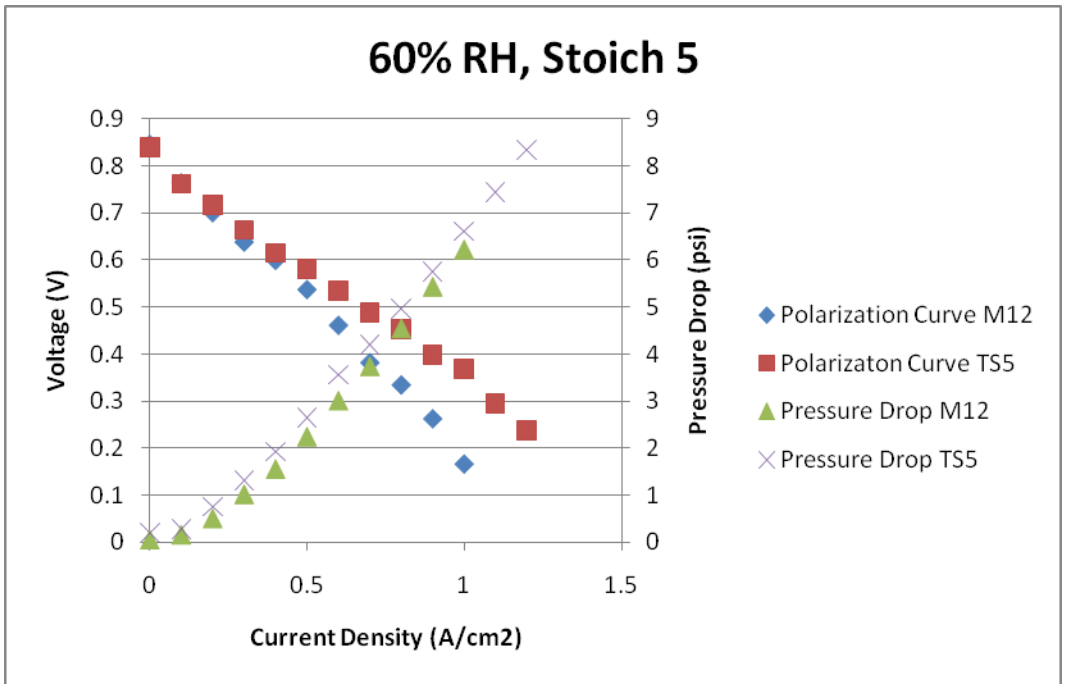

Figure 6.9 Comparison between the Murray 1 and triple serpentine flow fields at 60% cathode relative humidity and a cathode air stoichiometric ratio of 5

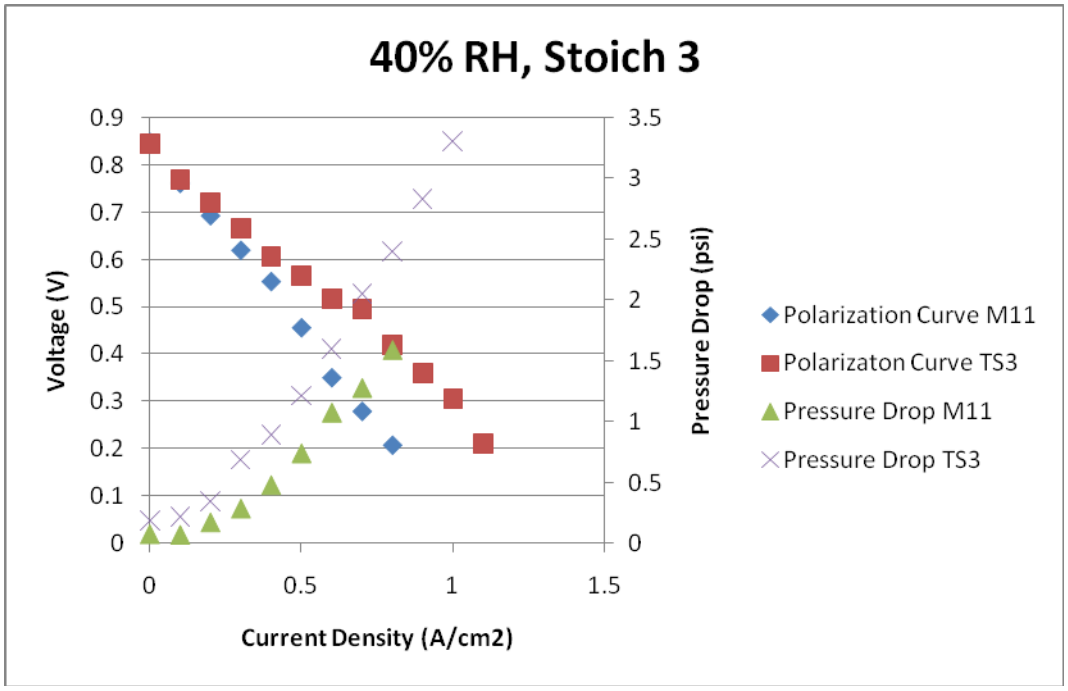

Figure 6.10 Comparison between the Murray 1 and triple serpentine flow fields at 40% cathode relative humidity and a cathode air stoichiometric ratio of 3

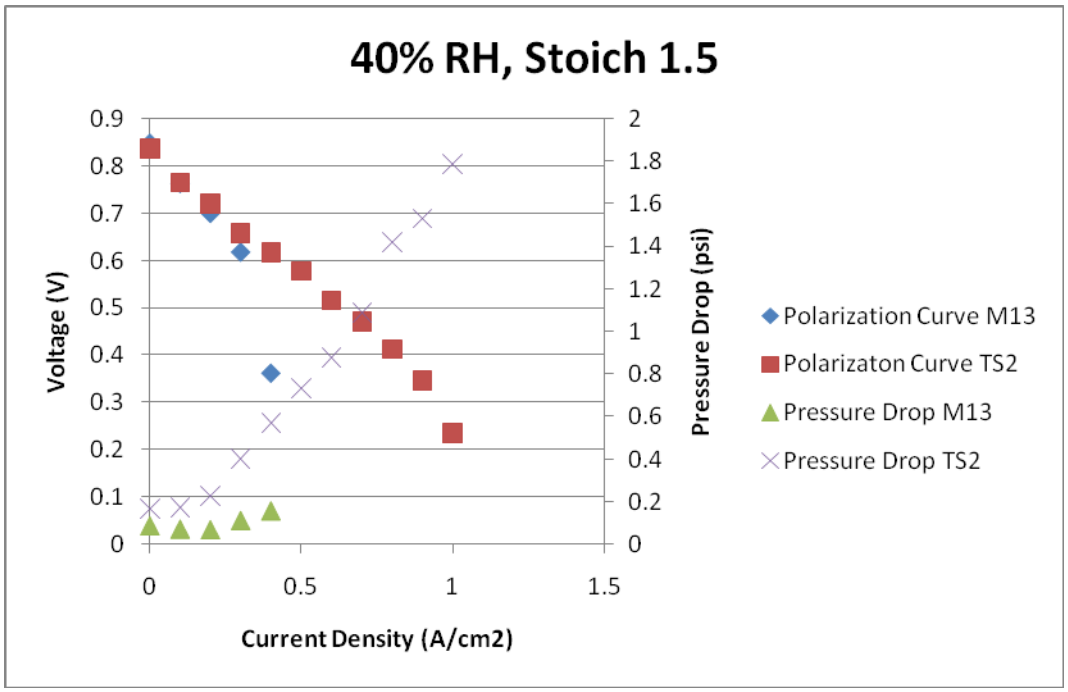

Figure 6.11 Comparison between the Murray 1 and triple serpentine flow fields at 40% cathode relative humidity and a cathode air stoichiometric ratio of 1.5

In summary, the tests show a much lower pressure drop with the Murray 1 flow field compared to the triple serpentine design. This is consistent with its branched design and also with the predictions of the 2-D simulation. A lower pressure drop reduces the parasitic power required to provide the cathode air flow. There is also evidence of better oxidant distribution from the lower concentration polarization at high current density in the low humidity case where liquid water build-up was minimized. On the other hand, the same reduced pressure drop also reduces the pressure force available to move liquid water from the individual branches. As the results showed, this can significantly reduce the fuel cell's ability to operate at high current density.

7 Conclusions

Biomimetic design techniques were applied to the redesign of a PEM fuel cell flow field. The particular problem that was investigated was distribution of fuel and oxidant across the surface of the gas diffusion layer. Using a keyword search of an undergraduate biology text book, phenomena were identified that could inspire solutions to this problem. From these phenomena, new concepts of flow field designs were developed. Numerical models of a PEM fuel cell with the different flow fields were developed to simulate the performance to validate the concepts. Computational limitations did not allow the final simulation to be solved. As a result, a physical model of the strongest design was produced and tested. Though the complete 3D flow field simulation could not be finished at this time, having a complete 3D straight channel has the opportunity to provide insight into other fuel cell processes, aiding further fuel cell research.

The flow field design that was produced and tested was based on Murray's law of branching in plants. The results showed that liquid water formation caused poor performance at low flow rates for the Murray's law inspired flow field. However, when a high flow rate was used, the performance of the Murray's law inspired flow field matched that of the triple serpentine flow field used as a control for testing. In addition, an improvement in pressure drop across the low field was found in the Murray's law inspired flow field. This suggests that this new flow field design could help reduce parasitic loads when applied in a fuel cell with high flow rate.

Thus, biomimetic design was found to be useful in inspiring design solutions for a PEM fuel cell flow field. Since liquid water was identified as a significant problem in this flow field, biomimetic design could be employed again to try and solve this aspect of the problem. A keyword like 'bypass' for bypassing the liquid water to get to the reaction sites could be a starting point in identifying new biological phenomena.

On the other hand, there is significant research on-going into the development of high temperature proton exchange membranes that can operate at temperatures above 100°C where water is always in the vapour state. A Muuray's law flow field combined with a high temperature membrane could offer a significant mass transfer improvement at high current densities combined with a lower parasitic loss.

References

Akbari, M.H. and Rismanchi, B. "Numerical investgtion of flow field configuration and contact resistance for PEM fuel cell performance." Renewable Energy. 33 (2008) 1775-1783.

Altshuller, G.S., *Creativity as an Exact Science*, Gordon and Breach Science Publishers Inc., New York, 1988.

Amphlett, J.C., Baumert, R.M., Mann, R.F., Roberge, P.R. and Harris, T.J. "Perforance modeling of the Ballard Mark IV solid polymer electrolyte fuel cell." Journal of the Electrochemical Society." 142 (1995) 1-8.

Atwell, B., P. Kriedmann, C. Turnbull, 2001, *Plants in Action: Adaptations in Nature, Performance in Cultivation*, MacMillian Publishers Australia Pty. Ltd., South Yarna.

Barreras, F., Lozano, A., Valino, L., Marin, C. and Pascau, A. "Flow distribution in a bipolar plate of a proton exchange membrane fuel cell: experments and numerical simulation studies." Journal of Power Sources. 144 (2005) 54-66.

Barreras, F., Lozano, A., Valino, L., Mustata, R. and Marin, C. "Fluid dynamics performance of different bipolar plates - Part I. Velocity and pressure fields." Journal of Power Sources. 175 (2008) 841-850.

Baschuk, J.J. and Li, X. "Modelling of polymer electrolyte membrane fuel cells with variable degrees of water flooding." Journal of Power Sources. 86 (2000) 181-196.

BASF Gas Diffusion Electrode

Bernardi, D.M. and Verbrugge, M.W. "A mathematical model of the solid polymer electrolyte fuel cell." Journal of the Elctrochemical Society. 139 (1992) 2477-2491.

Bernardi, D.M. and Verbrugge, M.W. "Mathematical model of a gas diffusion electrode bonded to a polymer electrolyte." AIChE Journal. 37 (1991) 1151-1163.

Chiu, I., L.H. Shu, 2005, "Bridging cross-domain terminology for biomimetic design," *Proceedings of ASME DETC/CIE*, Long Beach, CA. DETC2005-84908 (DTM).

COMSOL AB, 2007, *COMSOL Multiphysics User's Guide,* Version: October 2007 COMSOL 3.4, Stockholm.

Debe, M.K. and Herdtle, T. "Design and development of a novel flow field for Pem fuel cells to obtain unform flow distribution." Electrochemical Society Transctions. 1 (2006) 581-604.

DuPont Nafion PFSA Membranes – NE-1135, N-115, N-117, NE-1110 (2005) (used N-117)

Fuller, E.N., Schettler, P.D. and Giddings, J.C. "A new method for predicton of binary gas phase difusion coefficients." Industrial and Engineering Chemistry. 58 (1966) 19-27.

Fuller, T.F. and Newman, J. "Water and thermal mangament in solid-polyer-electrolyte fuel cells." Journal of the Electrochemical Society. 140 (1993) 1218-1225.

Gazzarri, J.I. and Kesler, O. "Electrochemical AC impedance model of a solid oxide fuel cell and its application to diagnosis of multiple degradation modes." Journal of power Sources. 176 (2007) 100-110.

Gurau, V., Liu, H., and Kakac, S. "Two-dimensional model for proton exchange membrane fuel cells." American Institute of Chemical Engineers Journal. 44 (1998) 2410-2422.

Hacco, E., L.H. Shu, 2002, "Biomimetic Concept Generation Applied to Design for Remanufacture", *Proceedings of ASME DETC/CIE*, Montreal, QC, Canada, DETC2002/DFM-34177.

He, W., Yi, J.S. and Van Nguyen, T. "Two-phase model of the cathode of PEM fuel cells using interdigitated flow fields." American Institute of Chemical Engineers Journal. 46 (2000) 2053-2064.

Heinzel, A., Nolte, R., Ledjeff-Hey, K. and Zedda, M. "Membrane fuel cells - concepts and system desgn." Electrochmica Acta. 43 (1998) 3817-3820.

Hinatsu, J.T., Mizuhata, M., and Takenaka, H. "Water uptake of perfluorosulfonic acid membranes from liquid water and water vapour." Journal of the Electrochemical Society. 141 (1994) 1493-1498.

Hsieh, S.-S. and Huang, Y.-J. "Measurements of current and water distribution for a micro-PEM fuel cell with different flow fields." Journal of Power Sources. 183 (2008) 193-204.

Hung, A.-J., Sung, L.-Y., Chen, Y.-H. and Yu, C.-C. "Operation-relevant modelling of an experimental proton exchange membrane fuel cell." Journal of Power Sources. 171 (2007) 728-737.

Hwnag, J.J., Chang, W.R., Peng, R.G., Chen, P.Y. and Su, A. "Experimental and numerical studies of local current density." International Journal of Hydrogen Energy. 33 (2008) 5718-5727.

Jeon, D.H., Greenway, S., Shmpalee, S. and VanZee, J.W. "The effect of serpentine flow field designs on PEM fuel cell performance." International Journal of Hydrogen Energy. 33 (2008) 1052-1066.

Jones, F.E. *Evaporation of Water: With Emphasis on Applications and Measurements*. Lewis Publishers. Chelsea, Michigan: 1992.

Jung, G.-B., Su, A., Tu, C.-H., Lin, Y.-T., Weng, F.-B. and Chan, S.-H. "Effects of cathode flow fields on direct methanol fuel cells - simulation study." Journal of Power Sources. 171 (2007) 212-217.

Kim, S. and Hong, I. "Effect of flow field design on the performance of a proton exchange membrane fuel cell (PEMFC)." Journal of Industrial Engineering Chemistry. 13 (2007) 864-869.

Kloess, J.P., Wang, X., Liu, J., Shi, Z. and Guessous, L. "Investigation of bio-inspired flow channel designs for bipolar plates in proton exchenge membrane fuel cells." Journal of Power Sources. 188 (2009) 132-140.

Li, X. and Sabir, I. "Review of bipolar plates and PEM fuel cells: Flow-field designs." International Journal of Hydrogen Energy. 30 (2005) 359-371.

Li, X., 2006, *Principles of Fuel Cell*, Taylor & Francis Group, New York.Lin, G., He, W. and Van Nguyen, T. "Modeling liquid water effects in the gas diffusion and catalyst layers of the cathode of a PEM fuel cell." Journal of the Electrochemical Society. 151 (2004) A1999-A2006.

Liu, H.C., Yan, W.M., Soong, C.Y., Chen, F., and Chu, H.S. "Reactant gas transport and cell performance of proton exchange membrane fuel cells wth tapered flow field desgn." Journal of Power Sources. 158 (2006) 78-87.

Majsztrik, P.W., Satterfield, M.B., Bocarsly, A.B., and Benziger, J.B. "Water sorption, desorption and transport in nafion membranes. Journal of Membrane Science. 301 (2007) 93-106.

Marr, C. and Li, X. "Composition and performance modelling of catalyst layer in a proton exchange membrane fuel cell." Journal of Power Sources. 77 (1999) 17-27.

Natarajan, D. and Van Nguyen, T. "A two-dimensional, two phase, transient model for the cathode of a proton exchange membrane fuel cell using conventional gas distributors." Journal of the Electrochemical Society. 148 (2001) A1324-A1335.

Okudan, G.E., M. Ogot, R. Shirwaiker, 2006, “An investigation on the effectiveness of design ideation using TRIZ,” *Proceedings of ASME DETC/CIE*, Philadelphia, PA, DETC2006-99483.

Otto, K.N., K.L. Wood, 2001, *Product Design Techniques in Reverse Engineering and New Product Development,* Prentice-Hall, Inc. New Jersey, USA.

Purves, W.K., D. Sadava, G.H. Orians, H.C. Heller, 2001, *Life, The Science of Biology, 6/e*, Sinauer Associates, Sunderland, MA.

Ross, V.E., "A Comparison of Tools Based on the 40 Inventive Principles of TRIZ," *The TRIZ Journal*, 2006. [Online] Accessed: January 15, 2008. Available: http://www.triz-journal.com/archives/2006/11/01.pdf.

Schütz, P., 1989, "Prevention of Membrane Dehydration in PEM Fuel Cells," *Proceedings of the Symposium on Fuel Cells*, eds. White, R.E., Appleby, A.J., The Electrochemical Society, Inc., PVP-Vol. 89(14): 87-93.

Sherman, T.F. "The meaning of murray's law." The Journal of General Physiology. 78 (1981) 431-453

Shi, Z. and Wang, X. "Comparison of darcy's law, the brinkman equation, the modified n-s equation and the pure diffusion equation in PEM fuel cell modeling." Proceeding of the COMSOL Conference 2007, Boston.

Shu, L.H., H. Hansen, A. Gegeckaite, J. Moon, C. Chan, 2006, "Case Study in Biomimetic Design: Handling and Assembly of Microparts," *Proceedings of ASME DETC/CIE*, Philadelphia, PA, DETC2006-99398 (DTM).

Siegel, N.P., Ellis, M.W., Nelson, D.J. and von Spakovski, M.R. "A two-dimensional computational model of a PEMFC with liquid water transport." Journal of Power Sources. 128 (2004)173-184.

Singh, D., Lu, D.M., and Djilali, N. "A two-dimensional analysis of mass transport in proton exchange membrne fuel cells." International Journal of Engineering Science.37 (1999) 431-452.

Sinha, P.K., Wang, C.-Y. and Beuscher, U. "Effect of flow fiels design on the performance of elevated-temperature polymer electrolyte fuel cells." International Journal of Energy Research. 31 (2007) 309-411.

Sinha, P.K., Wang, C.-Y. and Beuscher, U. "Transport phenomena in elevated temperature PEM fuel cells." Journal of the Electrochemical Society. 154 (2007) B106-B116.

Smith, C.W., Vincent, J.F.V. "Biomimetics: Technology transfer from biology to engineering." Philisophical Transactions: Mathematical, Physical and Engineering Sciences. 360 (1791) 155-157 (2002)

Springer, T.E., Zawodzinski, T.A. and Grottesfeld, S. "Polymer electrolyte fuel cell model." Journal of the Electrochemical Society. 138 (1991) 2334 - 2342.

Sui, P.C., Kumar S. and Djilali, N. "Advanced computational tools for PEM fuel cell design Part 1. Development and base case simulations." Journal of Power Sources. 180 (2008) 410-422.

Turhan, A., Heller, K., Brenizer, J.S. and Mench, M.M. "Passive control of liquid water storeage and distribution in a PEFC through flow field design." Journal of Power Sources. 180 (2008) 773-783.

Vakili, V., L.H. Shu, "Towards Biomimetic Concept Generation," *Proceedings of ASME DETC/CIE*, Pittsburgh, PA, 2001, DETC2001/DTM-21715.

Van Bussel, H.P.L.H, Koene, F.G.H., Mallant, R.K.A.M. "Dynamic model of solid polymer fuel cell water management." Journal of Power Sources. 71 (1998) 218-222

Van Nguyen, T. and White, R.E. "A water and heat managament model for proton-exchange-membrane fuel cells." Journal of the Electrochemical Society. 140 (1993) 2178-2186.

Vincent, J.F.V., Mann, D.L. "Systematic technology transfer from biology to engineering." Philisophical Transactions: Mathematical, Physical and Engineering Sciences. 360 (1791) 159-173 (2002)

Wang, X.-D., Duan, Y.-Y., Yan and W.-M. "Novel serpentine-baffle flow field design for proton exchange membrane fuel cells." Journal of Power Sources. 173 (2007) 210-221.

Wang, X.-D., Duan, Y.-Y., Yan, W.-M. and Peng, X.-F. "Effects of flow channel geometry on cell performance for PEM fuel cells with parallel and interdigitated flow fields." Electrochemica Acta. 53 (2008) 5334-5343.

Weng, W.-C., Yan, W.-M., Li, H.-Y. and Wang, X.-D. "Numerical simulation of cell performance in proton exchange membrane fuel cells with contracted flow field design." Journal of the Electrochemical Society. 155 (2008) B877-B886.

Wesselingh, J.A. and Krishna, R. *Mass Transfer in Multicomponent Mixtures*. Delft University Press. Delft, The Netherlands: 2000.

Yan, W.M., Liu, H.C., Soong, C.Y., Chen, F. and Cheng, C.H. "Numerical study on cell performance and local transport phenomena on PEM fuel cells with novel flow field designs." Journal of Power Sources. 161 (2006) 907-919.

Ye, Q. and Van Nguyen, T. "Three-dimensional simulation of liquid water distribution in a PEMFC with experimentally measured capillary functions." Journal of the Electrochemical Society. 154 (2007) B1242-B1251.

Yi, J.S. and Van Nguyen, T. "Multicomponnent transport in porous electrodes of proton exchange membrane fuel cells using the interdigitated gas distributors." Journal of the Electrochemical Society. 146 (1999) 38-45.

Yi, J.S., Van Nguyen, T. "An along-the-channel model for proton exchange membrane fuel cells." Journal of the Electrochemical Society. 145 (1998) 1149-1159

Zawodzinski, T.A., Neeman, M., Sillerud, L.O. and Gottesfeld, S. "Determination of water coefficients in perfluorosulfonate ionomeric membranes." Journal of Physcal Chemistry. 95 (1991) 6040-6044.

Appendices

Appendix A: Drawings of the Flow Fields

The following are drawings of the Fuel Cell Technolgies Inc. triple serpentine low field and the Murray 1 flow field.

A.1 FCT Triple Serpentine Flow Field

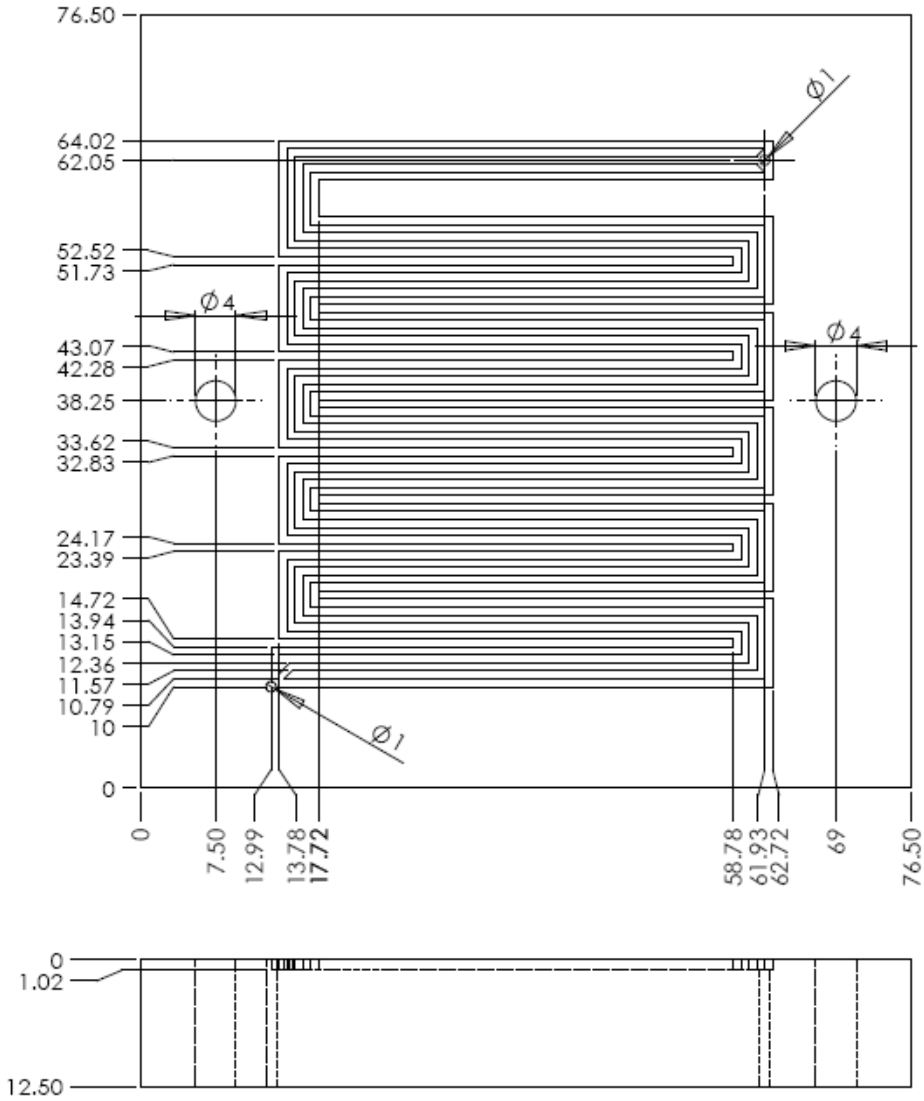

A.2 Murray 1 Flow Field